ON THE DOMAIN OF DOMINANCE OF THE ASYMPTOTIC ELASTODYNAMIC CRACK-TIP FIELDS

Thesis by

Sridhar Krishnaswamy

In Partial Fulfillment of the Requirements

for the Degree of

Doctor of Philosophy

California Institute of Technology

Pasadena, California

1989

(Submitted September 30, 1988)

To my parents

ACKNOWLEDGMENTS

I would like to thank Prof. Ares Rosakis for his active support and guidance throughout my stay at Caltech. I am grateful to Prof. Knauss for the use of the high-speed camera and laser set-up. I would also like to thank Prof. G. Ravichandran of the University of California, San Diego, who eased my way (dragged me feet first?) into the realm of computational mechanics.

The entire solid mechanics group has been very supportive. In particular, I greatly appreciate the help of Dr. Alan Zehnder and, especially, the many, many useful discussions with Richard Pfaff.

I must thank Lou Johnson of Central Engineering Services, George Lundgren of the Aero Shop and Ken Wang for their timely help with specimen preparation.

The experimental aspects of this work were funded by the Office of Naval Research through contract N00014-85-K-0599. The computations were performed using the facilities of the San Diego Supercomputer Center and were made possible through NSF grant MSM-84-51204.

ABSTRACT

A substantial part of the experimental data in dynamic fracture mechanics has been obtained under the assumption that the two-dimensional asymptotic elastodynamic stress-intensity factor field (the K_I^d-field) is dominant over at least the region around the crack-tip over which the experimental measurements are made. The validity of this assumption is investigated in this thesis both experimentally and through finite-element simulations of the experiments.

The experiments reported in this work were on 4340 steel, three-point bend specimens loaded dynamically using a drop-weight tower. The two cases of dynamically loaded stationary cracks and dynamically propagating cracks were considered. An optical configuration is proposed that leads to a *bifocal* high-speed camera capable of focussing on two different planes simultaneously. This was used in conjunction with the method of caustics to measure the apparent stress-intensity factor simultaneously from two different regions (initial-curves) around the crack-tip. If the initial-curves lie within the domain of dominance of the asymptotic field, the measured values of the dynamic stress-intensity factor must agree to within experimental error. By suitably adjusting the optical set-up, a range of initial-curves was scanned in an attempt to map the domain of dominance of the K_I^d-field.

The impact hammer and supports of the drop-weight loading device were instrumented in order to monitor the time dependent loads acting on the specimen. These loads were subsequently used as boundary tractions in dynamic two- and three-dimensional finite-element simulations of the experiments. The simulations were carried only up to the point of crack initiation. Comparison of the numerical simulations with the experimental results help in identifying the role of three-dimensionality and transient conditions on the measured stress-intensity factor values.

On the basis of both the experimental results as well as the numerical simulations, no sizeable annulus of dominance for the asymptotic elastodynamic field was found for the laboratory situation studied. It appears that the assumption of an underlying K_I^d-dominant (or two-dimensional) field might not hold to a level of accuracy that would warrant many of the conclusions made in the literature regarding the crack-initiation toughness values as well as the uniqueness of the dynamic fracture toughness – crack velocity relation or its specimen and acceleration dependence.

TABLE OF CONTENTS

CHAPTER I

INTRODUCTION

The mechanics of crack initiation and propagation under conditions where material inertial effects are important – either due to rapid crack propagation or due to transient loading – fall into the broad field of study of dynamic fracture mechanics. The interest in this field arises, from a practical standpoint, from the need to understand the conditions under which an existing macro-crack in a structure might initiate dynamically and begin to grow catastrophically through the structural component, seriously jeopardizing its integrity and function. Catastrophic crack growth in nuclear pressure vessels or in the bulkheads of airplanes could have rather undesirable consequences. The rapid disintegration of natural-gas pipelines, where the internal gas pressure might initiate and drive a crack for many kilometers prior to arrest, is a particularly graphic example of the kind of problems that is to be prevented. The endeavor of the engineer in these cases is, ideally, to obtain conditions under which a crack would never grow unstably, or failing this, to at least configure the structural system so as to build in a tendency for an initiated crack to arrest as rapidly as possible before serious damage is sustained.

While the micro-mechanical aspects of the actual cleavage or void coalescence that are an essential part of the fracture process are inaccessible through a continuum description, much of the theoretical basis of dynamic fracture mechanics derives from continuum analyses. The rationale for this rests on the intuitive argument that the behavior and response of any *confined* non-continuum region (process zone) around the crack-tip must be controlled by the engulfing continuum field and, as such, whatever critical parameters govern the progress of fracture in the process zone must have their counterparts in the continuum region. It is not the purpose of this work to inquire into the physical basis of the above argument. Rather, at-

tention shall be confined here to cases where a continuum description is known – empirically – to be adequate.

The attempt to characterize the initiation and dynamic propagation of a crack in a material is typically done in two parts. A fracture criterion is first postulated which would relate some parameter in a continuum solution to a material specific property. For example, a crack might be postulated to initiate and propagate when the strain at some prescribed point along the crack-line reaches a critical value which is supposedly a material property determinable only through experiments. The correctness and utility of such a fracture criterion must then be established by showing its validity under different geometric and loading configurations. That is, while the details of the stress and strain fields might depend on the particular geometric and loading conditions, the critical values at which a crack would initiate and grow must be configuration independent.

By far the most widely quoted fracture criterion in the dynamic fracture of nominally brittle materials – defined here as materials where no extensive plastic deformation occurs prior to or during crack growth – is that based on the stress-intensity factor. This is a parameter that arises naturally from certain mathematically idealized crack problems and, since its measurability and utility as a fracture criterion form the subject of inquiry of this thesis, it is probably instructive at this point to delve into its origins.

1.1 The Asymptotic Field

The first dynamic fracture problems to be analytically solved were those where the material was modelled as linear elastic and the geometry and loading were taken to conform to plane strain conditions. The crack solutions of Yoffe (1951), Craggs (1960), Broberg (1960), Baker (1962) and Freund (1972) all fall into this category. While the problems they considered differed in some vital respects – some

were transient while others were steady-state, for example – a common outcome of all their solutions was the nature of the asymptotic stress field. Indeed, as has been shown by Freund and Clifton (1974), the stress field with reference to a Cartesian coordinate system moving with the crack-tip (see Figure 1.1) of 'all plane elastodynamic solutions for (smoothly turning) running cracks, for which the total internal energy is finite,' can be asymptotically described by the square-root singular expression

$$\sigma_{\alpha\beta} = \frac{K_I^d(t)}{\sqrt{2\pi r}}\,\Sigma_{\alpha\beta}^I(\theta,\dot{a}) + \frac{K_{II}^d(t)}{\sqrt{2\pi r}}\,\Sigma_{\alpha\beta}^{II}(\theta,\dot{a}) + O(1), \qquad \text{as } r \to 0. \tag{1.1}$$

Here (r,θ) is a polar coordinate system travelling with the crack-tip, $\Sigma_{\alpha\beta}^I$ and $\Sigma_{\alpha\beta}^{II}$ are known functions of θ and crack velocity $\dot{a}$ (with respect to some fixed coordinate frame), and K_I^d and K_{II}^d are the so-called stress-intensity factors in mode-I and mode-II respectively dependent only on the specific geometric and loading conditions of a problem. In this work, attention will be confined to only the mode-I case and the relevant asymptotic expressions from Freund and Clifton (1974) are collected here for purposes of later reference:

$$\sigma_{\alpha\beta} = \frac{K_I^d(t)}{\sqrt{2\pi r}}\,\Sigma_{\alpha\beta}^I(\theta,\dot{a}) + O(1), \qquad \text{as } r \to 0 \tag{1.2}$$

where,

$$\Sigma_{11}^I = A\left((1+2\alpha_l^2-\alpha_s^2)\frac{\cos(\theta_l/2)}{\gamma_l^{1/2}} - \frac{4\alpha_l\alpha_s}{(1+\alpha_s^2)}\frac{\cos(\theta_s/2)}{\gamma_s^{1/2}}\right) \tag{1.3}$$

$$\Sigma_{12}^I = 2A\alpha_l\left(\frac{\sin(\theta_l/2)}{\gamma_l^{1/2}} - \frac{\sin(\theta_s/2)}{\gamma_s^{1/2}}\right) \tag{1.4}$$

$$\Sigma_{22}^I = A\left(-(1+\alpha_s^2)\frac{\cos(\theta_l/2)}{\gamma_l^{1/2}} + \frac{4\alpha_l\alpha_s}{(1+\alpha_s^2)}\frac{\cos(\theta_s/2)}{\gamma_s^{1/2}}\right) \tag{1.5}$$

and

$$A = \left(\frac{(1+\alpha_s^2)}{4\alpha_l\alpha_s - (1+\alpha_s^2)^2}\right) \tag{1.6}$$

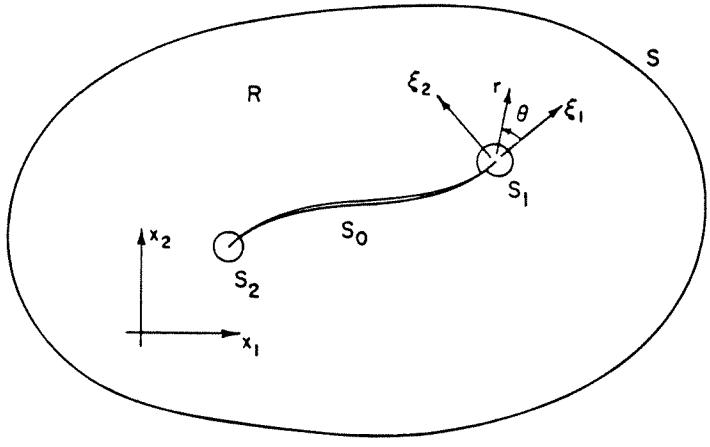

Figure 1.1: Cross-sectional geometry of the elastodynamic plane crack problem; the Cartesian coordinate system (ξ_1, ξ_2) translates with the crack-tip of interest (from Freund and Clifton (1974)).

and

$$\gamma_{l:s} = (\cos^2(\theta) + \alpha_{l:s}^2 \sin^2(\theta))^{-1/2} \tag{1.7}$$

$$\tan(\theta_{l:s}) = \alpha_{l:s} \tan(\theta) \tag{1.8}$$

and

$$\alpha_{l:s} = \left(1 - \frac{\dot{a}^2}{c_{l:s}^2}\right)^{1/2}, \tag{1.9}$$

where c_l and c_s are the longitudinal and shear wave speeds of the material. The above will henceforth be referred to as the dynamic stress-intensity factor field or, more concisely, the K_I^d-field. Note that this is strictly asymptotic and that any attempt to use it over a finite extent must be justified by showing that the asymptotic solution dominates (to within some acceptable error) over this region. A region where the above field dominates will then be referred to as a region of K_I^d-dominance.

The situation of a stationary crack that is loaded dynamically is less clear but the few analytical solutions that exist – de Hoop (1958) and Achenbach (1973) – do exhibit a stress-intensity factor field such as (1.2-9) with $\dot{a} \to 0$. While the universality of such a field has not been rigorously established for all stationary cases, the leeway provided by the unspecified extent of validity of the asymptotic field has allowed for the assumption that the stress-intensity factor field is descriptive of all plane elastodynamic crack problems. It has of course been recognized that the asymptotic field as given above leads to singular stresses at the crack tip and, as such, plasticity and other non-linear effects must come into play near the crack tip. The possible relevance of the stress-intensity factor field thus arises from an argument of confined plasticity similar to that used for the confined process zone: if the length scale over which plasticity effects are important is much smaller than the length over which the asymptotic K_I^d-field is dominant, then the stress-intensity

factor field must characterize the plastic and process zones and hence the fracture process itself. This is the so-called small-scale yielding concept.

Finally, in an attempt to model the more realistic problem of fracture in thin plates, the asymptotic field for conditions of plane-stress are formally obtained through suitable modifications of the material parameters. 'Formal' in the sense that no attempt is made to inquire into the acceptability of the plane stress approximation in the vicinity of a crack tip.

1.2 Fracture Criteria

The presumed universality of the stress-intensity factor field for problems of small-scale yielding thus provides a possible fracture criterion of the form

$$K_I^d(t) = K_{ID} \tag{1.10}$$

where the left side is the stress-intensity factor, in principle entirely determined through an analysis of a boundary-initial value problem, and the right side represents a material quantity called the dynamic fracture toughness that can only be determined through experiments. The dynamic stress-intensity factor $K_I^d(t)$ is known to be a function of crack length $a(t)$, crack velocity $\dot{a}(t)$, and some generalized measure of the applied load $P(t)$. It has also been suggested, based on perceived changes in the resistance to crack propagation with changes in rate of loading, that the dynamic fracture toughness must be dependent on crack velocity. Thus the fracture criterion as given in (1.10) becomes

$$K_I^d(a(t), \dot{a}(t), P(t)) = K_{ID}(\dot{a}(t), ...) \tag{1.11}$$

which is then an evolution equation for crack growth (equation of motion for the crack-tip) and therein lies the attractiveness of (1.10) as a fracture criterion.

The primary focus of dynamic fracture mechanics has been the determination of the fracture toughness and its possible dependence on parameters such as crack

velocity, acceleration and temperature. The extensive experimental effort that has gone into this task over the past two decades has generated a large amount of data without really conclusively deciding on the appropriateness of (1.10) as a fracture criterion. For the most part, experimental techniques that *assume* the dominance of the asymptotic K_I^d-field over some region around the crack tip have been utilized to argue about the functional dependence of the dynamic fracture toughness on crack velocity, acceleration, et cetera. Using this approach, some authors – Kobayashi and Dally (1977), Bilek (1980), Rosakis, Duffy and Freund (1984) and Zehnder (1987) – have found that the dynamic fracture toughness depends in a one-to-one manner on the crack velocity while others – Kobayashi and Mall (1978), Ravi-Chandar (1982) and Ravi-Chandar and Knauss (1984) – do not find support for such a relation. Takahashi and Arakawa (1987) have argued for an acceleration dependence of the dynamic fracture toughness while Eshelby (1969) has pointed out that 'a crack tip exhibits no inertia.' A few experimentalists – Dahlberg, Nilsson and Brickstad (1980) and Kalthoff (1983) – have even found specimen dependence of the supposedly material property, which, if correct, should surely have robbed the stress-intensity factor-based fracture criterion of all residual meaning. The causes for these disagreements have been widely debated but a reasoned consensus is yet to emerge. For the most part, the variations have been attributed to differences in material response; this has a measure of validity because the failure modes of brittle materials such as Homalite-100 are quite different from those fracturing in a locally ductile manner, as was pointed out by Rosakis, Duffy and Freund (1983).

Of late, however, attention has been increasingly drawn toward another possible source of divergence, namely that the interpretation of the experimental data has, to a large extent, required the assumption that the asymptotic field be valid at least over the region where the measurements were made. Realizing that this

might be a source of error, Dally, Fourney and Irwin (1985) proceeded to develop 'higher-order solutions' to the two-dimensional, dynamic, steady crack propagation problem to aid in the interpretation of their experimental photo-elastic fringes. However, questions regarding the validity of these solutions and the errors associated with time-averaging the field over large domains, at least insofar as truly transient problems are concerned, have been raised by Knauss and Ravi-Chandar (1985). While Dally, Fourney and Irwin (1985) are probably correct in maintaining that the asymptotic field might not be adequate for transient problems, it is precisely these problems that are also not amenable to the kind of steady-state higher-order solution that they propose.

The realization that a much larger source of error might be the assumption that two-dimensional fields could be descriptive of the near-tip continuum structure is of much more recent origin. Among the first to study this question were Rosakis and Ravi-Chandar (1986) who experimentally sought to determine the extent to which three-dimensionality affected measurements made using the method of caustics under static conditions. Their finding was that the three-dimensional effects were confined to within a radial distance of one-half plate thickness around the crack-tip beyond which they found the two-dimensional static stress-intensity factor field prevailing over some distance. Supporting analytical basis for this work was provided by Yang and Freund (1985) who again find that the three-dimensional character of the field is confined to about one-half of the plate thickness beyond which the *imposed* asymptotic plane stress field is recovered. A full-field, three-dimensional, elastostatic analysis of the compact tension specimen was reported by Parsons, Hall and Rosakis (1986) providing further evidence that the three-dimensional region is confined to a radial distance of one-half the plate thickness. A detailed numerical study of the three-dimensional elastostatic near-tip field was reported by

Nakamura and Parks (1987) with essentially similar results, and Smith and Freund (1988) adopted the same approach to the dynamic, steady-state propagating crack problem. Both these analyses, however, *impose* the plane-stress, asymptotic field at some arbitrary distance from the crack-front. These studies also find that the three-dimensional zone is confined to a region around the crack-tip of radius about one-half plate thickness. Further, they suggest that the asymptotic K_I-field should be obtained outside this region. Too much importance, however, should not be attached to this latter result in view of the fact that this outcome was most definitely influenced by their having *prescribed* the K_I-field at some *definite* distance *greater* than one-half of plate thickness. (Specifically, the results certainly would have been different if the K_I-field had been imposed at, say, one-quarter of the plate thickness, and probably would have been different if something other than the K_I-field had been prescribed as the far-field boundary condition.)

Apart from the works mentioned above, many analytical and numerical studies have attempted to incorporate non-linearity of material response. Among these, Freund and Douglas (1982), Lam and Freund (1985) and Freund and Hutchinson (1985) adopt the small-scale yielding approach; i.e., it is assumed that a K-dominant field surrounds the non-linear zone and the details of the continuum structure in the plastic region are obtained in this context. In particular, Freund and Lam (1985) have sought to provide an analytical basis for the postulated uniqueness of the $K_{ID} - \dot{a}$ relation by assuming a more fundamental fracture criterion inside the plastic zone and then studying its ramifications for the surrounding K_I^d-field. Essentially the same approach is taken by Freund and Hutchinson (1985) where a material exhibiting rate-dependent plastic behavior is considered. For the purposes of this thesis, the point to note is that the common thread underlying all these studies – and many others of no immediate relevance to this work – is the acceptance

of a K-dominant field over some annulus around the crack-tip.

1.3 Overview of Thesis

This thesis documents an effort to systematically investigate the validity and extent of dominance of the stress-intensity factor field under conditions of dynamic loading and propagation. The need for such a study becomes apparent when one realizes that a concept that had its origins in an asymptotic two-dimensional idealization has come to be rather widely used in many analytical problems investigating non-linear or three-dimensional effects near the crack-tip and, more importantly, in laboratory situations involving finite-sized specimens of definite thickness – with little attempt to show that such a concept retains its validity under these conditions. The question that this work addresses is the following: *Is there a region around the crack-tip where the stress and displacement fields could be said to be modelled by the two-dimensional dynamic stress-intensity factor field?* This will be answered within the context of a three-point bend specimen loaded dynamically in a drop-weight tower – an experimental configuration that has been extensively used in the past by Kalthoff (1985), Zehnder (1987) and Zehnder and Rosakis (1988). The findings of this work are specific to this particular configuration. Extrapolations to other settings must therefore be done with care and then, only in a qualitative sense. The questions raised here and the methodology adopted in trying to answer them, of course, have a wider applicability.

The idea behind the experimental set-up is described in Chapter II. A simple modification that can be incorporated into virtually any high-speed photography set-up is proposed and the way in which this experimental configuration can be used in conjunction with the method of caustics to determine the domain of dominance of the asymptotic field is discussed. Chapter III presents the details of the experiments. The optical high-speed photography set-up for obtaining a time sequence of caustic

patterns and the instrumentation used to record the dynamic traction boundary conditions experienced by the specimen are both discussed. Finally, the results and implications of the optical part of the experiment are given. In Chapter IV, the details of numerical simulations of the experiments are provided. Two- and three-dimensional elastodynamic finite element analyses using experimentally obtained traction boundary conditions are attempted. The numerical simulations help in identifying possible reasons for the experimentally observed behavior. In conclusion, Chapter V describes the implications of the findings of this work and attempts to review some of the experimental and analytical results in the literature in light of the results of this study.

CHAPTER II

THE METHOD OF BIFOCAL CAUSTICS

The optical method of caustics has found extensive application in fracture mechanics studies in general and in dynamic fracture experiments in particular – Rosakis (1980,1982), Beinert and Kalthoff (1981), Ravi-Chandar (1982), Ravi-Chandar and Knauss (1984) and Zehnder and Rosakis (1988). It is a technique that has been used both for transparent materials in transmission and opaque materials in reflection. In this, it has the advantage over photo-elasticity, though attempts to extend photo-elasticity techniques to non-transparent materials by the use of bi-refringent coatings on the opaque test material have been reported by Kobayashi and Dally (1980). While there are ongoing efforts to use interferometry in dynamic fracture experiments (Pfaff (1988)), and other techniques – such as the stress-intensity factor tracer of Kim (1985) – have been proposed, the method of caustics has remained up to now essentially the only viable optical technique for the study of dynamic fracture of opaque materials such as steel. This being so, it is essential to understand the constraints under which the method of caustics – or photo-elasticity for that matter – is expected to produce useful results. For a successful interpretation of the measured data, the method of caustics as it is customarily used requires that the form of the near-tip stress or out-of-plane displacement field be known *a priori* up to a multiplicative constant. The method of caustics can *then* be used to successfully yield the actual value of this multiplicative constant which, in linear elastic fracture mechanics, is the stress-intensity factor. Photo-elasticity as well as the stress-intensity factor tracer method also suffer from similar restrictions. It is instructive to bear in mind that this stipulation is no different from the requirement that there be a homogeneous deformation field in a tension specimen if one were to set about obtaining material stress-strain behavior.

In this chapter, a brief discussion of the method of caustics as it pertains to this thesis is given. The issue of what is required to adapt this method to determine whether the assumed stress or out-of-plane displacement field does indeed prevail is then addressed with respect to both the static and dynamic fracture problems. Finally, in what is probably at the core of the experiment discussed in this thesis, an optical configuration that makes possible the experimental determination of the domain of dominance of the assumed crack-tip fields is proposed.

2.1 The Method of Caustics

A detailed exposition of the history and theory of the method of caustics can be found in Manogg (1964) and Rosakis and Zehnder (1985). Here only a brief outline of the method of caustics in reflection will be presented. A schematic diagram of the experimental method is shown in Figure 2.1. A collimated laser beam is incident on a polished, optically flat fracture specimen and the reflected light is collected and imaged in a camera. The camera is set to focus on a virtual object plane at a distance z_0 behind the specimen. When the specimen is loaded, its surface gets deformed by, say, $x_3 = -f(x_1, x_2)$, where (x_1, x_2) are points on the specimen. Due to this deformation, a light ray incident at a point (x_1, x_2) on the specimen gets mapped to a point (X_1, X_2) on the virtual object plane of the camera. The mapping can be shown to be given by

$$\underline{X} \approx \underline{x} - 2z_0 \underline{\nabla} f \tag{2.1}$$

where it has been assumed that $z_0 \gg \max|f(x_1, x_2)|$ which is true for all experiments reported in this thesis.

Caustics in Elastostatic Fracture:

Consider a fracture specimen made of an isotropic, homogeneous, nominally linear elastic solid. Under static, mode-I, generalized plane-stress conditions, following

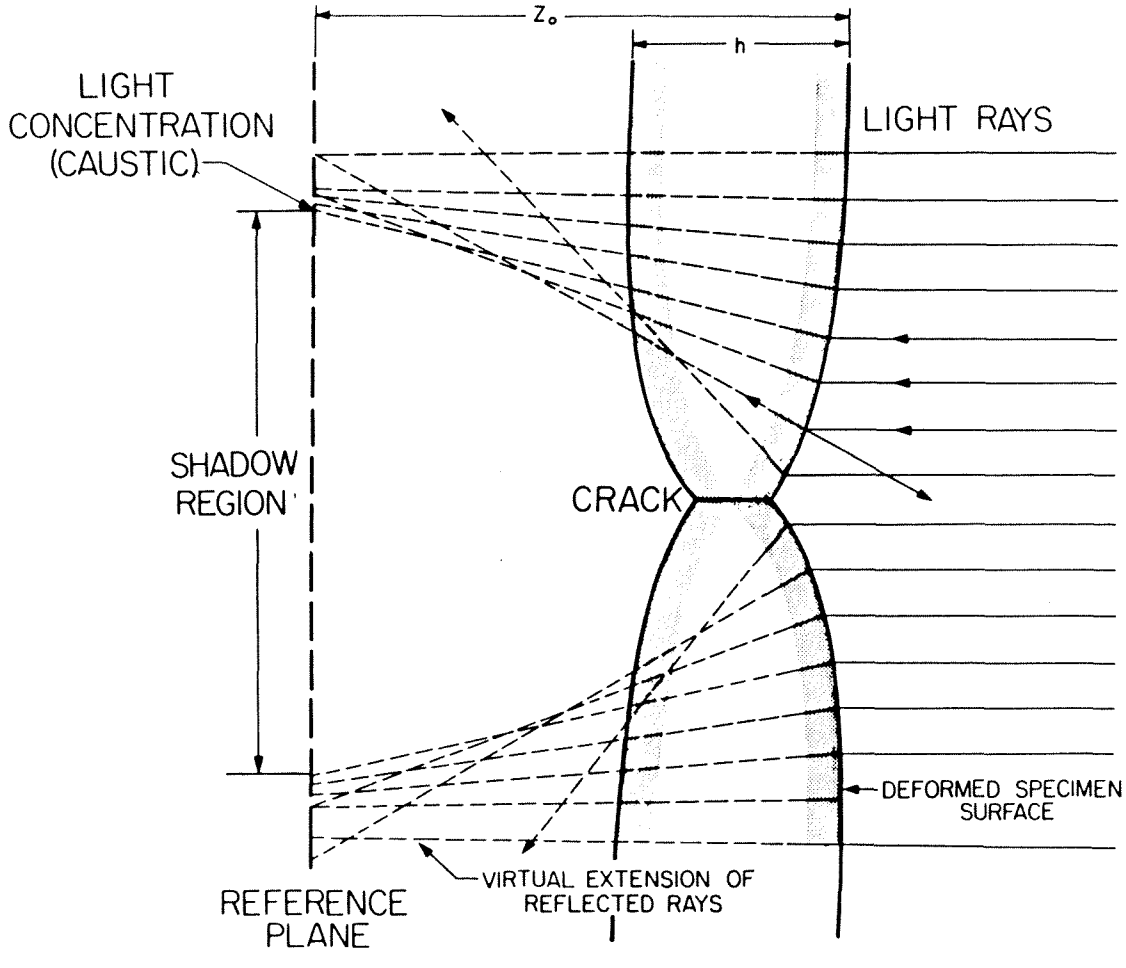

Figure 2.1: Schematic diagram of the method of caustics in reflection.

Williams (1957), the asymptotic out-of-plane displacement field can be shown to be given by

$$u_3 = \frac{-\nu h}{E}\frac{K_I}{\sqrt{2\pi r}}\cos\left(\frac{\theta}{2}\right) + O(1), \qquad \text{as } r \to 0 \tag{2.2}$$

where (r, θ) is a polar coordinate system centered at the crack-tip, E is the Young's modulus of the material, ν is the Poisson's ratio of the material, and h is the specimen thickness.

The out-of-plane displacement field is seen to be singular at the crack-tip but, in reality, non-linear and non-continuum effects in a process zone surrounding the crack-tip invalidate the strict application of (2.2) as $r \to 0$. However, as an engineering approximation, the idea of small scale yielding was propounded by Rice (1968) and is now widely held to be valid, under which the surface deformation is assumed to be given by

$$u_3 = \frac{-\nu h}{E}\frac{K_I}{\sqrt{2\pi r}}\cos\left(\frac{\theta}{2}\right), \qquad r_{in} < r < r_{out} \tag{2.3}.$$

Here $'r'_{out}$ is some relevant specimen in-plane geometry parameter and $'r'_{in}$ is dictated by the size of one or more of the following: (1) the process zone which is the region of non-continuum behavior (2) the plastic or non-linear zone and (3) a region where the assumptions of two-dimensional plane-stress analysis break down and the field is inherently three-dimensional. The domain where equation (2.3) is applicable will be referred to as a region of K_I-dominance.

The caustic mapping of the surface given by (2.3) leads to a characteristic shadow spot – a dark region where no light rays get mapped, surrounded by a bright epicycloid called the caustic (Fig. 2.2). The caustic diameter D can be related to the stress-intensity factor K_I through

$$K_I = \frac{ED^{5/2}}{10.7 z_0 \nu h}. \tag{2.4}$$

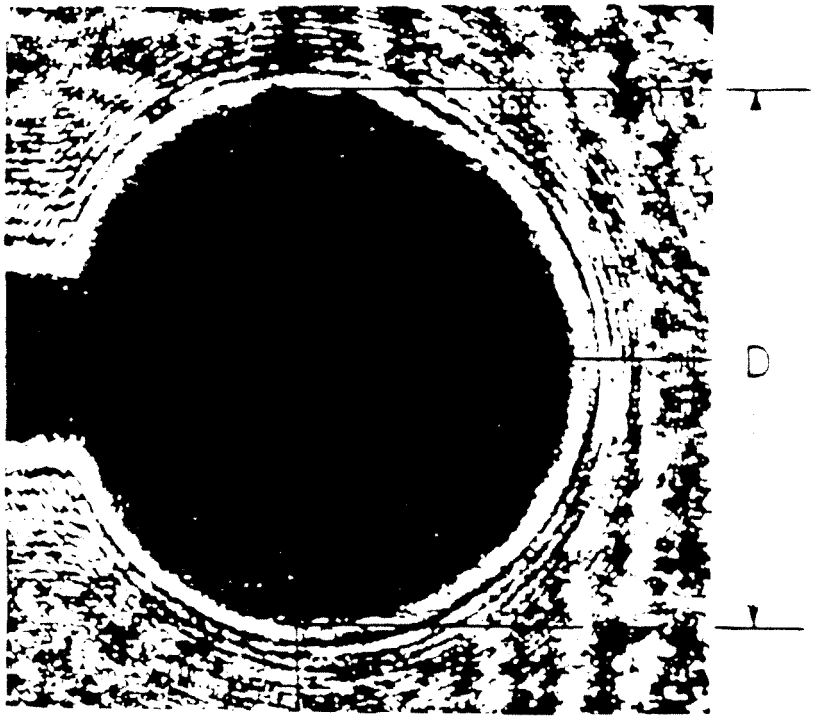

Figure 2.2: Representative caustic pattern from a statically loaded fracture specimen.

It is important to note that the locus of points on the specimen surface that map on to the caustic curve forms a circle called the initial-curve whose radius r_0 is given by

$$r_0 = 0.316D = \left(\frac{3h\nu K_I z_0}{2\sqrt{2\pi}E}\right)^{2/5}. \tag{2.5}$$

The information about the caustic diameter and hence the stress-intensity factor comes essentially from the local field prevailing around the initial-curve. Symbolically one may write $r_0 = \widehat{r}_0(K_I, z_0)$ and it is precisely this dependence that can be exploited to provide an *indirect* check of whether the assumed displacement profile (2.3) actually prevails or not. For the static case, this issue was investigated by Rosakis and Ravi-Chandar (1986) in a rather straight forward manner. By keeping the load constant, the same value of the stress-intensity factor K_I can be maintained and by varying the object plane distance z_0, the region r_0 from which the caustics are obtained could be varied. Now if, for the range over which r_0 is varied, the out-of-plane displacement field is given by (2.3), then the resulting values for the apparent stress-intensity factor as computed through (2.4) must be the same.* From their experiments, Rosakis and Ravi-Chandar (1986) concluded that for $r_0/h > 0.5$ equation (2.4) remains accurate, while for smaller r_0/h the value of the stress-intensity factor as obtained through (2.4) is under predicted. (see Fig. 2.3).

Caustics in Elastodynamic Fracture:

Consider a fracture specimen made of a linear elastic, homogeneous, isotropic solid subject to mode-I, generalized plane-stress conditions. Suppose that inertial effects need to be included either due to dynamic loading of a stationary crack or due to rapid crack propagation. By means of an interior asymptotic expansion, Freund

* The assumption that the displacement field is not expected to behave pathologically (leading to a multiply folded mapping) is implicitly made here.

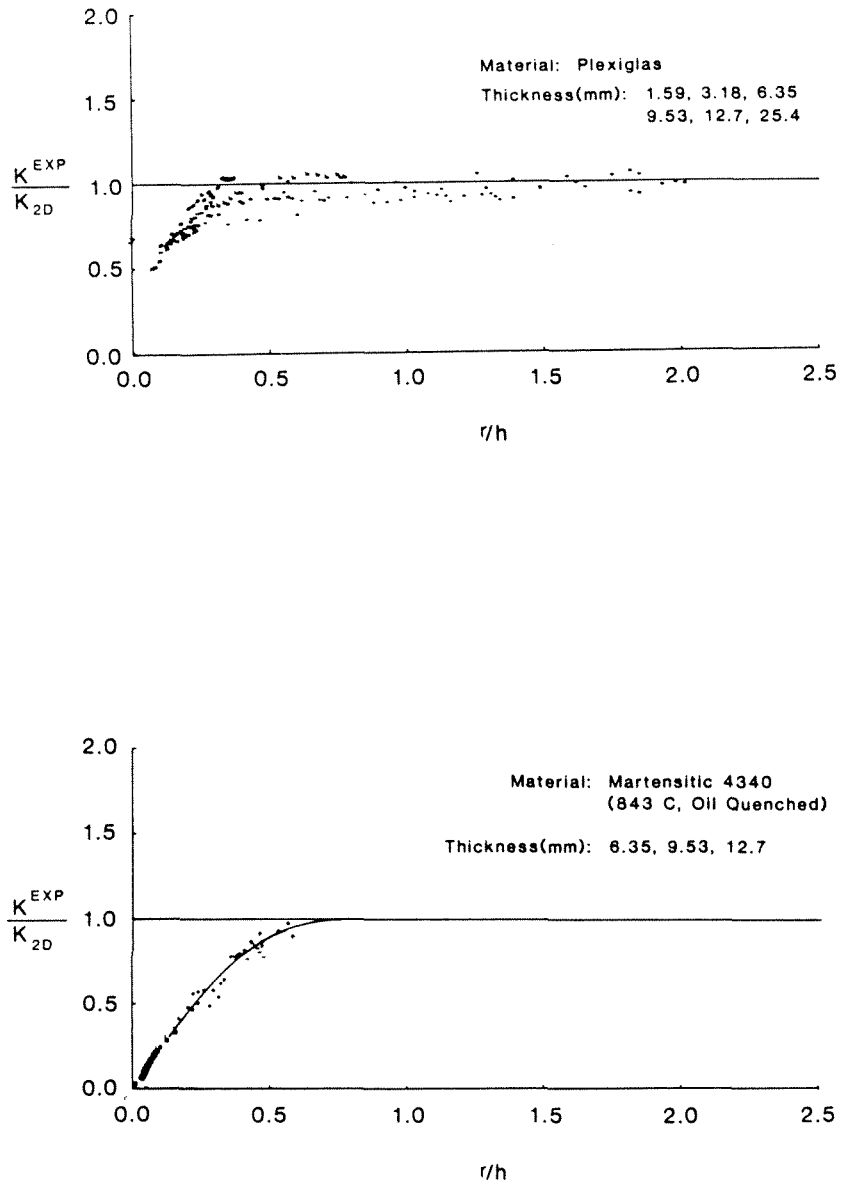

Figure 2.3: Variation in the measured stress-intensity factor with radius of the initial-curve of the caustic. From Rosakis and Ravi-Chandar (1986) who attribute the deviation to near-tip three-dimensionality.

and Clifton (1974) have shown that the asymptotic stress field with reference to a polar coordinate system translating with the crack-tip is now given by

$$\sigma_{\alpha\beta} = \frac{K_I^d(t)}{\sqrt{2\pi r}} \Sigma_{\alpha\beta}(\theta, \dot{a}) + O(1), \qquad \text{as } r \to 0 \tag{2.6}$$

where $K_I^d(t)$ is now a time-dependent dynamic stress-intensity factor and $\Sigma_{\alpha\beta}$ are known universal functions of θ and crack velocity $\dot{a}$ (see the introductory chapter). As given in detail in Rosakis (1982), the out-of plane displacement field corresponding to (2.6) can be obtained, the caustic map of which yields the characteristic shadow-spot whose transverse diameter D (now varying with time) can be related to the instantaneous stress-intensity factor through

$$K_I^d = \frac{ED^{5/2}}{10.7 z_0 \nu h} F(\dot{a}) C(\alpha_l) \tag{2.7}$$

where,

$$F(\dot{a}) = \frac{4\alpha_l \alpha_s - (1+\alpha_s{}^2)^2}{(1+\alpha_s{}^2)(\alpha_l{}^2 - \alpha_s{}^2)} \tag{2.8}$$

and

$$C(\alpha_l) = (6.8 + 14.4\alpha_l - 2.6\alpha_l{}^2)/18.6 \tag{2.9}$$

and

$$\alpha_{l:s} = \left(1 - (\dot{a}/c_{l:s})^2\right)^{1/2}. \tag{2.10}$$

As discussed in Rosakis (1982), the initial-curve for this case is no longer a circle. Nevertheless for sufficiently small crack velocities ($\dot{a} < 0.3c_s$) the initial-curve is very nearly circular and its instantaneous nominal radius can be approximated by

$$r_0(t) = \left(\frac{3h\nu K_I{}^d(t) z_0}{2\sqrt{2\pi E}}\right)^{2/5} F(\dot{a})^{(-2/5)}. \tag{2.11}$$

The above equations in the limit $\dot{a} \to 0$ are valid for the case of a dynamically loaded stationary crack. In a typical experiment, a high-speed camera would be

used to obtain a time sequence of caustics from whose diameter $D(t)$, the stress-intensity factor $K_I^d(t)$ would be computed using (2.7). From (2.11), one finds that $r_0(t) = \widehat{r}_0(K_I^d(t), z_0, \dot{a})$ and as $K_I^d(t)$ varies with time in a dynamic experiment, the radius of the initial-curve would perforce change during the course of the experiment. It is thus vital to know that (2.6) leads to a valid expression for the displacement field for at least the range of radii that the initial curve would cover during the event of interest. This issue is not quite so easily resolved as in the static case.

To make matters a bit more explicit, suppose that during the event of interest (which could be the crack propagation phase of a test) the initial-curve radius is known from previous experience to vary in the region $r_{min} \leq r_0 \leq r_{max}$ for some choice of the object plane distance z_0. Suppose further, as has become traditional, in analogy to the small-scale yielding approximation for the static case it is recognized that non-continuum, non-linear and three-dimensional effects preclude the application of (2.6) in the limit $r \to 0$ and so the asymptotic field as given by (2.6) is actually held to be a good approximation to reality in an annulus surrounding the crack-tip as shown in Figure 2.4. Thus,

$$\sigma_{\alpha\beta} \approx \frac{K_I^d(t)}{\sqrt{2\pi r}}\, \Sigma_{\alpha\beta}(\theta, \dot{a}), \qquad r_{in} < r < r_{out}. \tag{2.12}$$

Since the domain of validity of (2.12) could in general be time-dependent as well, let $'r'_{in}$ and $'r'_{out}$ be such as to give the smallest annulus in which (2.12) holds for all times during the entire event of interest. For a valid interpretation of the caustics, the inequalities

$$r_{in} < r_{min} \leq r_0 \leq r_{max} < r_{out} \tag{2.13}$$

must be satisfied in order to have the initial-curve fall in a region of K_I^d-dominance.

The first attempts to address the issue of the validity of (2.12) are reported in Ravi-Chandar and Knauss (1987). A series of tests was performed using the

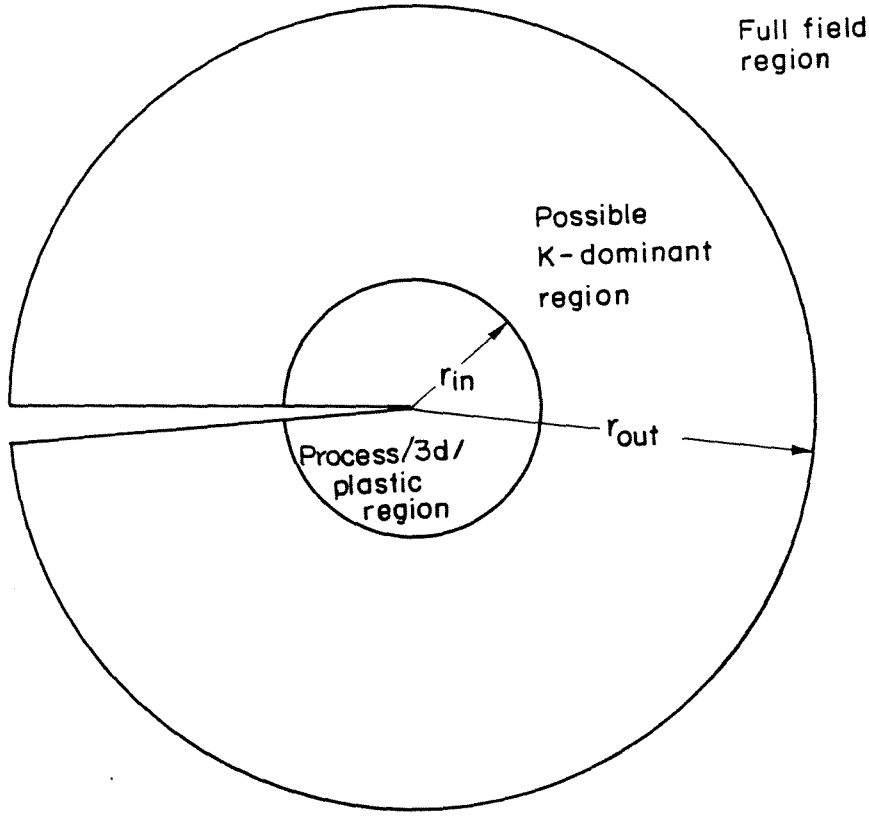

Figure 2.4: Possible region of K_I^d-dominance around the crack-tip.

method of caustics in transmission on identical specimens under identical stress-wave loading, varying from test to test only the object plane distance z_0. In this manner a range of initial-curve radii was scanned and since, presumably, the actual stress-intensity factor history $K_I^d(t)$ for the various tests must be identical, the apparent stress-intensity factors measured from caustics obtained from different object planes must also agree, at least for those times when the requirements of (2.13) are met. Based on their findings, Ravi-Chandar and Knauss (1987) indicate that the assumption behind (2.12) might not be tenable. Since a substantial part of the extant dynamic fracture data has been obtained through the use of either photoelasticity or the method of caustics, the ramifications of this result are potentially far-reaching and thus deserve greater scrutiny.

In particular, it would be preferable to obtain the apparent stress-intensity factor values from different initial-curves around the crack-tip for the same specimen at any given instant in time. While comparison of experimental results across tests can be made with confidence for the loading regime of the experiments, it becomes more difficult in the crack propagating phase since, as will be seen shortly, small variations in the crack motion history could lead to large variations in the values for the measured stress-intensity factor. It is in an attempt to avoid this problem that one would like to be able to obtain caustics from different initial-curves simultaneously from the same experiment. Conceptually, to set up an experiment to do this is an easy matter. The light reflected off a dynamically-loaded fracture specimen could be split into many paths (using beam-splitters) which could then be piped into a series of cameras each of which is set to focus on a different object plane. The resulting caustics imaged in these cameras would have been obtained from different initial-curves at each instant of time. Here, however, an alternate scheme is proposed that could, in fact, be incorporated into essentially any high-speed

photography system. An optical configuration that would allow for the *simultaneous* acquisition of dynamic caustics from *two* different object planes using only a *single* high-speed camera will now be discussed.

2.2 The Bifocal High-Speed Camera

In a previous section it was noted that the initial-curve is the region from which the caustic gets mapped and thus it is the region from which the apparent stress-intensity factor value is measured. Also, for a given stress-intensity factor value, it is the distance between the specimen and the camera (virtual) object plane that determines the radius of the initial curve. Thus if two different object planes can be simultaneously brought into focus in a single camera, stress-intensity factor information from two different initial-curves would be obtained at the same time. Figure 2.5 shows a schematic of the optical set-up required to bring two different object planes simultaneously into focus in a single camera. The set-up entails the use of two beam-splitters and two mirrors by which two optical paths of different path lengths are established between the specimen and the high-speed camera. With reference to the figure, let the high-speed camera be set up to focus at a distance f from the camera lens. Along path(1) this would mean that the virtual object plane is located at a distance z_{01} behind the specimen. Along path(2) however, by virtue of the increased length ($2L$) between the specimen and the camera lens, the object plane would now fall only at a distance $z_{02} = z_{01} - 2L$ behind the specimen. Thus the caustics obtained from the two paths would be from two different initial-curve radii. They could be made to appear on the film track of the high-speed camera either superposed or side by side.

For nomenclatural convenience, the pairs of dynamic caustics obtained by use of this bifocal high-speed camera will henceforth be referred to as 'bifocal caustics,' with the implicit understanding that such caustics are obtained from two different

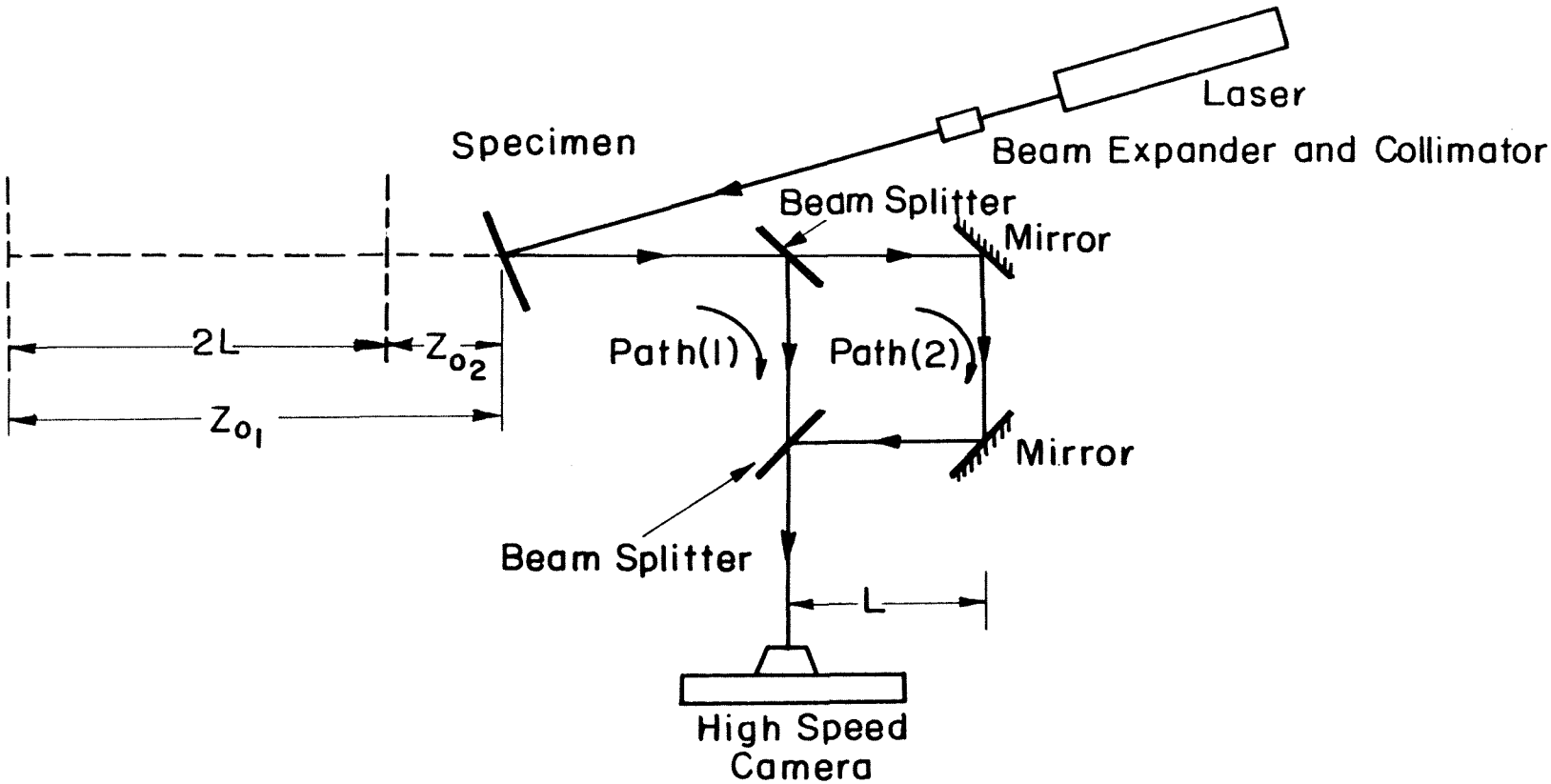

Figure 2.5: Schematic diagram of the bifocal set-up.

initial-curves on the same specimen at the same time.* By changing the distance L from test to test or by changing the focal plane of the camera, one could of course scan various sets of initial-curves. The comparison of whether the apparent stress-intensity factors obtained from the bifocal caustics agree over some range of r_0 would however be done solely within each test for reasons stated earlier.

Since the largest measurement uncertainties are in the crack velocities, one could check for the following ratio (as obtained from (2.7))

$$\frac{K_{I1}^d}{K_{I2}^d} = \left(\frac{z_{02}}{z_{01}}\right)\left(\frac{D_1}{D_2}\right)^{5/2} \tag{2.14}$$

where subscript '1' refers to quantities corresponding to path(1) and subscript '2' to path(2). This ratio should be unity if the initial-curve corresponding to z_{01} and z_{02} both fall within the K_I^d-dominant region. Any substantial deviation from unity of this ratio is then an indication of a lack of K_I^d-dominance over the corresponding region. The above ratio has the added advantage that the picture magnification and plate thickness get scaled out as well. Thus the measurement uncertainty in evaluating the above ratio of apparent stress-intensity factors through (2.14) is less than in the evaluation of the individual apparent stress-intensity factors through (2.7).

---

* There is, of course, a time delay of $2L/c$ because of the finiteness of the speed of light c, but this is negligible for values of L used in practice.

CHAPTER III

THE EXPERIMENT

The experiments reported in this work are designed to measure: (a) the apparent stress-intensity factor history using the bifocal caustics technique described in the previous chapter and (b) the time history of the traction boundary conditions that the specimen experiences for subsequent input into a dynamic finite-element analysis. These will help in the investigation of the domain of dominance of the asymptotic elastodynamic crack-tip fields. In this chapter, the experimental details will be described and the results of the bifocal caustics part of the experiments will be presented. The numerical simulation of the experiments will be described in the following chapter.

3.1 The Experimental Set-up

Specimen Preparation:

The specimens were made of either plain or vacuum-arc remelt AISI 4340 steel whose material composition is given in Table T1. The first step in the specimen preparation was to machine them to the nominal required dimensions as shown in Figure 3.1. A 25mm saw-cut was first made in all the specimens. For some specimens, the remaining length of the crack was cut by means of an electric discharge machine (EDM) leaving a somewhat blunt notch. In others, a smaller EDM cut was made and the notch was then increased in length by fatiguing to provide a sharp crack. The different crack-tip bluntnesses lead to a wider range of crack propagation velocities.

The specimens were heat-treated as follows: (1) normalized at 900^oC for one hour and air-cooled, (2) austenitized at 845^oC for one hour and oil-quenched and (3) tempered at 200^oC, 315^0C or 350^oC for one hour and air-cooled. This was

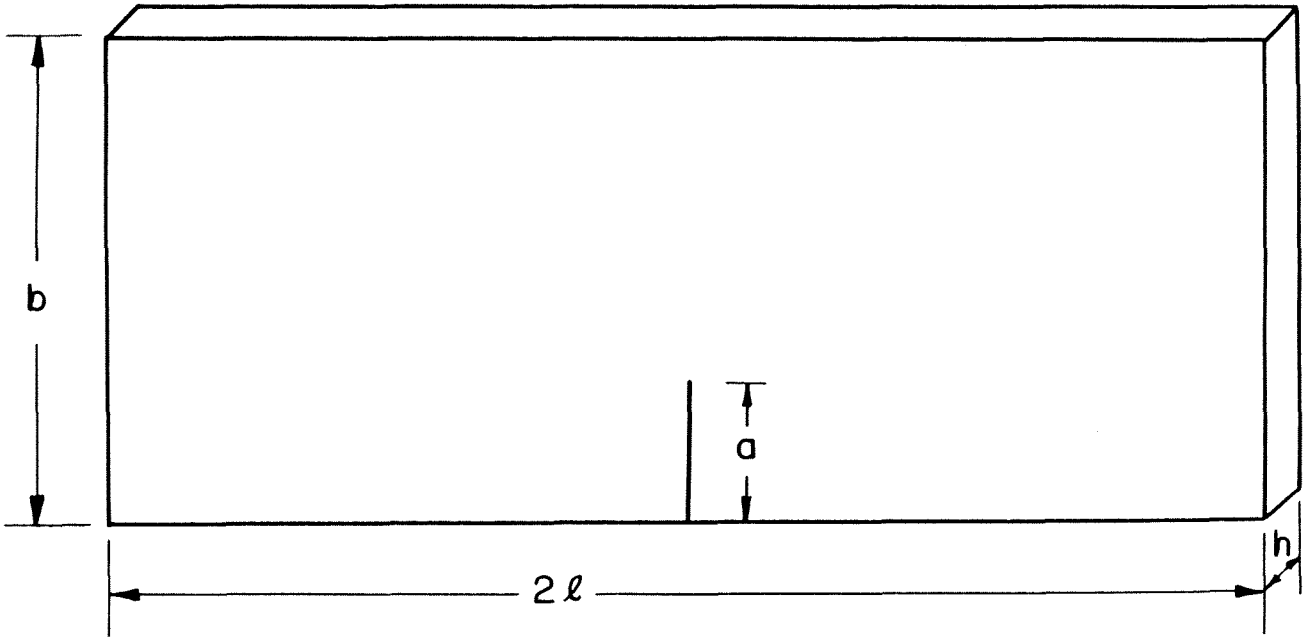

Figure 3.1: Specimen geometry.

done to obtain varying degrees of ductility of the material. After the preliminary machining and heat-treatment processes were completed, one face and the edges of each specimen were ground to ensure flatness and perpendicularity. The ground surface was then lapped in a lapping machine and polished using a diamond polishing compound through a sequence of 9, 6, 3 and 1 micron steps to obtain an optically-flat, highly reflective surface. In those specimens where a fatigue crack was grown, the fatiguing was done only after the polishing sequence was completed in order to avoid contamination of the crack-tip by any residue from the polishing process. The detailed make-up of each specimen is shown in Table T2.

Loading Device:

The specimens were loaded in a three-point bending configuration. The loading device used to dynamically load the specimens was the Dynatup 8100A drop-weight tower. A drop-weight whose mass and impact velocity can be varied to provide a range of impact energies, slides on two rails and can be raised by means of a chain to the desired height to obtain impact velocities of up to 10m/s. A pneumatic valve releases the weight from the chain in free-fall. The hammer mounted at the bottom of the falling drop-weight impacts the specimen which then gets dynamically loaded to the point of crack-initiation, whence the crack propagates dynamically through the specimen. A crack-tip loading rate of the order of $\dot{K}_I^d \approx 10^6 MPa\sqrt{m}/s$ is achieved.

To monitor the time-dependent tractions acting on the specimen boundaries during the impact event, both the hammer (the impact-tup) and one of the supports (the support-tup) are instrumented using strain-gauges and their readings are recorded on two channels of a Nicolet 4094 high-speed digital oscilloscope.

High-speed Photography:

A high-speed camera set-up (Figure 3.2) is used to obtain a sequence of dy-

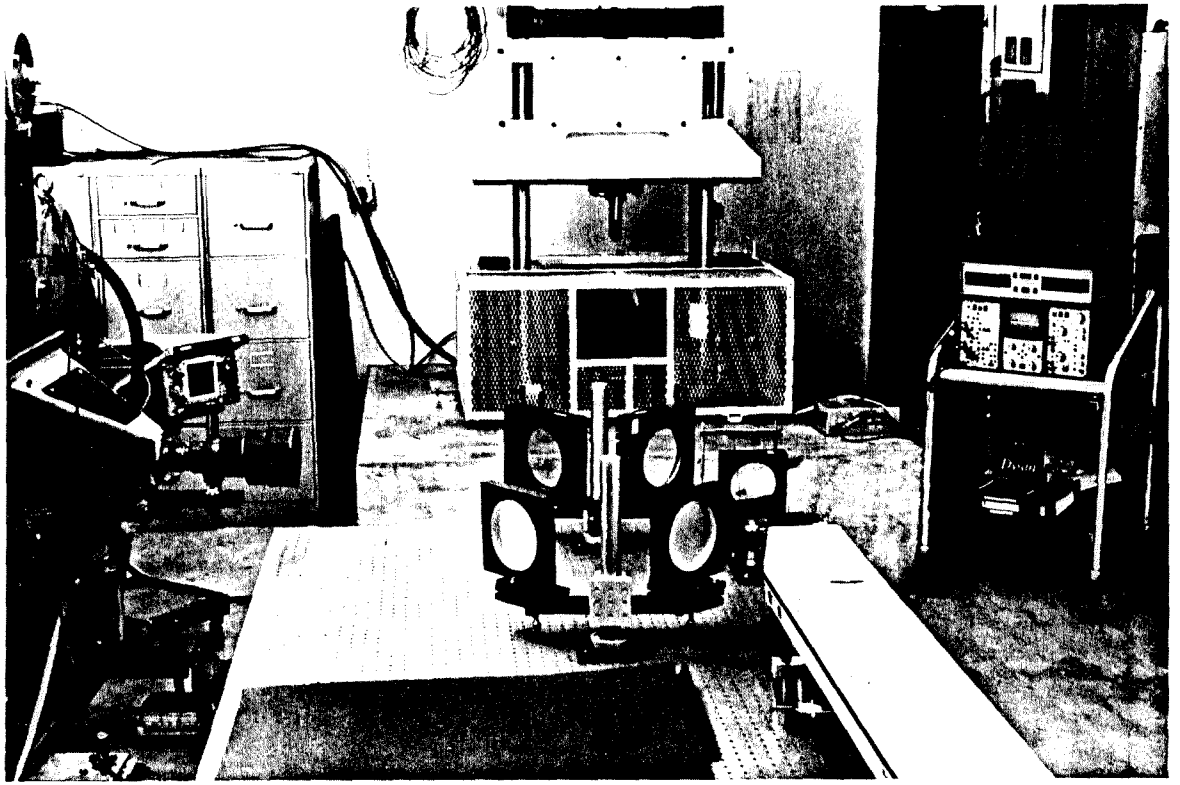

Figure 3.2: Picture of experimental set-up.

namic bifocal caustics. A Spectra Physics (model 166) argon-ion pulse laser is the light source. The laser beam is expanded by means of a beam-expanding lens. A collimating lens is then used to obtain a parallel beam 100mm in diameter. A reference grid is placed in the path of the collimated beam so that it lies in the object plane of the camera along one of the two bifocal paths. This grid provides the picture magnification. The laser beam then reflects off the polished specimen surface and splits into two paths at the first six-inch beam-splitter of the bifocal set-up which consists of an additional six-inch beam-splitter and two six-inch first surface mirrors to provide a direct and a detoured path as described earlier. Both the beams are then collected into a rotating-mirror high-speed camera through a series of lenses. The high-speed camera itself consists of a 45^o mirror mounted on the shaft of a high-speed rotating turbine. The in-coming light beam that enters the camera along the axis of the turbine is thus swept onto the film track by the mirror as it rotates. Details of the construction and operation of this high-speed camera can be found in Ellis (1954). To obtain discrete pictures, the pulsing circuit of the laser is nominally set to give 25ns exposure every 5μs for a total of 1ms from the time of an input trigger. Since the camera mirror is set to rotate at 800rps, the above settings ensure that picture blur is negligible and also avoid overlap of frames while providing an adequate time-window for filming the entire dynamic loading and crack-propagation event.

Sequence of Events:

Since the actual duration of the entire test is less than 1ms, the correct sequencing of various events is of critical importance. The input trigger that initiates the pulsing of the laser is provided by a mechanical interrupt type photo-diode switch mounted on the fixed tower of the drop-weight machine.The switch is so positioned that the falling weight itself would activate it at the moment of impact of the

hammer with the specimen. The same switch also triggers the Nicolet oscilloscope for recording the impact-tup and support-tup load histories. In addition, another photo-diode switch, positioned a little higher on the tower, provides a trigger some 20ms prior to impact and this signal is used to open a capping-shutter mounted on the camera. This shutter, which is used to minimize fogging of film due to room and other stray light entering the camera, stays open for another 33ms.

3.2 Results of the Bifocal Caustics Experiment

A number of experiments under different conditions were done. Figure 3.3a shows a representative sequence of bifocal caustics for the case of the dynamically loaded stationary crack at various times from the time of impact. The superposition of the two images from the bifocal set-up was here so arranged as to have the pairs of caustics (the two bright lines around the crack-tip) slightly shifted apart. Since a collimated laser beam was used as the light source, the smaller caustic corresponds to the smaller object plane distance (z_{02}) and the larger one to the larger z_{01}. Also seen are the reference lines used to obtain the picture magnification. Though these lines can be seen in the images corresponding to both bifocal paths, they are in focus only for one of these paths. A selection of high-speed photographs for the case of the dynamically propagating crack is shown in Figure 3.3b. Here, the pairs of bifocal caustics are one inside the other, with the inner caustic corresponding to the smaller object plane distance (z_{02}).

Measurement Error:

The pairs of caustics obtained at each instant of time are analyzed as described in chapter II to get the apparent stress-intensity factor histories. To first get an idea of the repeatability and measurement errors involved in the method of caustics, a few experiments were conducted without using the bifocal technique to obtain caustics from a single z_o. Care was taken in these tests to have the specimen geometry, the

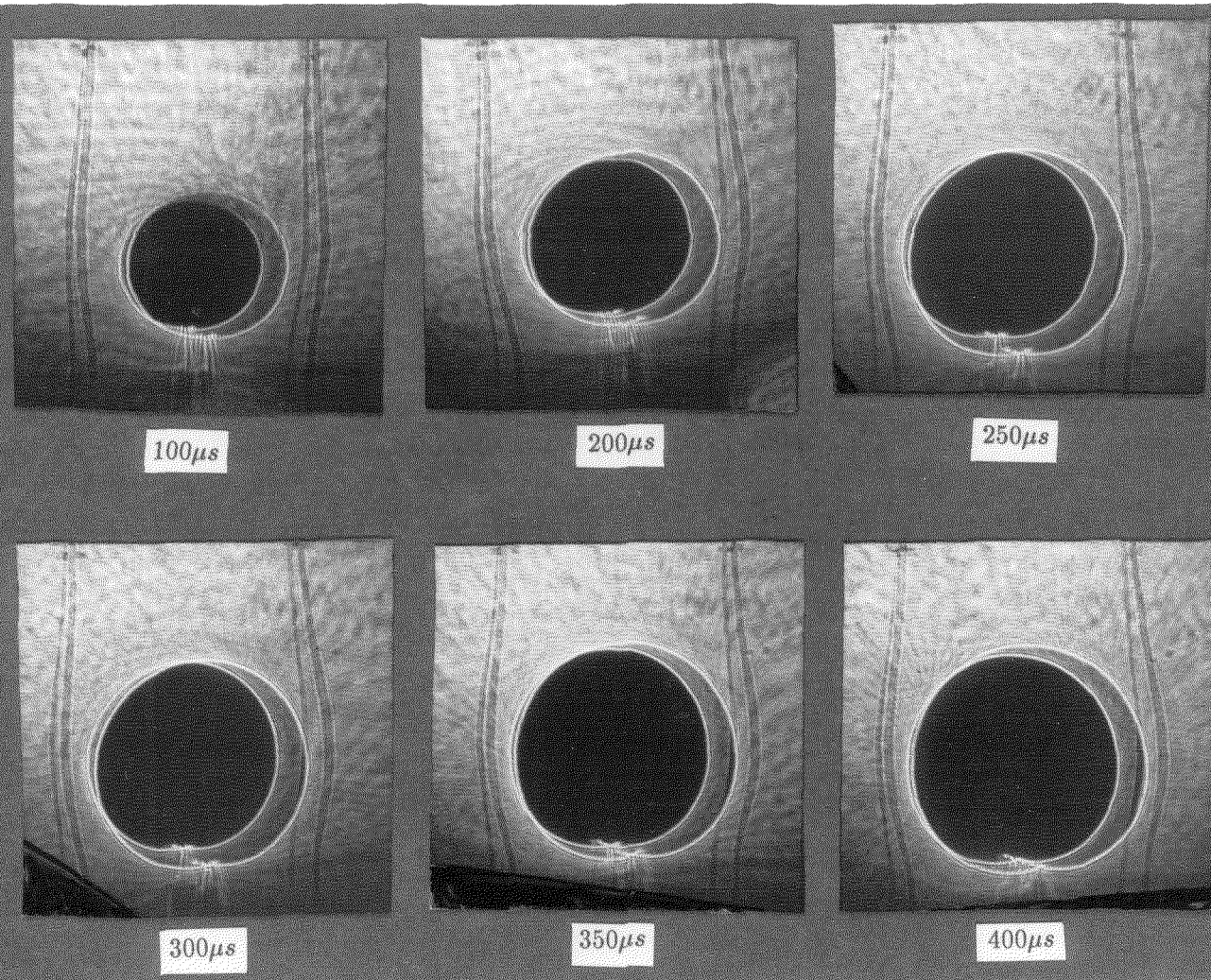

Figure 3.3a: Representative sequence of bifocal caustics for a dynamically loaded stationary crack.

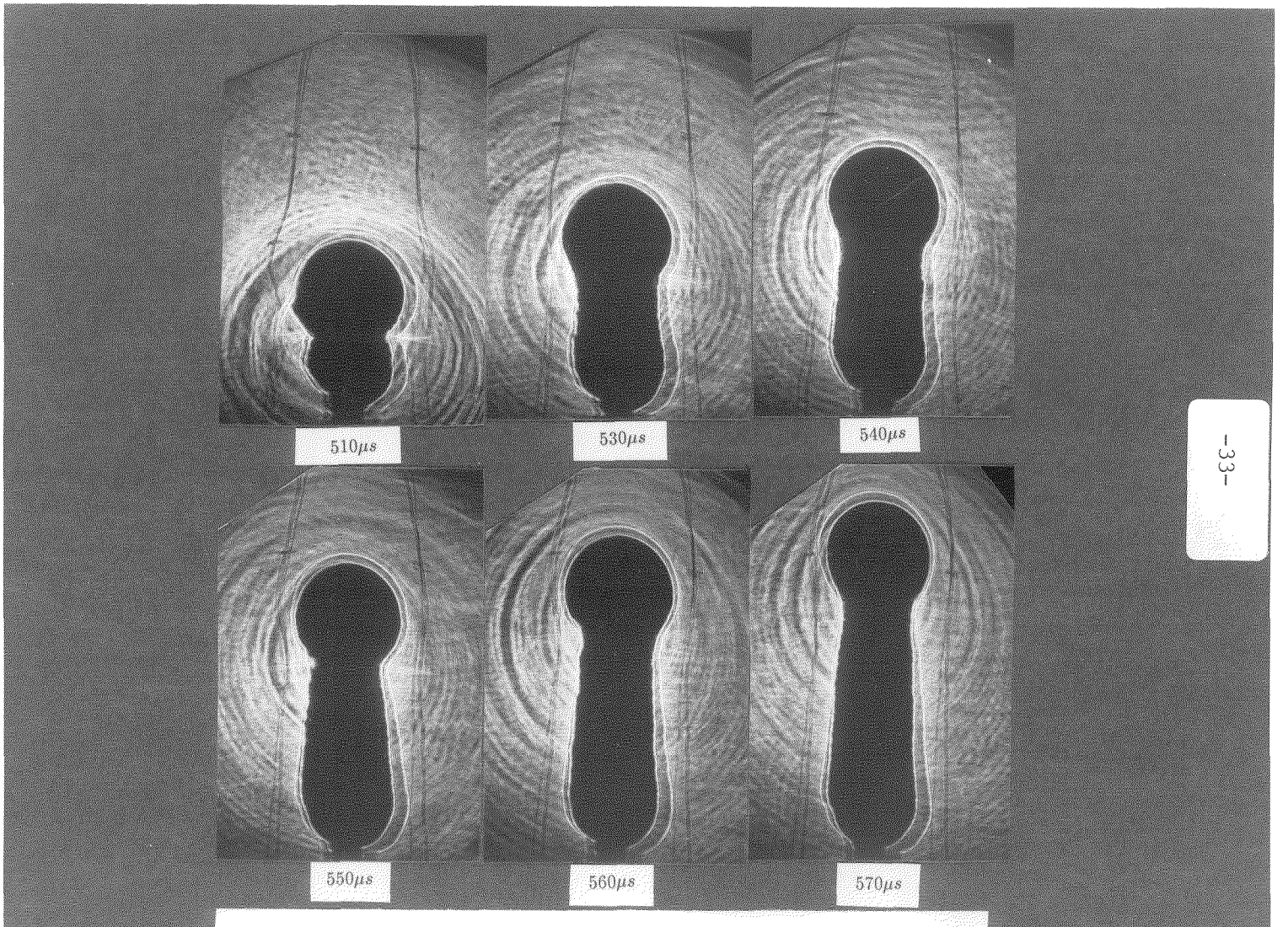

Figure 3.3b: Selection of bifocal caustics for the dynamically propagating crack.

loading, and the object plane distance (z_0) identical. The results from the loading phase of three different tests are shown in Figure 3.4a. Here, as in the other figures, the time of impact is taken as zero time. A z_0 of 2.5m was used for all these tests and the dynamic stress-intensity factor was computed from the caustic diameters through equation (2.7). Note that the experimental scatter in the apparent stress-intensity factor from three separate tests is seen to be about $\pm 5\%$. This is of the same order as the measurement error expected in a single test as obtained through an error analysis of equation (2.7). It should be emphasized that this is the error estimate *assuming* that equation (2.7) is valid. Thus it should be recognized that differences in the stress-intensity values from *bifocal caustics* that are less than the above value could arguably be attributed to measurement errors while larger differences would be an indication of a more fundamental *malaise* – namely the possible violation of the assumptions underlying equation (2.12).

The situation for the dynamically propagating crack, however, is different. Figure 3.4b shows the measured dynamic stress-intensity factor history from two ostensibly identical specimens. As was noted above, the results for the loading phase of these tests were virtually identical to within experimental error. The crack initiation times, however, do not coincide. Thus the rather large variations between the results of the two tests during the crack propagation phase arise not so much from experimental uncertainty as from the fact that the initiation times and, therefore, subsequent crack propagation histories are different. Unless the crack-tip bluntness is controlled to a degree of precision currently technically not feasible for metals, these differences are expected to be unavoidable. (This, of course, is the primary reason for resorting to the bifocal technique which circumvents the necessity of comparing results from different tests.)

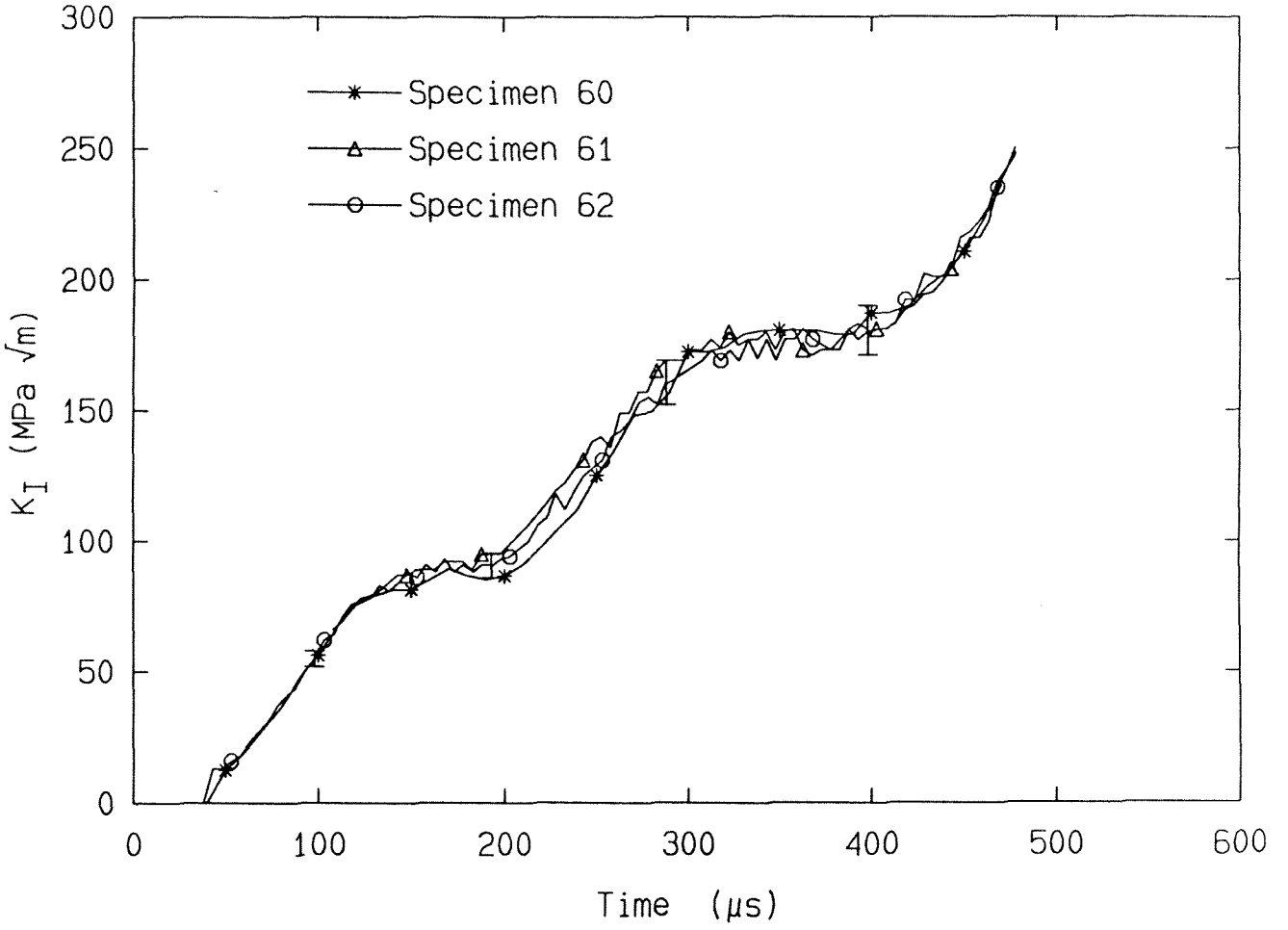

Figure 3.4a: Results for the loading phase from three identical tests.

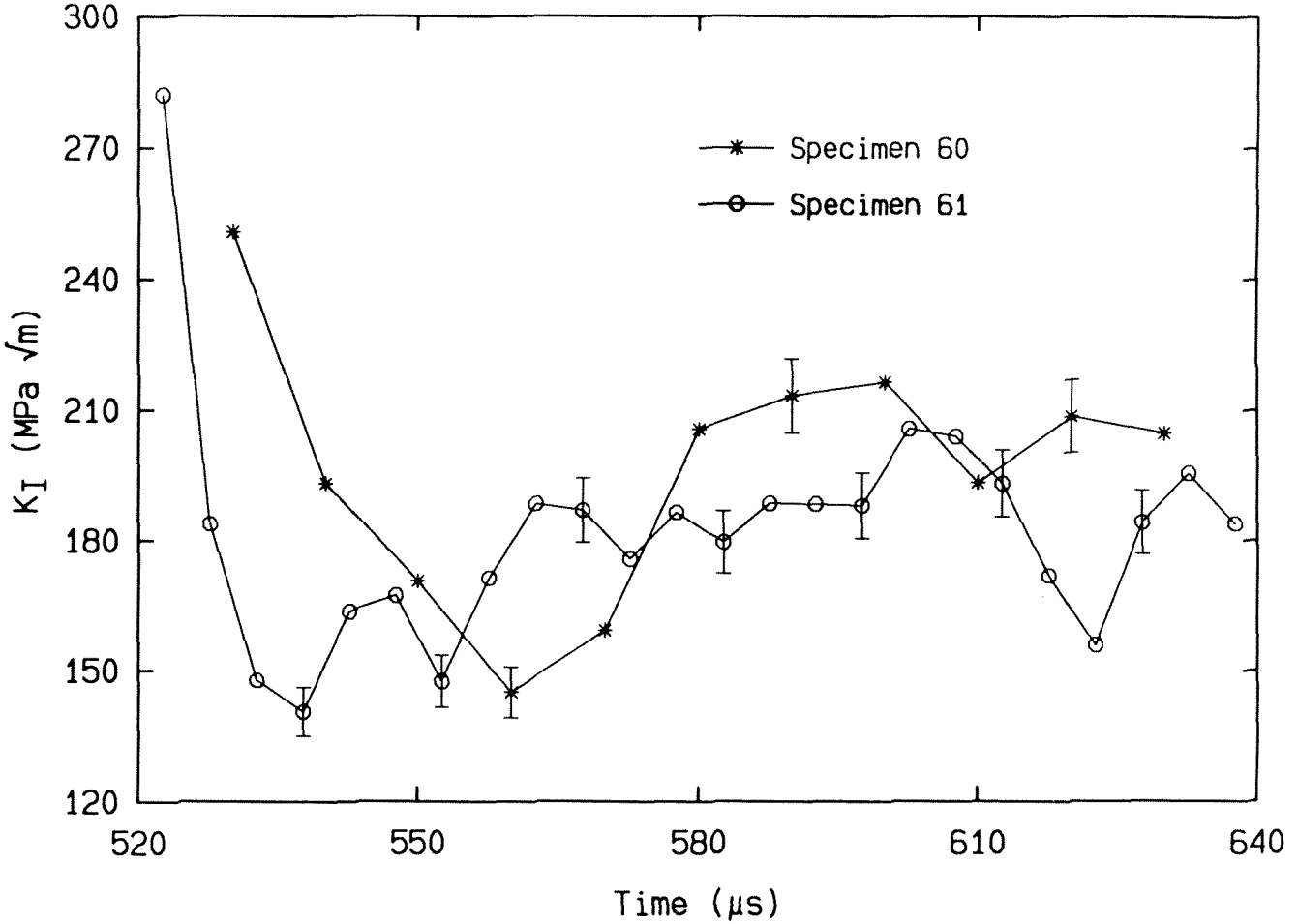

Figure 3.4b: Results for the propagating phase from two identical tests.

Dynamically Loaded Stationary Crack:

Turning now to the bifocal experiments, Figure 3.5a shows the results for the uninitiated dynamically loaded crack for specimen $\alpha - 3$. The two apparent stress-intensity factors obtained from the diameters of the bifocal caustics pairs are shown as functions of time from impact. The object plane distances used in this experiment were $z_{01} = 4.82$m and $z_{02} = 3.08$m. The region of possible measurement uncertainty is indicated by vertical error bars. Figure 3.5b is an alternate representation of the experimental results for specimen $\alpha - 3$. Here, the ratio K^d_{I1}/K^d_{I2} is plotted as a function of time from impact. As discussed previously, the experimental uncertainty in this ratio is less than in the individual values. For reference, the initial-curve radii (as computed through (2.11)) corresponding to the measured stress-intensity factor values for the two z_0s are also shown. It is seen that the apparent measured stress-intensity factor is not quite independent of the region from which the measurement is made. Indeed, differences of up to 60% are observed between the measured stress-intensity factors obtained from initial-curves whose radii vary by less than 20% of the plate thickness. Further, the larger measured stress-intensity factor corresponds to the larger object plane distance and hence larger initial-curve radius. Unlike the results of Rosakis and Ravi-Chandar (1986) for the static case, these differences persist even for $r_0/h \geq 0.5$.

Essentially similar results were found in the other experiments. As can be seen in Figures 3.6-3.9, results from experiments on different specimens with various choices of z_0s all indicate that the measured dynamic stress-intensity factor varies quite substantially with the initial-curve radius for the case of the dynamically-loaded stationary crack. This has implications with regard to the extraction of dynamic initiation fracture toughness values.

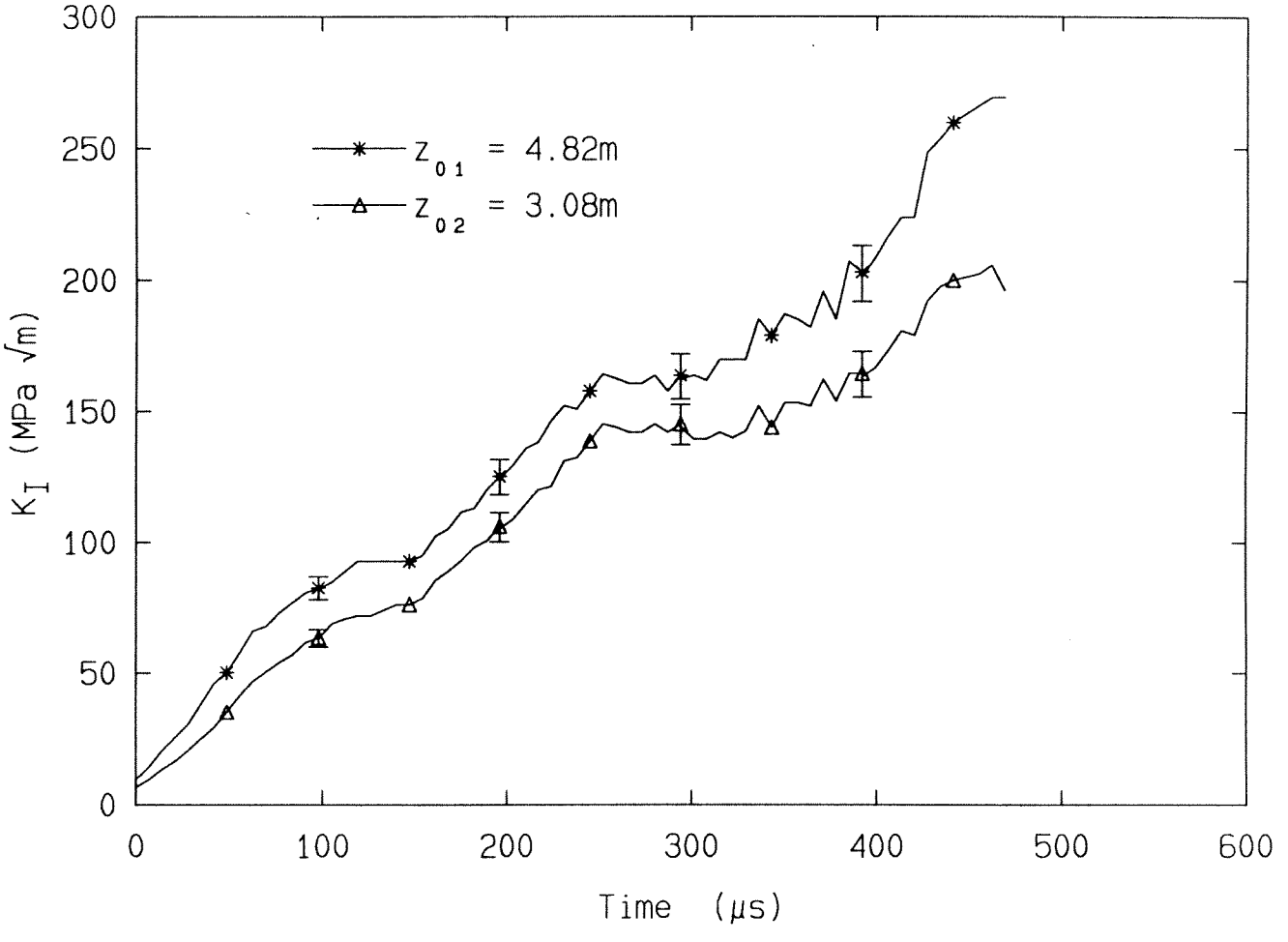

Figure 3.5a: Experimental results for the loading phase; specimen ($\alpha - 3$).

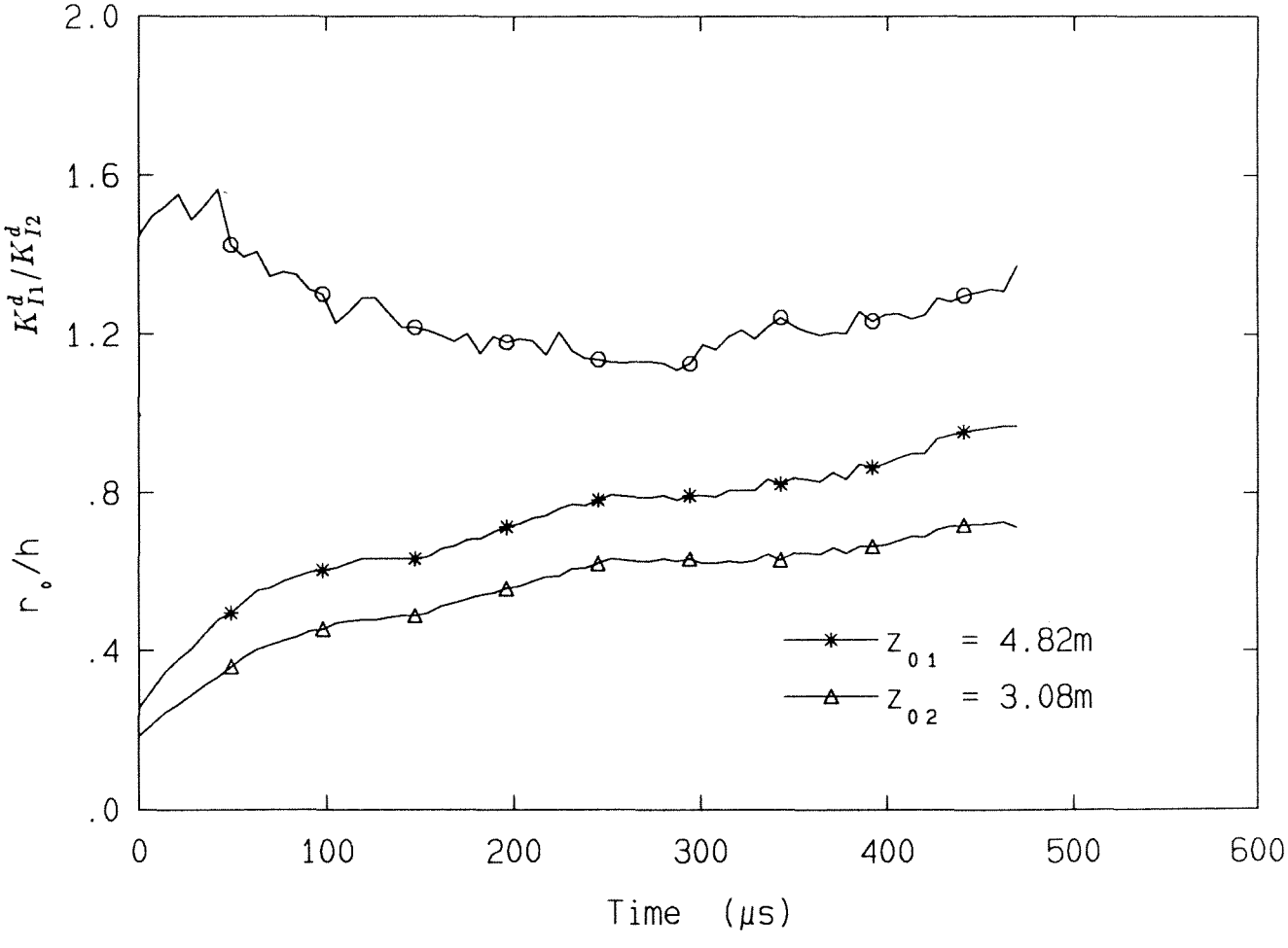

Figure 3.5b: Plot of K_{I1}^d/K_{I2}^d versus Time for specimen $(\alpha - 3)$.

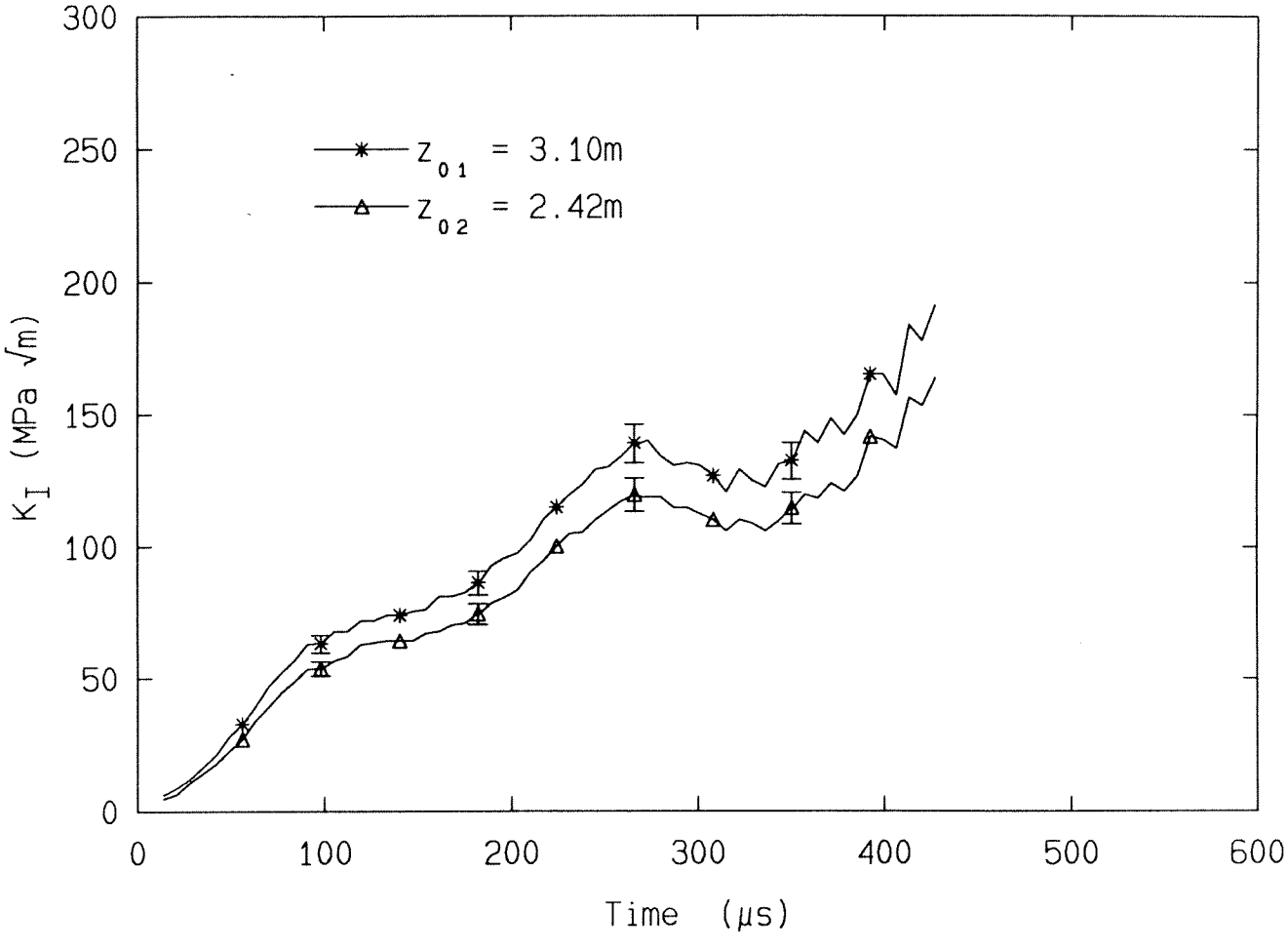

Figure 3.6: Experimental results for the loading phase; specimen $(\alpha - 4)$.

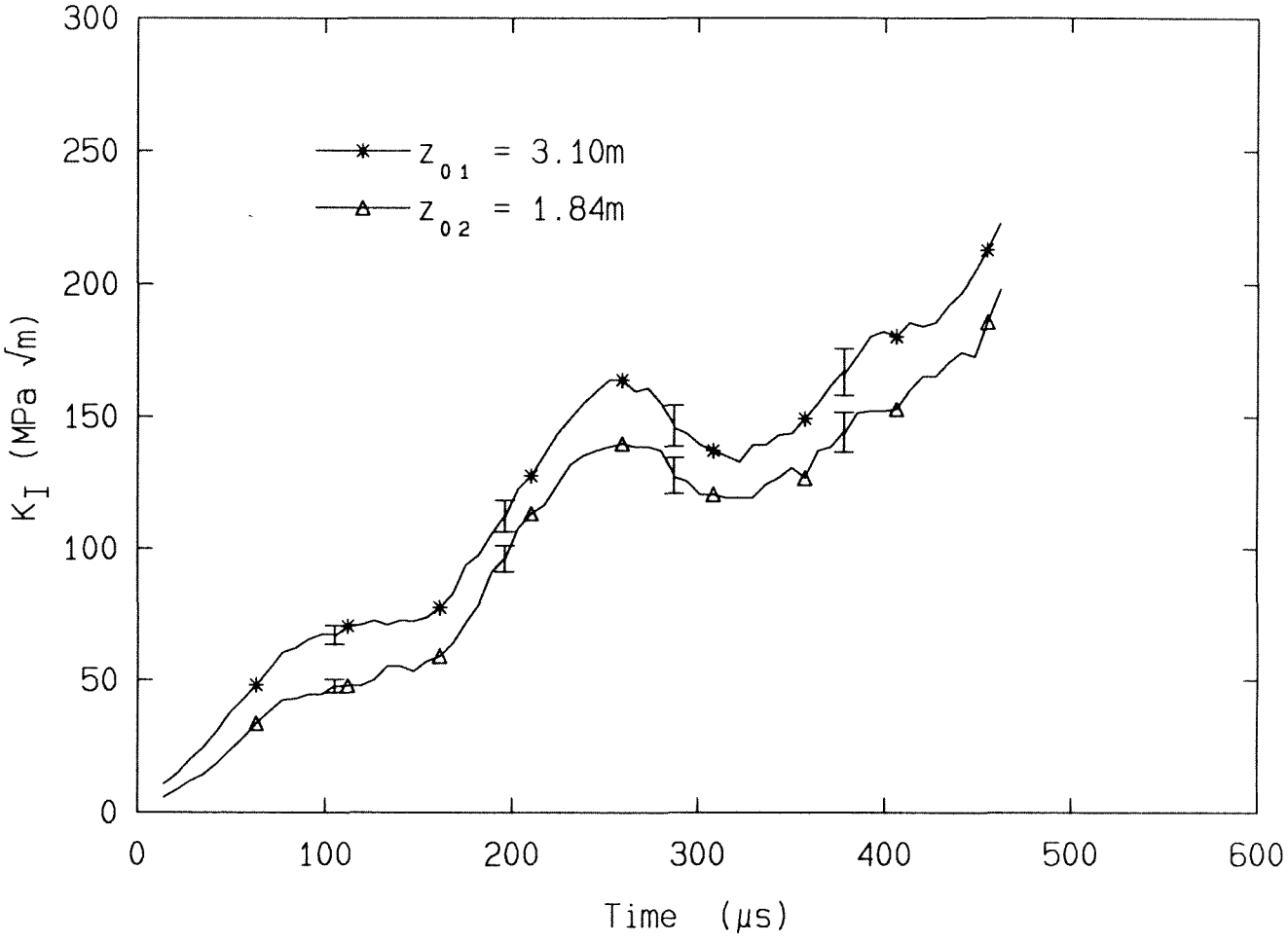

Figure 3.7: Experimental results for the loading phase; specimen ($\alpha - 5.$)

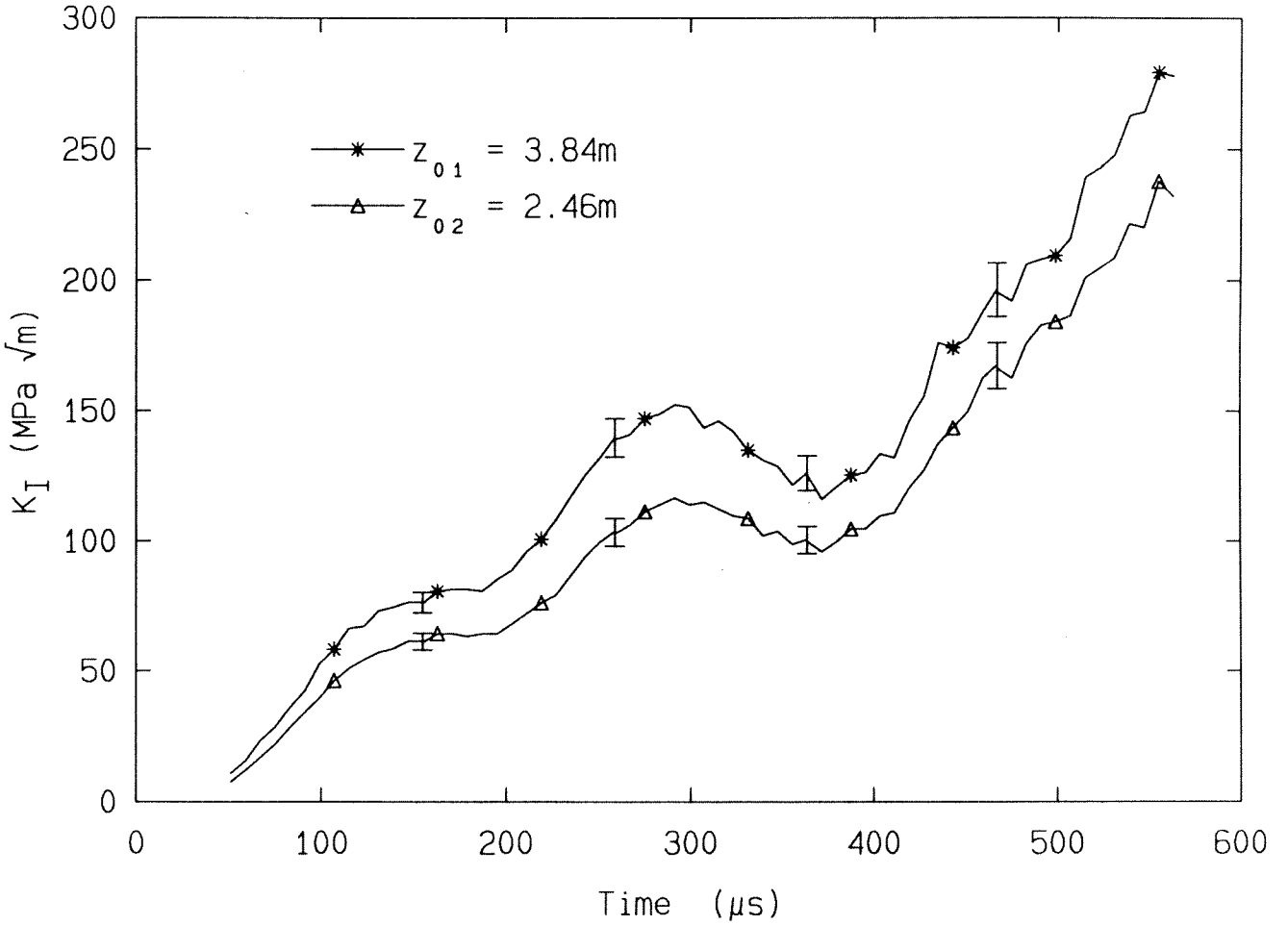

Figure 3.8: Experimental results for the loading phase; specimen ($v3s$).

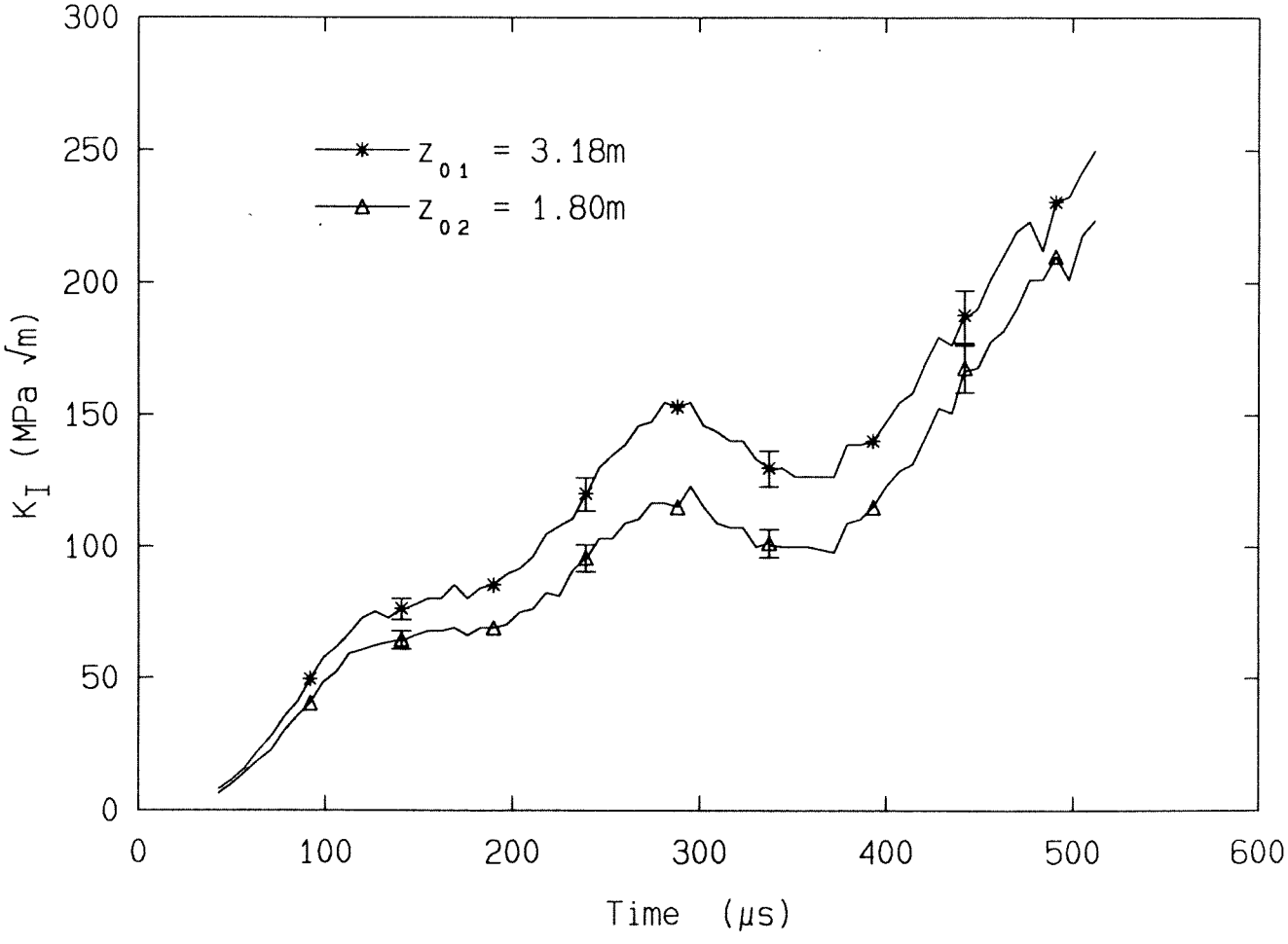

Figures 3.9: Experimental results for the loading phase; specimen ($3q$).

Dynamically Propagating Crack:

The results for the crack propagation phase are shown in Figures 3.10-3.16. Again, these are time history plots of the two measured dynamic stress-intensity factors from the bifocal caustics pairs. The larger initial-curve is again seen to give a larger apparent stress-intensity factor. Differences of up to 30% in the measured values are seen in these experiments. Note that in virtually all these tests, the initial-curve radii are almost always greater than one-half the specimen thickness during the crack-propagation phase. These differences, therefore, do not disappear for $r_o/h \geq 0.5$, unlike the static case. Results for the propagating case with an even wider range of z_0s could not be obtained because of the limitations of the experimental set-up.

With the results of both the dynamically-loaded stationary crack and the dynamically propagating crack tests at hand, the following tentative statement about the dynamically-loaded three-point bend specimen can be made: *the apparent dynamic stress-intensity factor as measured by the method of caustics increases with increasing initial-curve radius.* Of course, as was indicated in chapter II, this means that the assumption that equation (2.12) is dominant over this range of radius cannot be correct. The reasons and possible implications of this result will be taken up in later chapters. The next chapter, which details the numerical simulation of the dynamic experiments, is primarily a qualitative hunt to provide a possible reason for the apparent lack of a domain of dominance for equation (2.12).

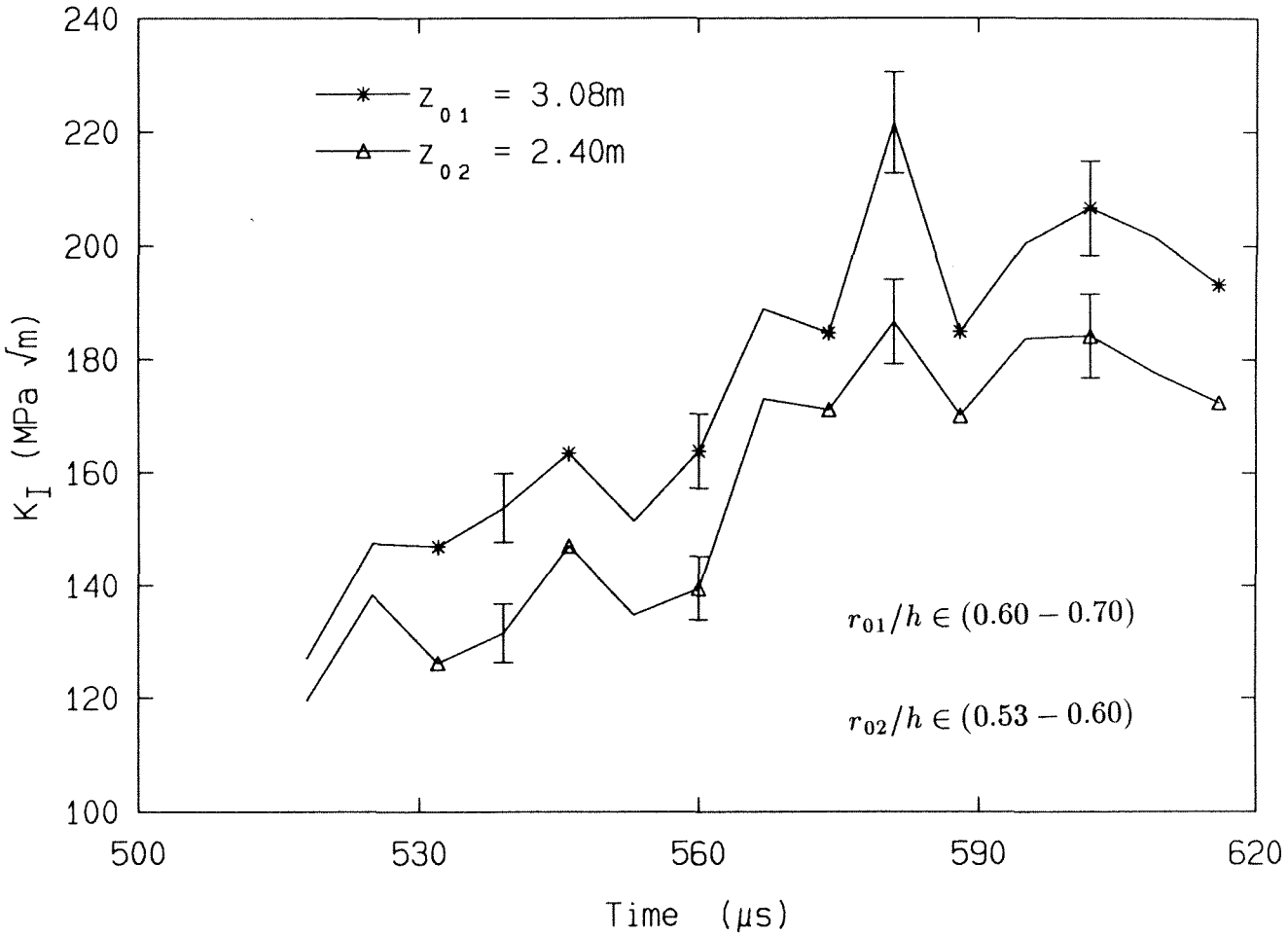

Figure 3.10: Experimental results for the crack-propagation phase; specimen ($\alpha - 4$).

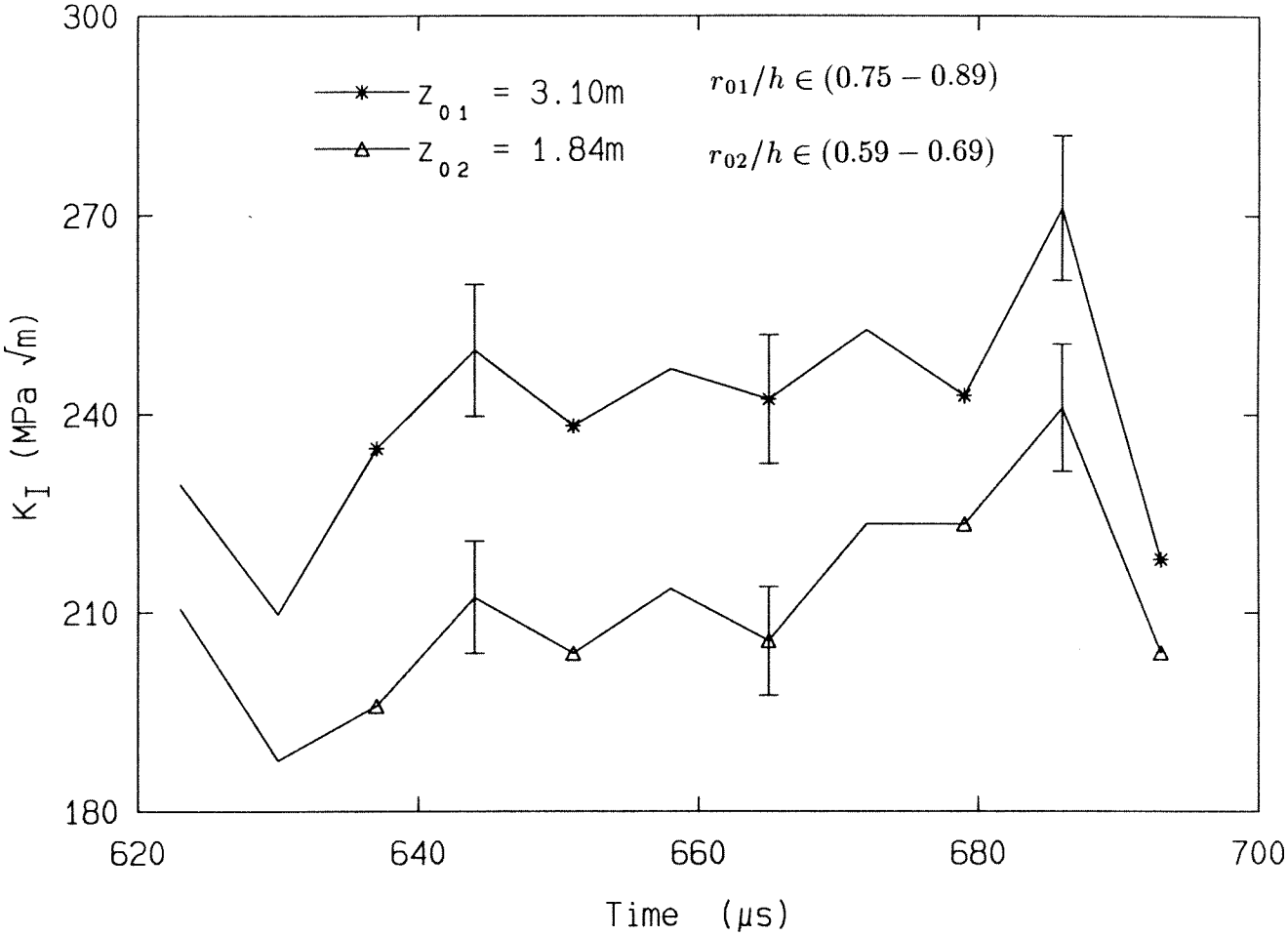

Figure 3.11: Experimental results for the crack-propagation phase; specimen ($\alpha - 5$).

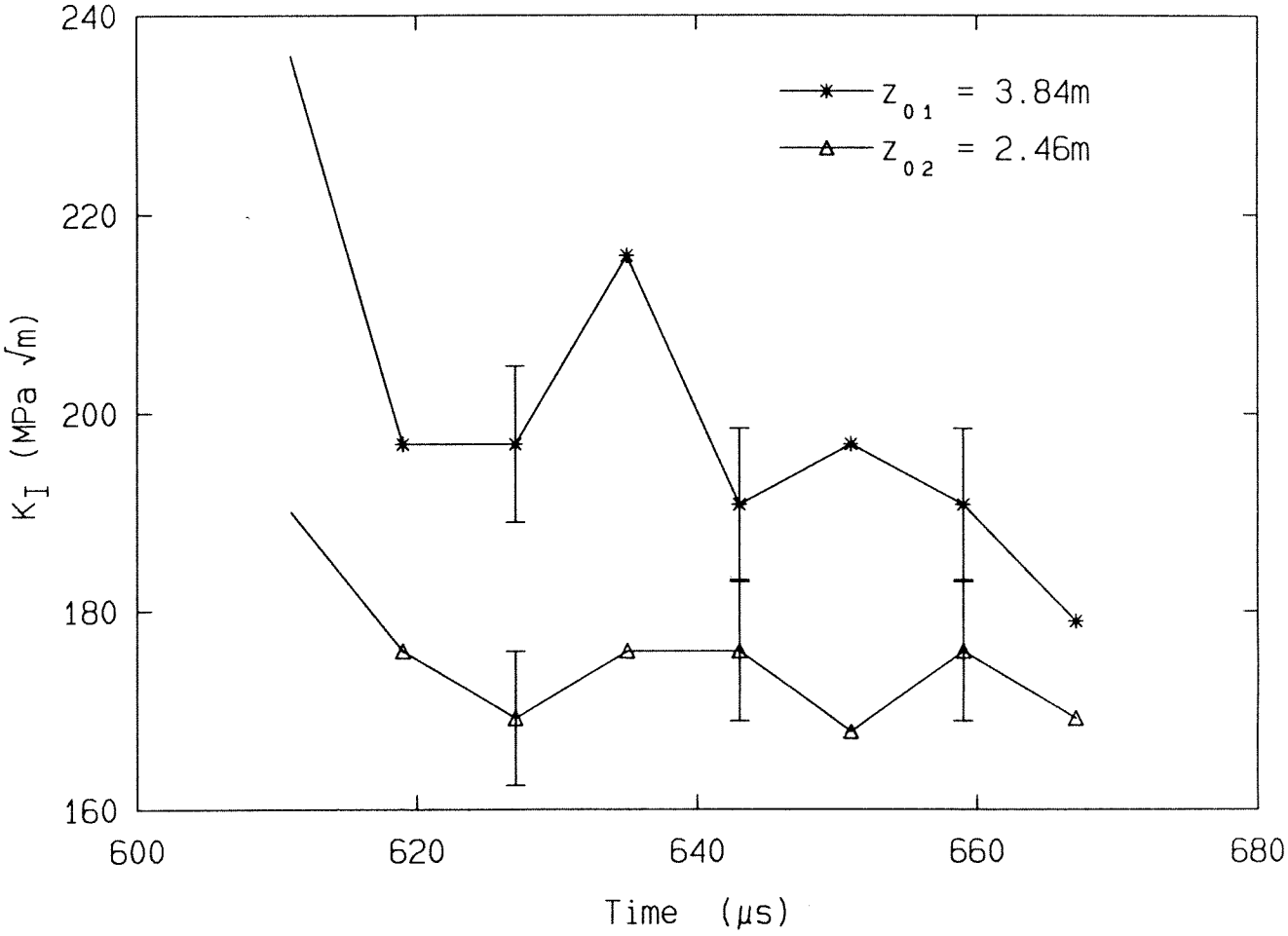

Figure 3.12: Experimental results for the crack-propagation phase; specimen ($v3s$).

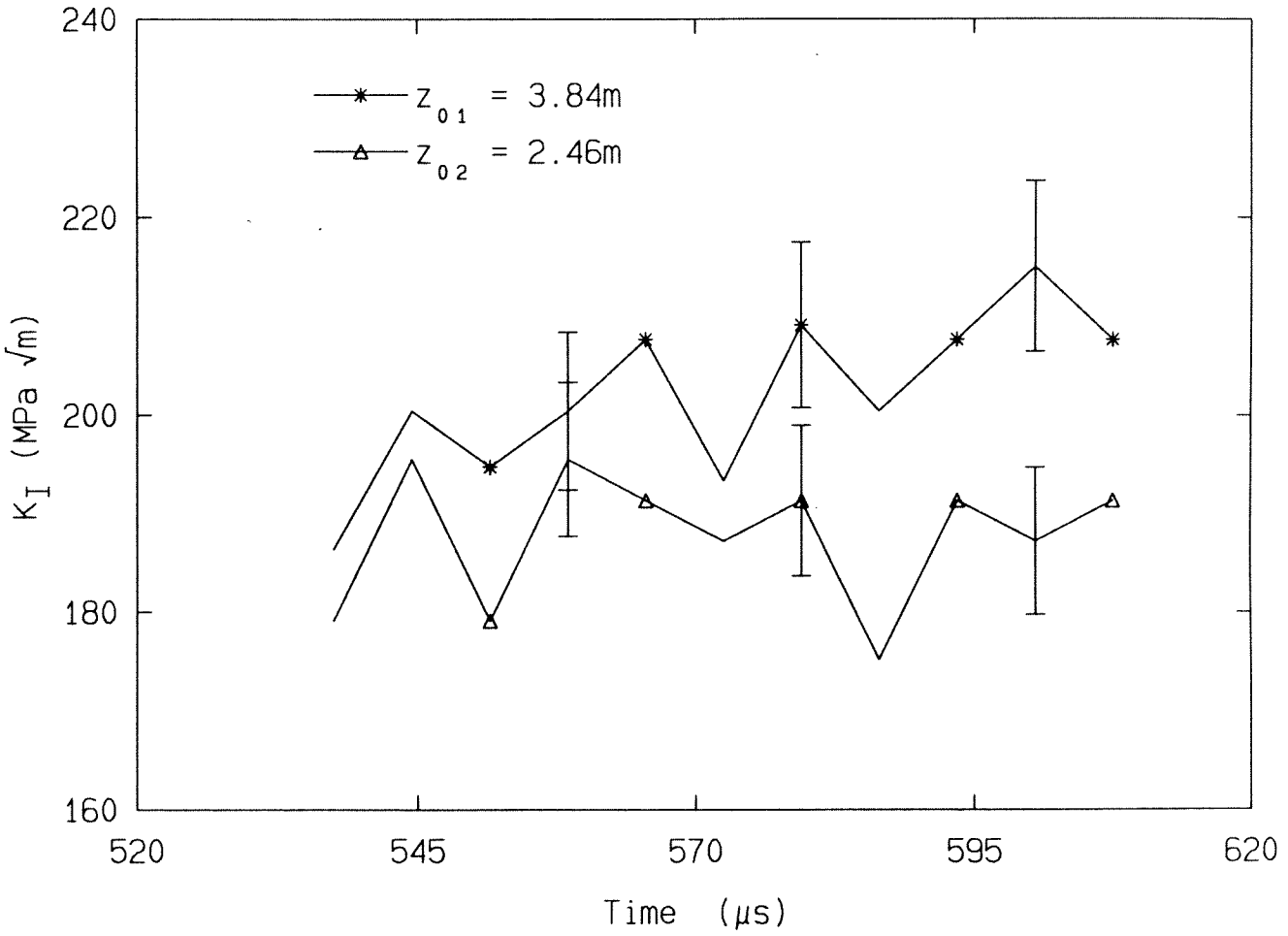

Figure 3.13: Experimental results for the crack-propagation phase; specimen (31).

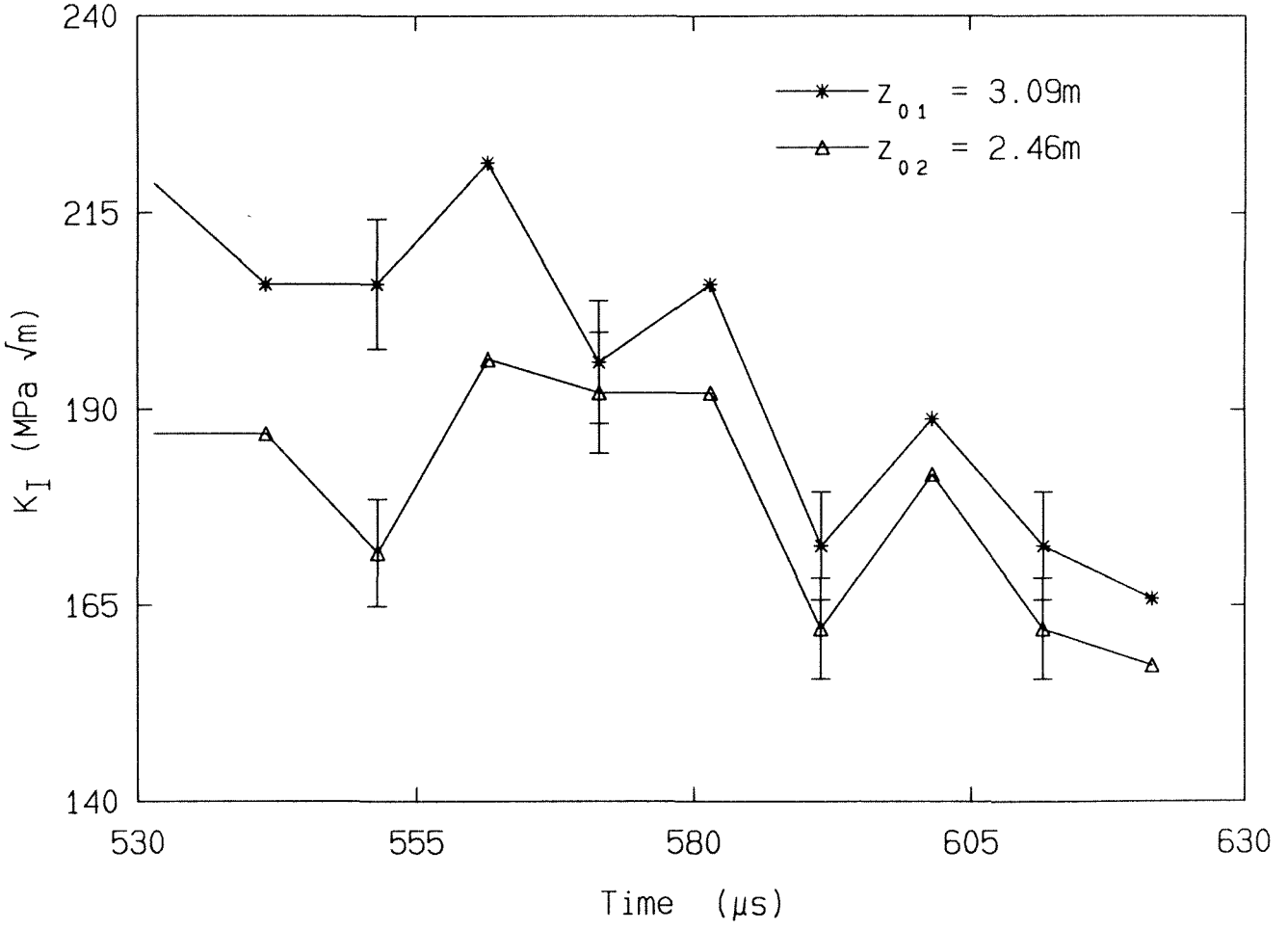

Figure 3.14: Experimental results for the crack-propagation phase; specimen ($v63$).

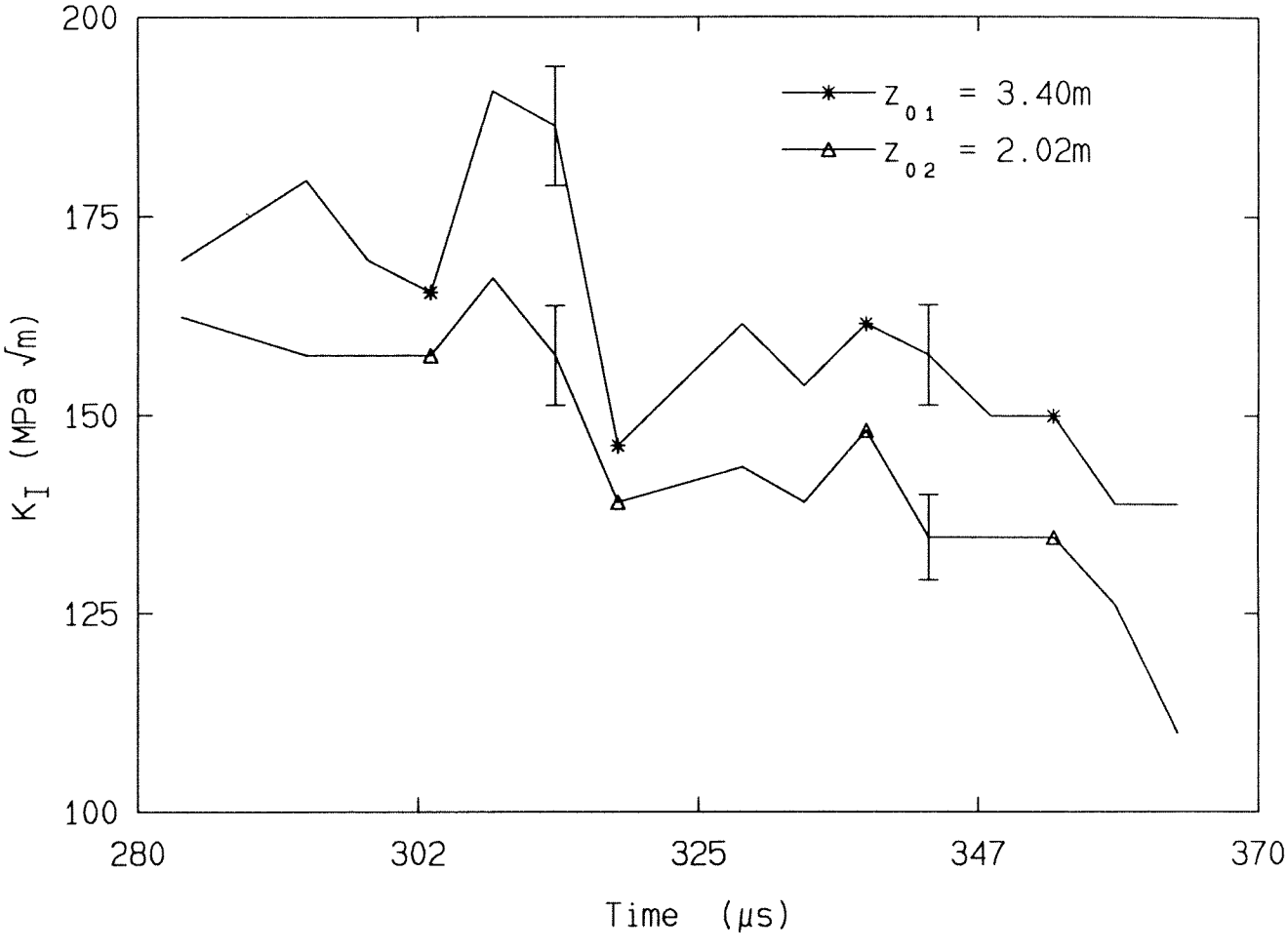

Figure 3.15: Experimental results for the crack-propagation phase; specimen ($v36f$).

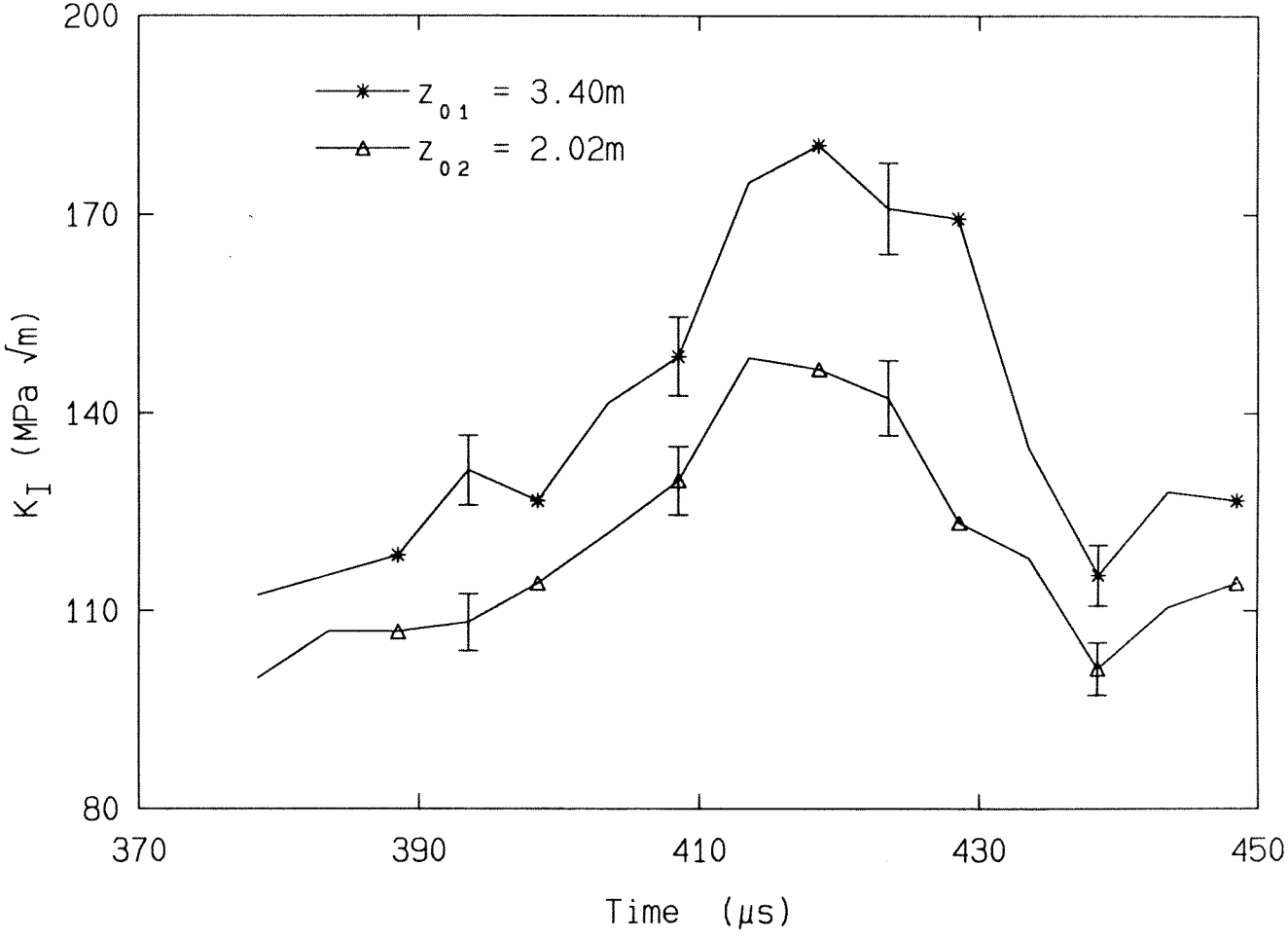

Figure 3.16: Experimental results for the crack-propagation phase; specimen ($65f$).

CHAPTER IV

NUMERICAL SIMULATION

In the previous chapter, it was observed that the apparent dynamic stress-intensity factor as measured by the method of caustics increases with increasing distance of measurement from the crack-tip (r_0) in a dynamically-loaded three-point bend specimen. This was the outcome of experiments using the bifocal caustics technique that allowed for the recording of dynamic caustic patterns corresponding to two object planes (and hence two initial-curves) at the same instant of time. Such variation was observed for both the uninitiated dynamically loaded crack as well as for the dynamically propagating crack. This result is at variance with the common tacit assumption that there exists a sizeable annulus around the crack-tip in which the dynamic stress-intensity factor field could be said to adequately characterize the continuum field. The implications of this result need to be studied further.

In this chapter, the finite-element method is used to investigate the issue of K_I^d-dominance in the dynamically loaded three-point bend specimen. To this end, a series of two- and three-dimensional finite-element simulations* of the drop-weight experiments were done using the experimentally recorded impact and support-point load histories as boundary tractions for the simulations (Figure 4.1). The simulations were undertaken in an effort to capture the essential features of the experimental results. Only the case of the dynamically loaded stationary crack was considered for the simulations. It was felt that attempting to simulate the propagating crack would be premature at this point, especially since it entails a high degree of uncertainty in terms of the nodal-release procedure that would have to be used. The primary interest here is in trying to identify the role of specimen geometry, dynamic

* All the numerical computations were done using a much-modified version of the finite-element analysis program FEAP whose ancestry traces back to Taylor (1977).

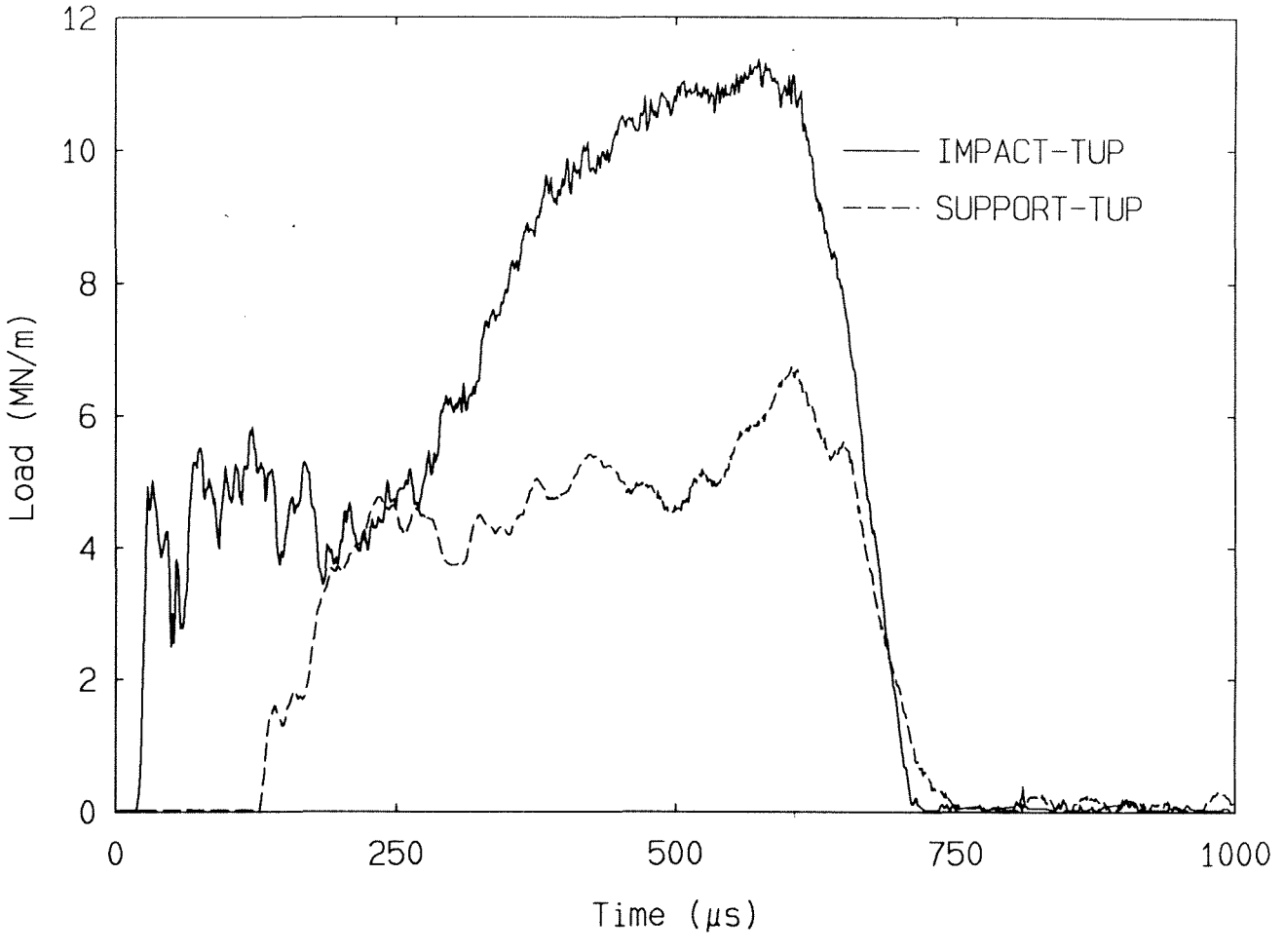

Figure 4.1: Experimental tup load records for specimen ($\alpha - 4$); these are used as input for dynamic finite-element simulation.

loading, and the three-dimensional structure of the crack-tip region (especially under transient conditions) insofar as these have a bearing on the K_I^d-dominance assumption on which the experimental method rests. Three issues are addressed. First, where relevant, direct comparisons of the numerical results with the corresponding asymptotic field are made to ascertain the adequacy of the K_I^d-field as a characterizer of the near-tip continuum fields. All field quantities presented are normalized in such a manner as to highlight salient points. Thus, full-field two-dimensional results are compared with the asymptotic field and three-dimensional results are normalized by the appropriate two-dimensional or asymptotic values. Secondly, virtual energy-release rate integrals are evaluated numerically to extract stress-intensity factor values in order to compare with the experimentally measured values. Appendix A1 describes in detail the numerical implementation of these integrals; also as a check of the accuracy of the numerical procedure used, a problem for which an analytical solution exists is numerically simulated.

Finally, the implications of the finite-element results are studied with regard to the experimental method of caustics in reflection. In an attempt to qualitatively recover the results of the bifocal experiments, an exact analog of the procedure used in the experiments is attempted in the following manner. The out-of-plane surface displacement fields obtained from the analyses are used to numerically generate (synthetic) caustic patterns for a range of initial-curves. That is, the numerically obtained surface out-of-plane displacement fields are subjected to the optical mapping relation (2.1) for a set of values for parameter z_0 (the object plane distance). These caustics are then interpreted exactly as in the experiments; i.e., the caustic diameters are related to the stress-intensity factor under the assumption that the underlying out-of-plane displacement field is K_I^d-dominant. Thus, the transverse diameters of the synthetic caustics are used in equation (2.4) to extract the appar-

ent stress-intensity factor values. Again, as in the experiments, if the displacement field is not actually K_I^d-dominant, this fact would be reflected as an apparent (erroneous) dependence of the stress-intensity factor on the radial distance from the crack-front.

As a final note, it must be pointed out that in the ensuing discussion of two-dimensional results, all in-plane lengths are normalized by the (actual) specimen thickness, h. For a two-dimensional problem, however, the plate thickness is not a relevant length scale. This is done here purely for ease of reference with subsequent three-dimensional results. Where necessary, alternate normalization with a more appropriate in-plane geometry parameter is given.

4.1 Two-Dimensional Elastodynamic Simulations

The simulations of the dynamic experiments were first attempted under the simplifying assumption that the specimens could be considered to be under essentially plane-stress conditions. Before delving into the simulations of the experiments one issue needs to be addressed. Since no special singularity elements were used in the finite-element analyses, it is essential that the discretization used must be such as to capture the expected singular crack-tip fields adequately. To this effect, preliminary two-dimensional elastostatic analyses of the three-point bend specimen were performed. Based on the results of these, the mesh discretization shown in Figure 4.2 consisting of 396 isoparametric linear quadrilateral elements (425 nodes) was found to be adequate. This mesh has a focussed region around the crack-tip of about one (actual) specimen thickness which is divided into 18 sectors and 10 concentric rings of elements as shown in Figure 4.2. For the two-dimensional elastostatic case, the solution given by Williams (1957) indicates that the crack-tip stress-fields must be square-root singular. As a check of whether the crack-tip singularity is captured by this discretization, a logarithmic plot of stress component

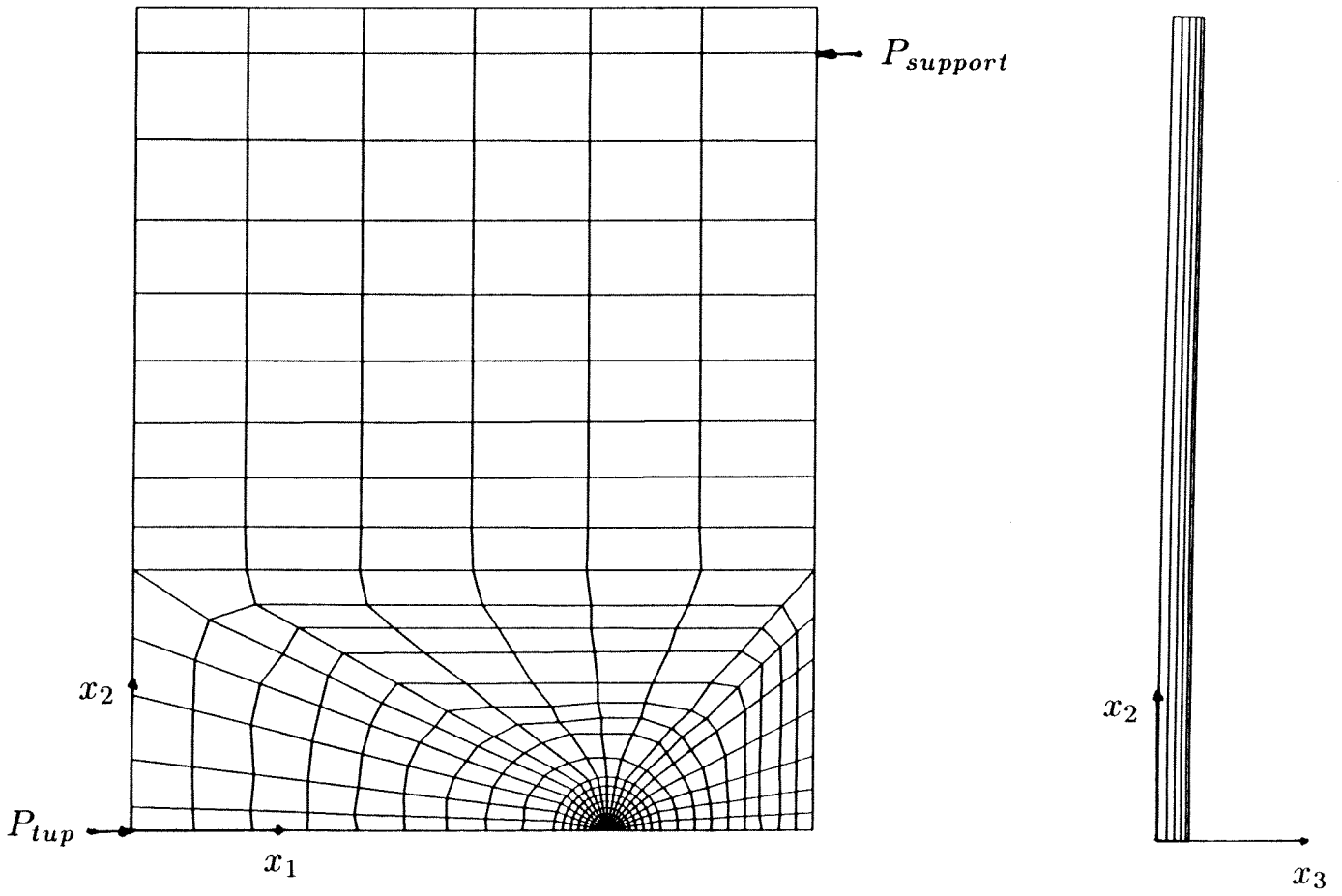

Figure 4.2: Finite-element discretization; on the right is shown the mesh gradation through half the specimen thickness used in the three-dimensional simulations.

σ_{11} along the $\theta = 45^o$ line is shown in Figure 4.3 as a function of the logarithm of radial distance to the crack-tip. Also shown are the corresponding asymptotic values with the magnitude of the stress-intensity factor obtained from the J-integral (computed using the domain integral formulation discussed in Appendix A1). The mesh discretization is seen to be adequate to model the square-root singular field in the elastostatic case and is thus expected to be suitable for the dynamic problem as well.

For the two-dimensional elastodynamic simulations, the loads as obtained from the experimental tup records were applied as the boundary conditions. That is, the impact-tup load history was applied to the node corresponding to the impact-tup and the support-tup load history was applied to the associated node as shown in Figure 4.2. From symmetry conditions, the uncracked ligament was constrained to move only along the x_1-direction. The rest of the boundary was left free of traction. An implicit Newmark predictor-corrector time integration scheme (see Appendix A2) was used for its virtue of unconditional stability which would allow for relatively large time steps and the attendant loss of high frequency information was deemed acceptable since it is not the intent here to monitor discrete stress waves in the body.

The (virtual) energy-release rate for a dynamically-loaded stationary crack is given by (see Appendix A1)

$$J = \lim_{\Gamma \to 0} \int_{\Gamma} \left((U + T) n_1 - \sigma_{ij} n_j \frac{\partial u_i}{\partial x_1} \right) d\Gamma \tag{4.1}$$

where U is the strain-energy density, T is the kinetic energy density, σ_{ij} is the stress-tensor, $\underline{u}$ is the displacement vector, and $\underline{n}$ is the unit outward normal to the contour of integration Γ. Here, $\Gamma \to 0$ symbolically indicates that the integration contour must be shrunk on to the crack-tip. In the simulations, the time history of this integral was computed using the equivalent domain integral form as explained

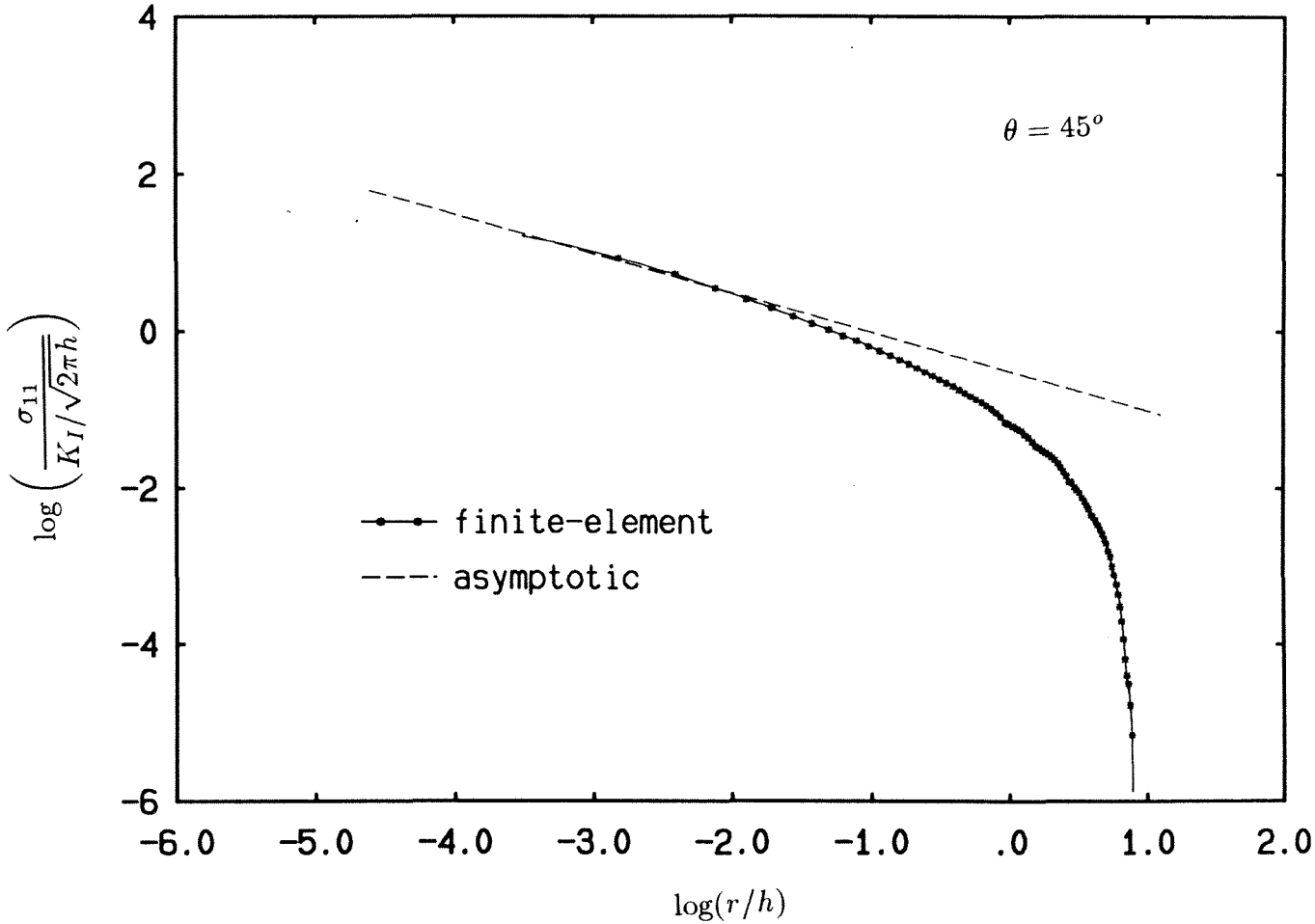

Figure 4.3: Plot of $log\left(\frac{\sigma_{11}}{K_I/\sqrt{2\pi h}}\right)$ versus $log(r/h)$ for the two-dimensional elastostatic case.

in Appendix A1. The dynamic stress-intensity factor was then computed through the relation between K_I^d and J in plane-stress,

$$K_I^d = \sqrt{EJ}, \tag{4.2}$$

where E is the Young's modulus of the material. Figures 4.4a,b show the experimentally obtained dynamic stress-intensity factor history in comparison with that from the numerical simulations for specimens (v3s) and $(\alpha - 4)$. Here K_{I1}^d and K_{I2}^d refer to the experimentally measured values corresponding to the two object plane distances z_{01} and z_{02} and K_j is that computed from the dynamic simulations (through the J-integral). It is seen that in both cases K_j has the same general trend as K_{I1} and K_{I2} except that the experimental values are sometimes substantially lower, while at other times equal to or higher than the simulated values. This discrepancy is attributable to two sources. First, there are uncertainties associated with the simulations in terms of how accurately the tup records provide the boundary tractions actually experienced by the specimens. Secondly, and more importantly, there is the possibility that the experimental values might not have been obtained from a region of K_I^d-dominance. This is in fact foreshadowed by the discrepancy between the two experimental records themselves.

In the above, it has been implicitly assumed that the asymptotic K_I^d-field has validity for this (two-dimensional) geometry and dynamic loading condition. However, as pointed out in the introductory chapter, the existence of a stress-intensity factor field around a dynamically-loaded stationary crack in a finite geometry has by no means been universally established. It is thus necessary to check whether a square-root singular asymptotic field is appropriate here. To this end, a logarithmic plot of stress component σ_{22} along the $\theta = 5^o$ line versus the logarithm of radial distance from the crack-tip is shown in Figure 4.5 for two representative times in the simulation. Comparison with the corresponding curves for the asymptotic field

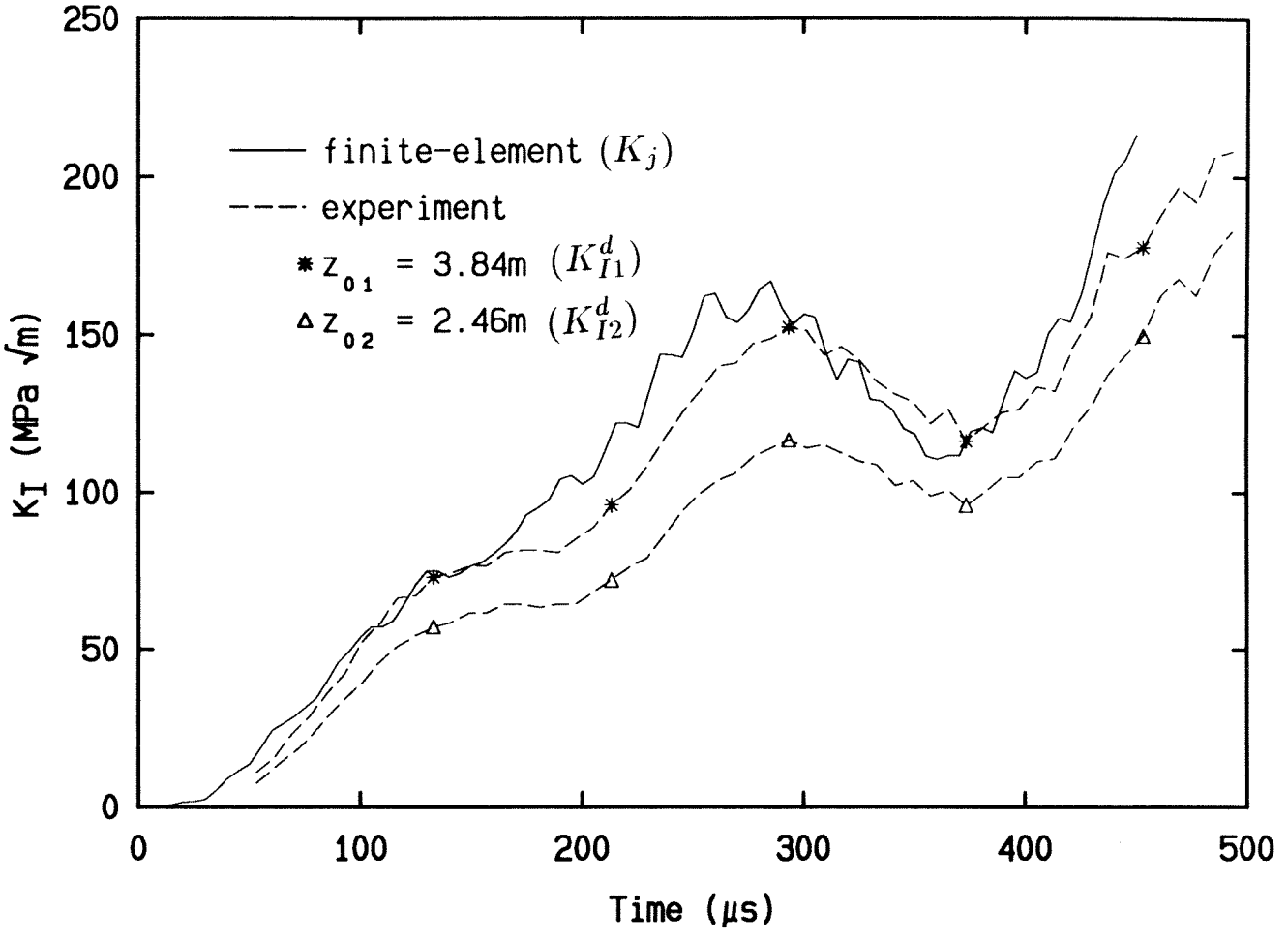

Figure 4.4a: Comparison of the experimentally obtained dynamic stress-intensity factor history with that computed from a two-dimensional simulation of specimen ($v3s$).

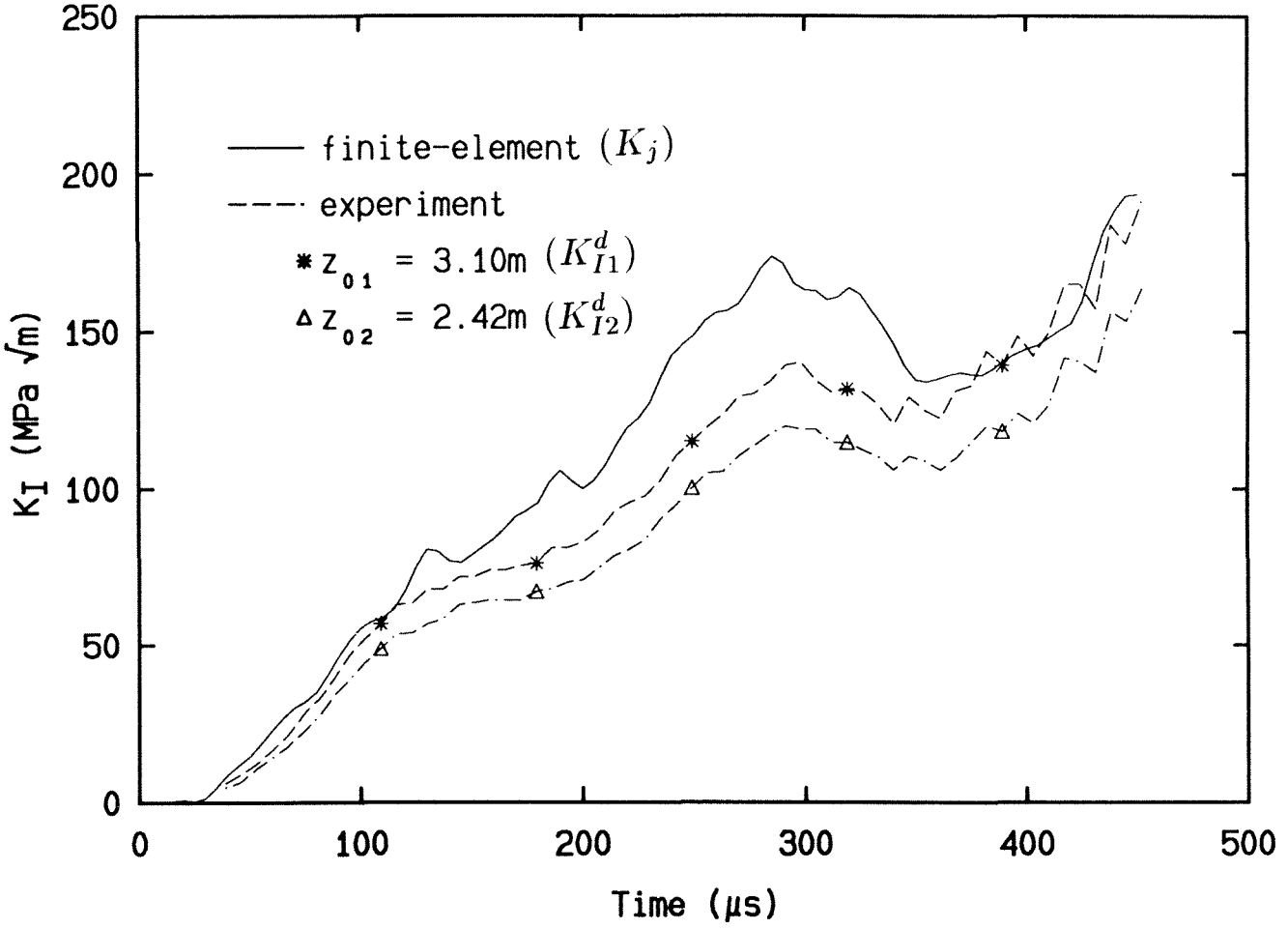

Figure 4.4b: Comparison of the experimentally obtained dynamic stress-intensity factor history with that computed from a two-dimensional simulation of specimen ($\alpha - 4$).

(with the values of the stress-intensity factor obtained from the J-integral) indicates that a square-root singular field is indeed asymptotically descriptive of the near-tip continuum structure for this case at least for the times shown.

As a measure of the extent of dominance of the asymptotic K_I^d-field, the angular variation of the stresses and displacements for a range of radial distance is shown in Figures 4.6a,b, for one particular time. Also shown for comparison are the corresponding asymptotic values. Note that the normalization used here is such that the asymptotic values are given by a single curve for *any* radial distance. This normalization enables distinct features of the stress-intensity factor field to be discerned in the near-tip full-field solution. The magnitudes, however, are seen to vary somewhat with radial distance from the crack-tip.

A quantity of fundamental interest for the method of caustics in reflection is the out-of-plane displacement field, u_3. The value of u_3 can be computed from the full-field plane-stress simulation from the relation

$$u_3 = -\frac{\nu h}{2E}(\sigma_{11} + \sigma_{22}) \tag{4.3}$$

and the angular variation of this is shown in Figure 4.7 for two radial distances from the crack-tip. Again, u_3 is normalized by the corresponding asymptotic quantity. It can be seen that the full-field quantity is in reasonable qualitative agreement with the asymptotic expression for $r/h \to 0$ with increasing deviation in magnitude as r/h increases. This was seen to be the case for other times in the simulation as well.

Finally, synthetic caustics were obtained from the out-of-plane displacement field as described previously for various times in the simulation. Since linear finite-elements were used and, in plane-stress problems, the out-of-plane displacement field is obtained from the in-plane stress field, a smoothing scheme as given in Hinton and Campbell (1974) was used to obtain the derivatives of the surface-displacement field required in the caustic-mapping of the surface. A representative set of these

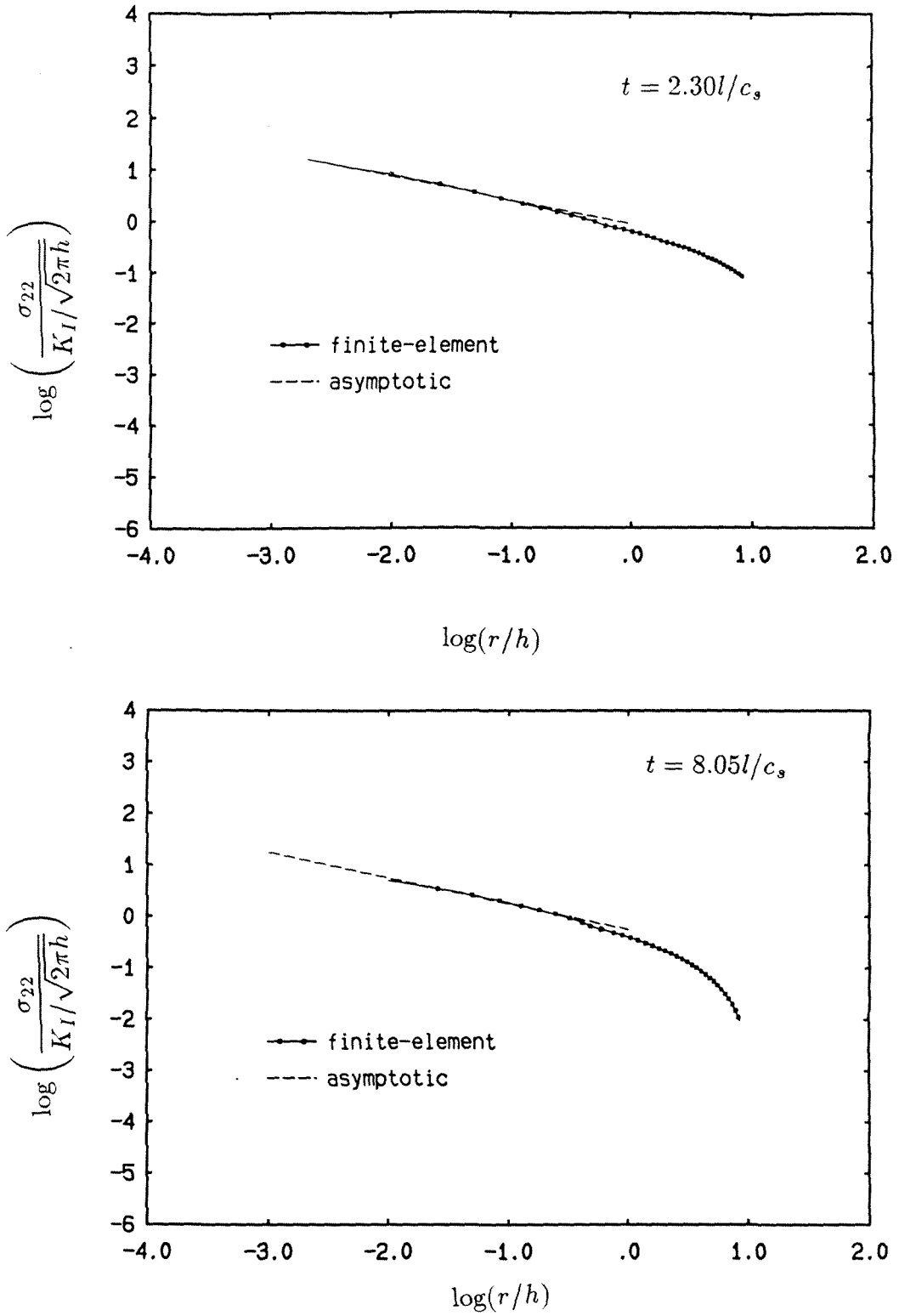

Figure 4.5: Plot of $log\left(\frac{\sigma_{22}}{K_I^d(t)/\sqrt{2\pi h}}\right)$ versus $log(r/h)$ for the two-dimensional elasto-dynamic case.

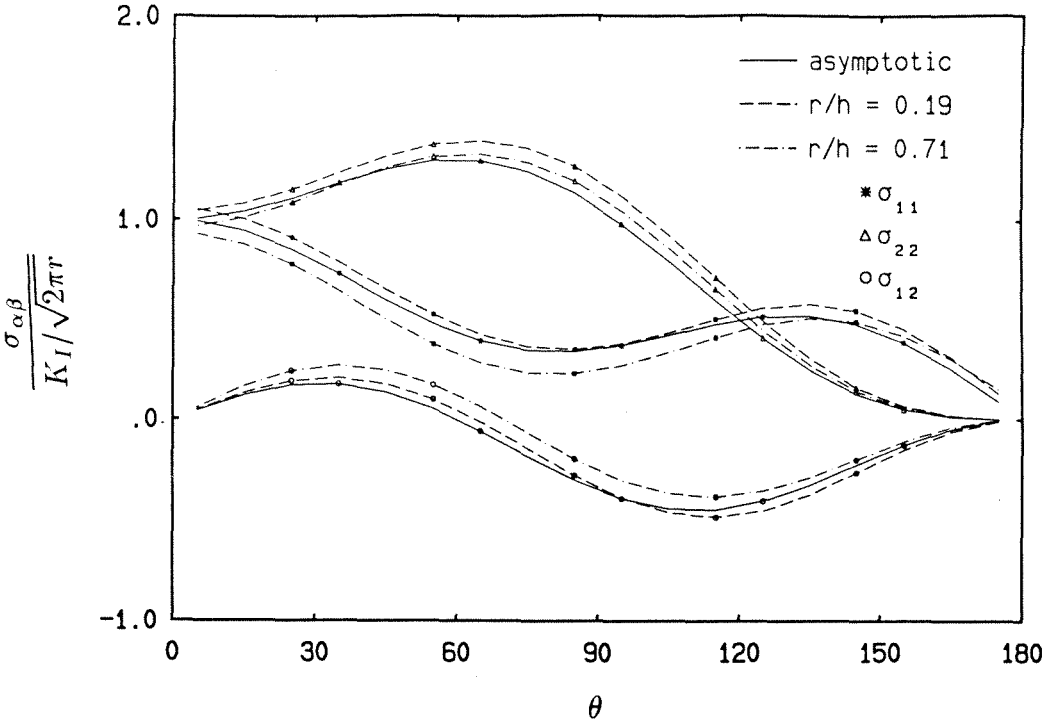

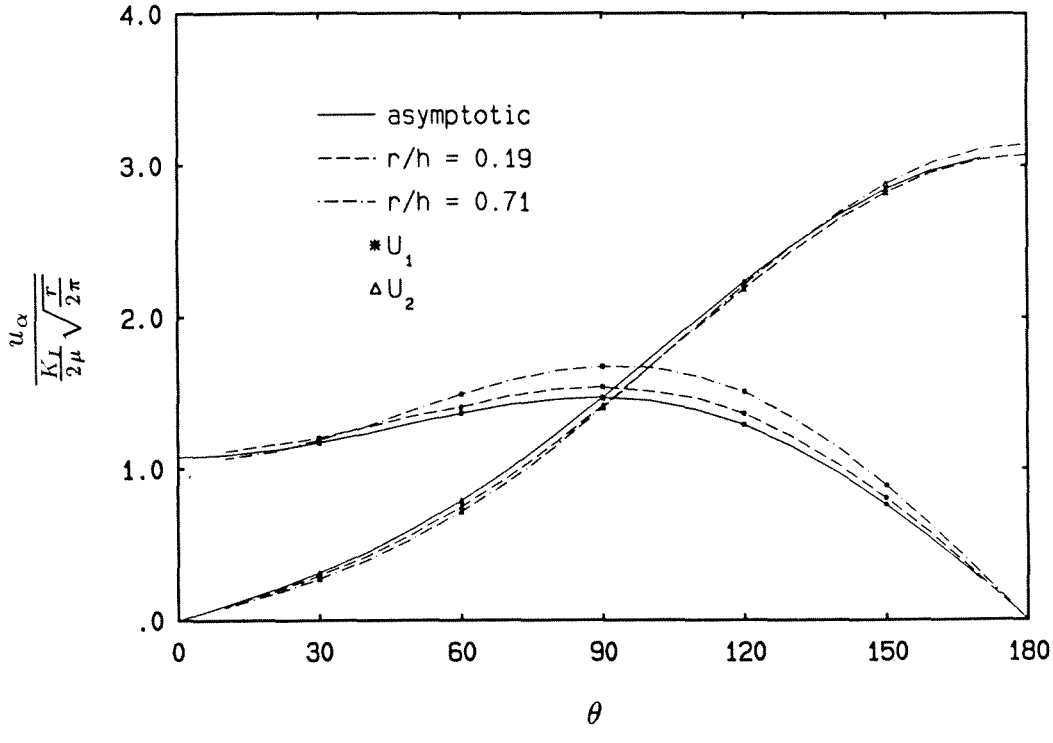

Figures 4.6a,b: Angular variation of near-tip field quantities for the two-dimensional elastodynamic case in comparison with the corresponding asymptotic values.

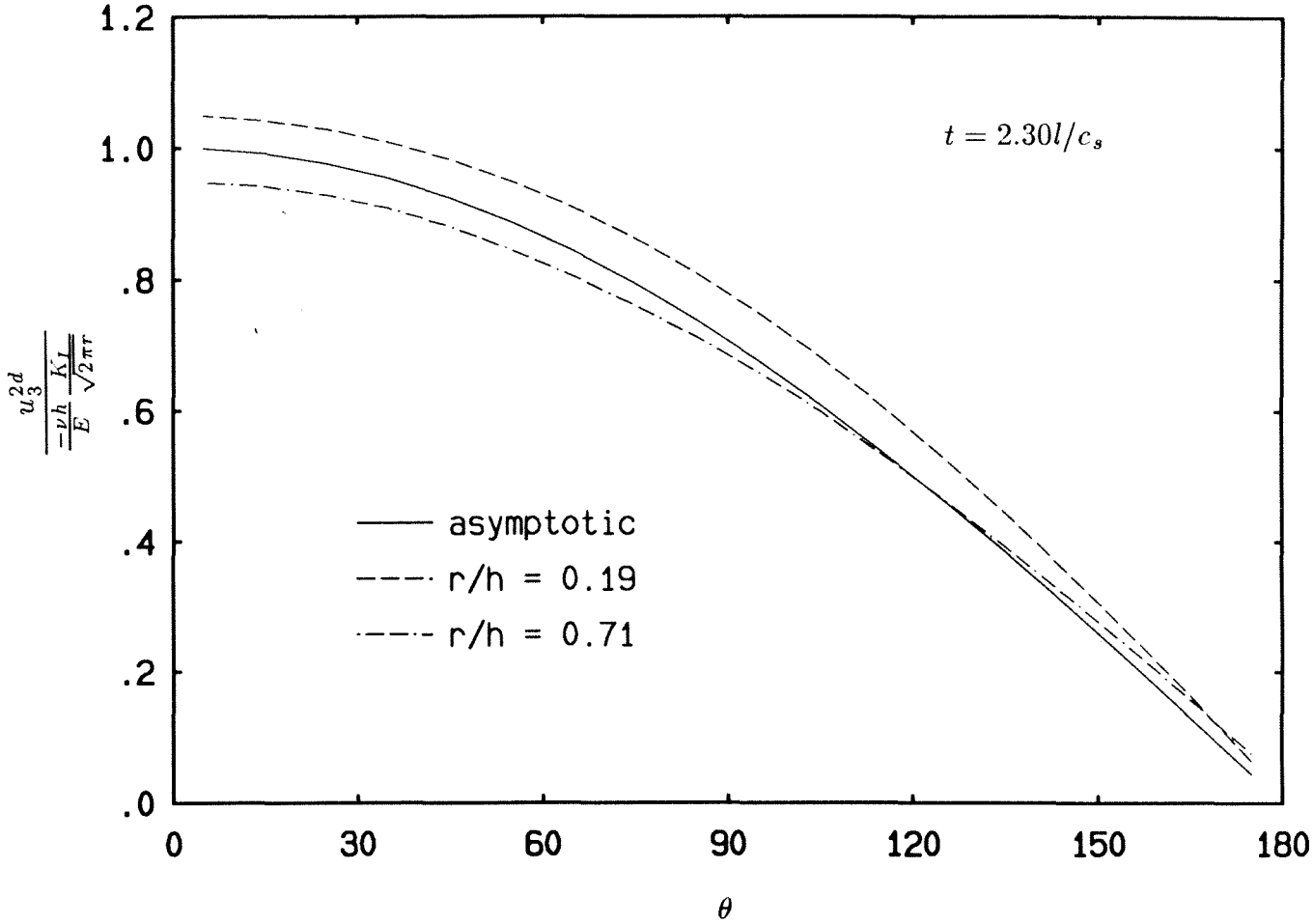

Figure 4.7: Angular variation of the computed out-of-plane displacements for the elastodynamic, plane-stress simulation in comparison with the corresponding asymptotic values.

caustic patterns is shown in Figure 4.8a for one particular time ($t = 2.3L/c_s$) in the simulation and for a set of z_0s. The corresponding initial-curve radii as computed from equation (2.5) on the basis of the caustic diameters range from r_0/h of 0.31 to 0.86. These caustics are seen to have the epicycloidal shape characteristic of those from the asymptotic solution. The ratio of the stress-intensity factor computed from the diameters of these synthetic caustics (denoted K_{caus}) to that obtained from the J-integral (K_j) are plotted in Figure 4.8b as a function of the initial-curve radius of the numerical caustic. While the apparent measured stress-intensity factor seems to increase as r_0/h increases, to within the accuracy warranted by the procedure used here, it appears that caustics should provide the stress-intensity factor value (to within 20%) for initial-curve radii in the range $r_0/h \leq 0.8$. Even though this error is definitely substantial, it is clear that two-dimensional transient effects alone would not seem to entirely account for the much larger variation in the stress-intensity factor observed in the experiments. Indeed, it is worth noting that the above result would indicate that caustics should always overestimate K_j which is not necessarily the case in the experiments (see Figures 4.4a,b).

4.2 Three-Dimensional Elastodynamic Simulation

It appears that the substantial variation observed between the experimentally measured stress-intensity factors from bifocal caustics cannot be explained purely in terms of (two-dimensional) dynamic effects affecting the caustic patterns. Thus additional reasons must be sought in terms of a) non-linear effects or b) three-dimensional effects under transient conditions. Visual evidence of the plastic deformation in the fractured specimens indicated that the initial-curves for the experimental caustics were well outside the plastic zone whose maximum extent was seen to be confined to $r_p/h \leq 0.15$. Based on the estimates of Rosakis and Freund (1981), the experimental results of Zehnder and Rosakis (1988), as well as elastoplas-

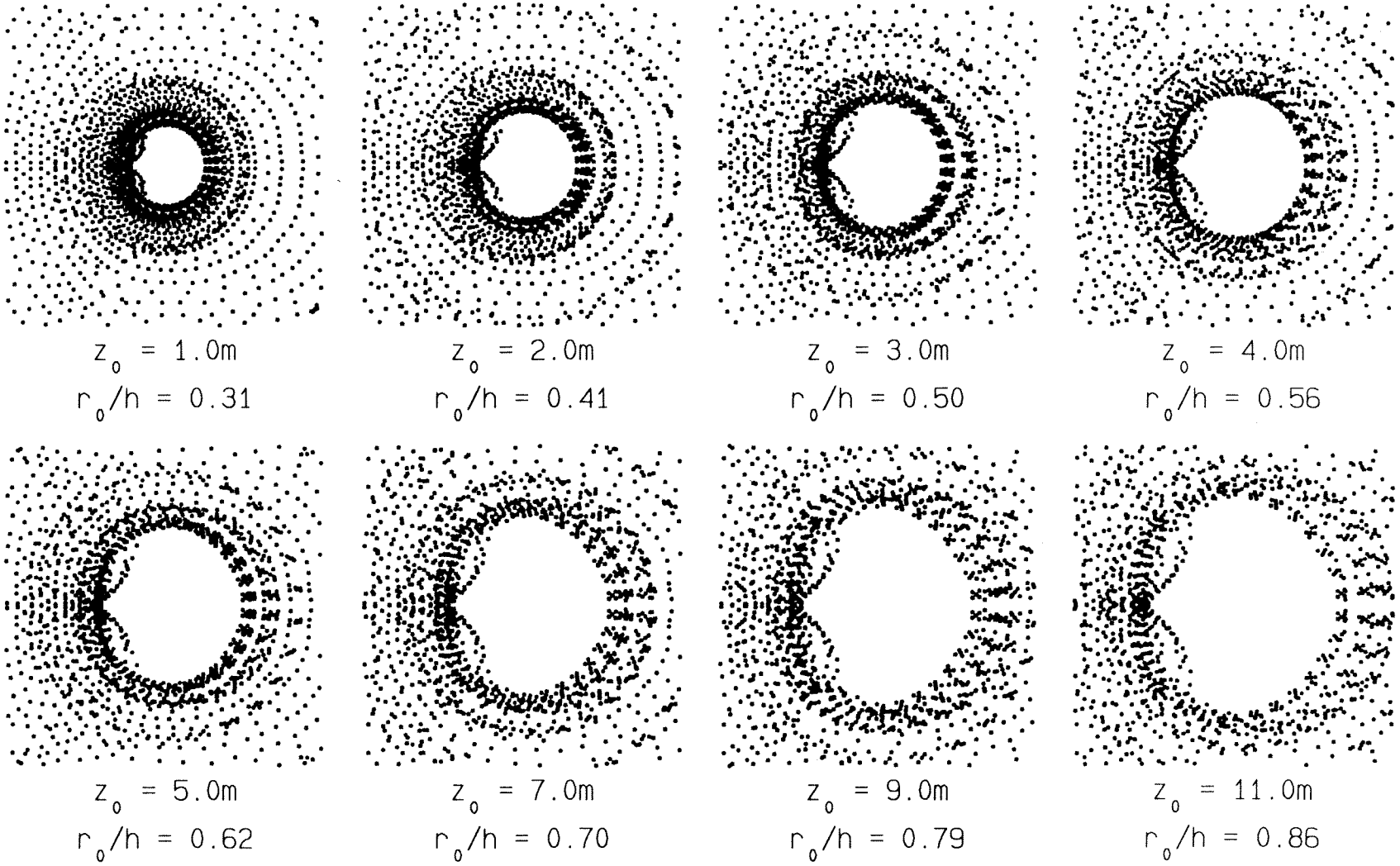

Figure 4.8a: Simulated caustics from the computed plane-stress out-of-plane displacements.

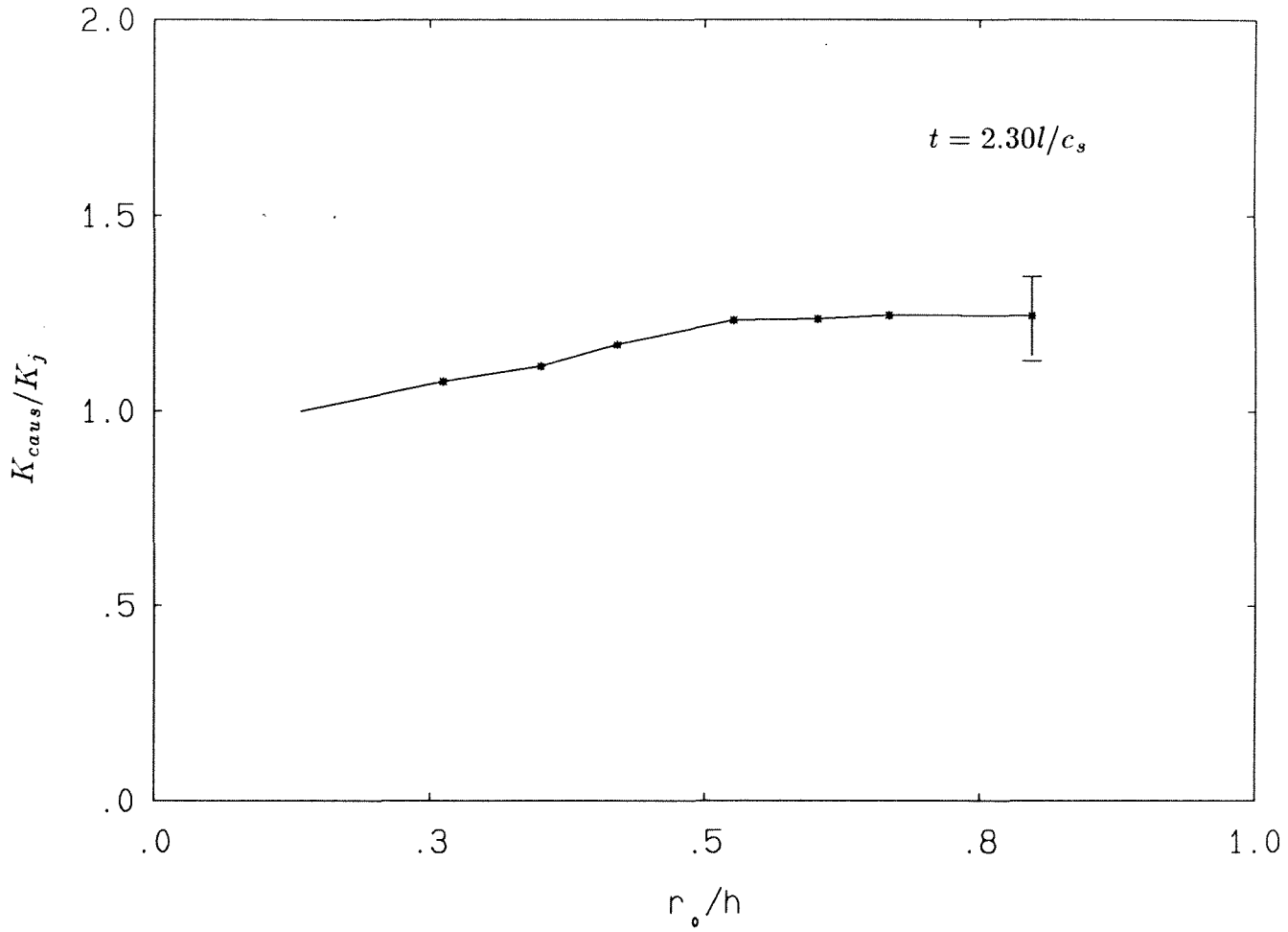

Figure 4.8b: Plot of K_{caus}/K_j versus r_0/h from the two-dimensional elastodynamic simulation.

tic simulations of the current experiments (reported in Krishnaswamy and Rosakis (1988)), plasticity effects are expected to be negligible. Thus attention will now be directed toward studying the effect of three-dimensionality near the crack-tip by means of a full-field three-dimensional elastodynamic simulation of the drop-weight experiments.

The mesh geometry used had an in-plane layout identical to that used for the two-dimensional cases. This enables the direct comparison of three-dimensional results with the corresponding plane-stress simulations and thereby helps identify the effect of three-dimensionality. Five layers of 8-noded brick elements through half the thickness leading to a total of 1960 elements (2250 nodes) were used to model one-quarter of the three-dimensional body. Recognizing that the largest through-thickness variations in field quantities occur near the free-surface, the mesh was graded in the thickness direction as shown in Figure 4.2. The experimentally obtained tup load histories interpreted as uniform line loads through the thickness were applied as boundary conditions to the appropriate nodes. The uncracked ligament surface and the specimen mid-plane were constrained suitably as dictated by symmetry considerations. The rest of the boundary was left traction-free. Once again, an implicit Newmark predictor-corrector scheme was used in order to be consistent with the algorithm used for the two-dimensional simulation.

The appropriate average dynamic energy-release rate integral here is (see Appendix A1)

$$J_{av} = \frac{1}{h} \lim_{S \to 0} \int_S \left((U + T) n_1 - \sigma_{ij} n_j \frac{\partial u_i}{\partial x_1} \right) dS, \tag{4.4}$$

where S is now a tubular surface through the specimen and $S \to 0$ symbolically indicates that this surface is shrunk onto the crack-front. In order to compare with experimental results, an 'average' stress-intensity factor can be extracted from J_{av} through relation (4.2). The average energy-release rate value obtained from the

three-dimensional simulation is shown in Figure 4.9 and is not much different from that computed in the plane-stress analysis. Thus, the plane-stress approximation might be adequate if one is interested in integrated energy-release rate type of quantities.

From the point of view of the method of caustics in reflection, the primary issue is the extent of deviation of the near-tip surface out-of-plane displacement field from the corresponding asymptotic plane-stress expression. This is shown in Figure 4.10a for a set of radial lines along $\theta = 0^o, 60^o$ and 140^o and for one typical time. The surface u_3-displacements as obtained from the three-dimensional solution are normalized by the corresponding asymptotic values. The two-dimensional counterpart along the radial line $\theta = 0^o$ is shown for comparison purposes. Two salient features can be identified from this figure. First, the *two-dimensional* full-field values seem to be in good agreement with the asymptotic for sufficiently small radial distances. The asymptotic expression seems to become increasingly inaccurate for larger radial distances. Secondly, it is precisely in those regions where the two-dimensional and asymptotic fields are in close agreement that the three-dimensional structure deviates the most from the asymptotic. In Figure 4.10b, the angular variations of the surface u_3-displacements are shown for a range of r/h. Under the normalization used, the asymptotic u_3-displacements are given by $\cos(\theta/2)$ – the solid line – for any radius. Again it is noted that the asymptotic field does not always model the actual three-dimensional structure very well. Indeed, the deviation from the asymptotic is seen to be pronounced toward the crack-tip. For larger r/h, the theta variation of u_3 seems to approach the asymptotic curve in form though not in actual magnitude. Thus it appears that the actual three-dimensional field is not quite captured by the asymptotic expression for the surface out-of plane displacements – toward the crack-tip because of substantial three-dimensional effects and away from

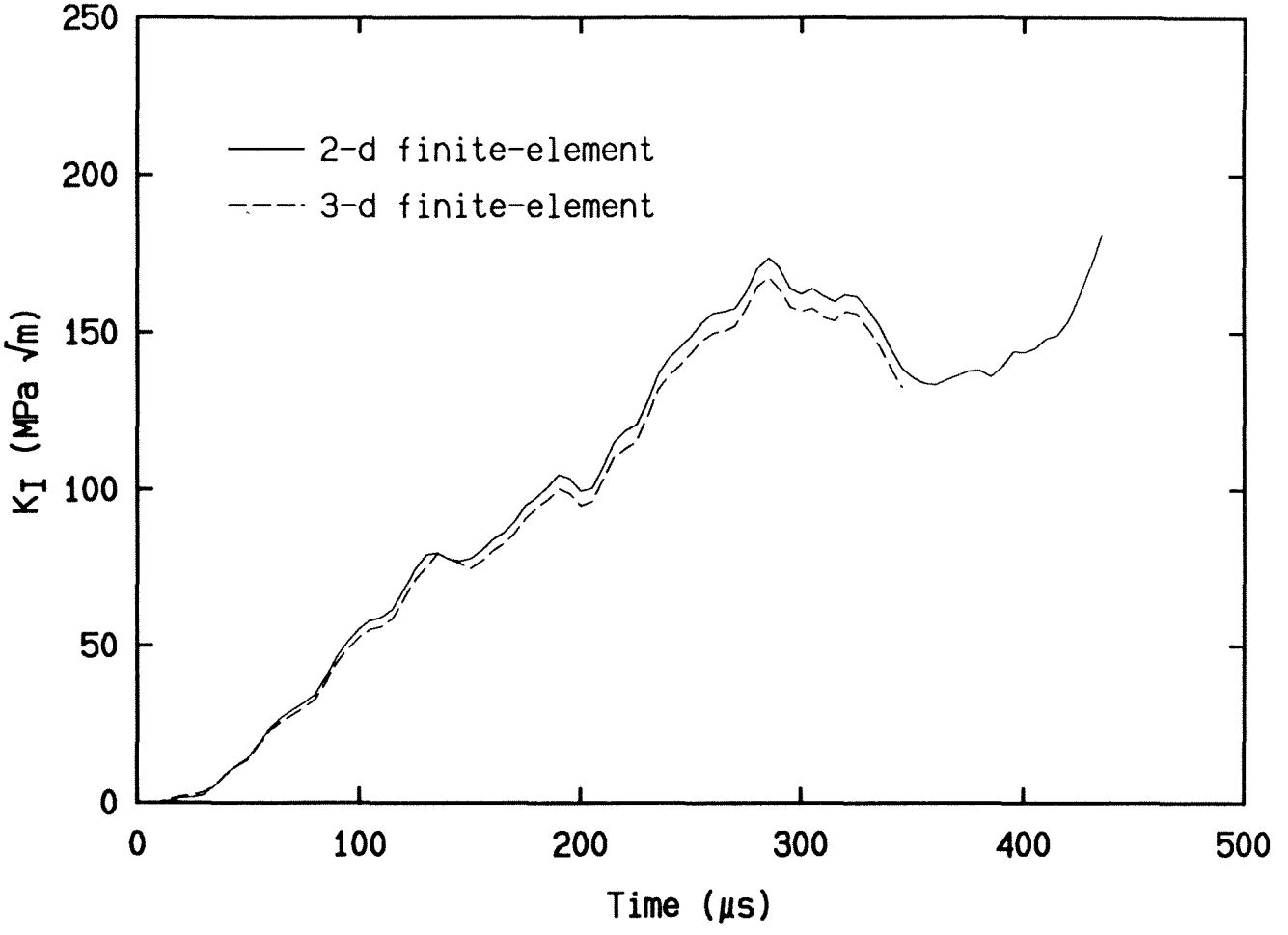

Figure 4.9: Comparison of the "average" dynamic stress-intensity factor history as computed from two- and three-dimensional simulations.

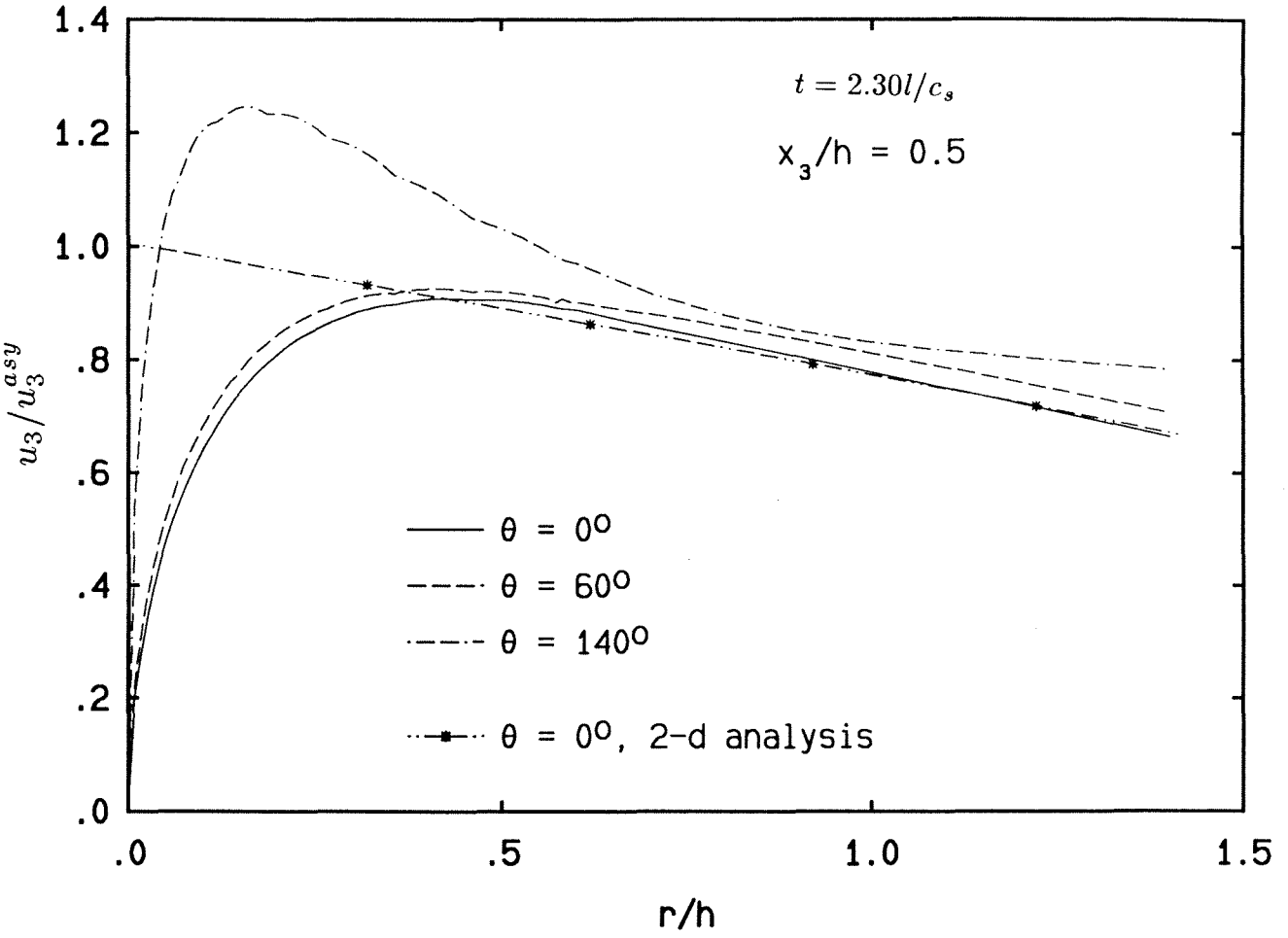

Figure 4.10a: Radial variation of the free-surface u_3-displacements in comparison with the corresponding asymptotic values.

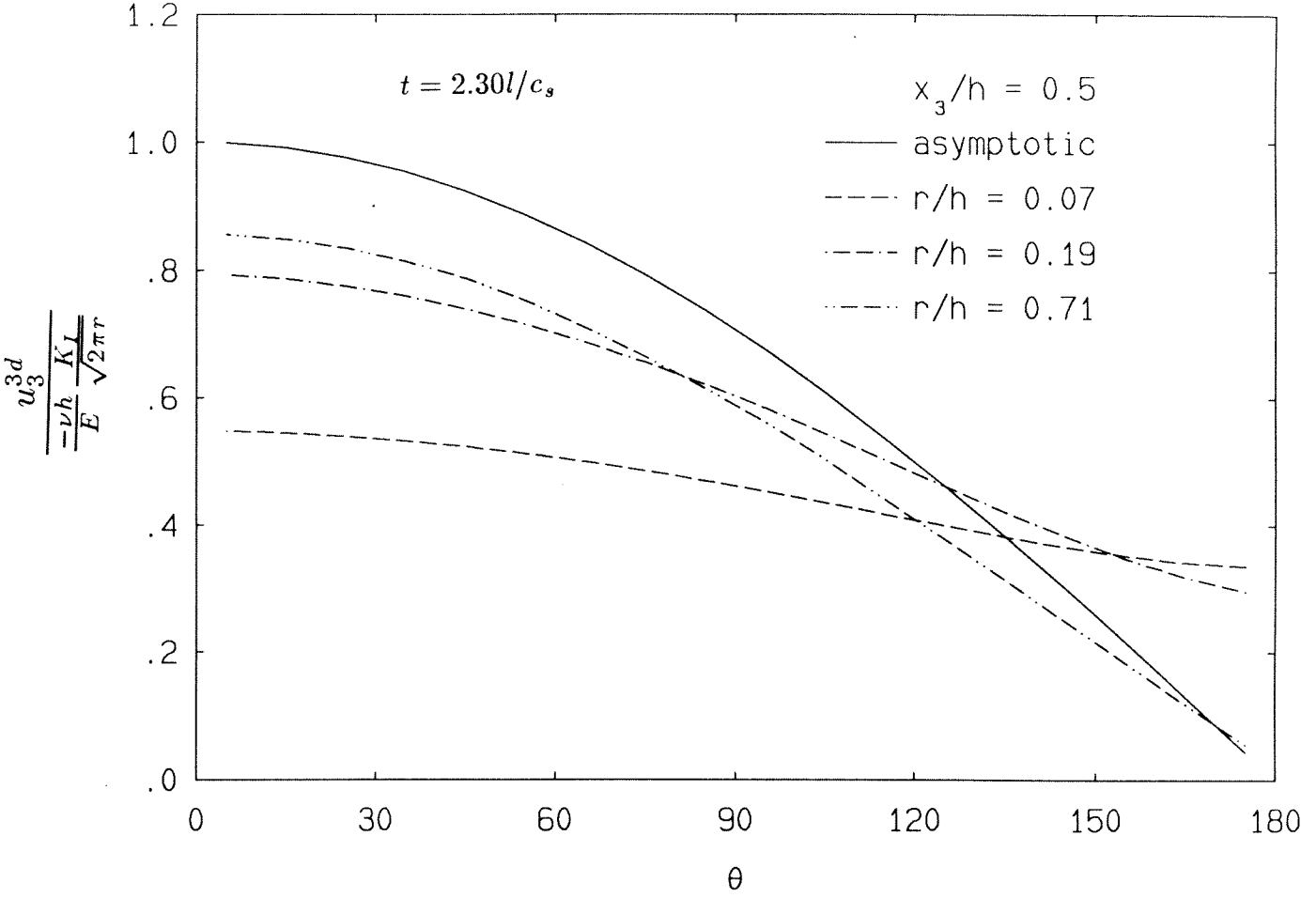

Figure 4.10b: Angular variation of the free-surface u_3-displacements in comparison with the corresponding asymptotic values.

it because the asymptotic expression becomes increasingly insufficient.

The qualitative effects of the above features insofar as these affect the method of caustics can now be evaluated. As described previously, the three-dimensional surface out-of-plane displacements obtained numerically for various times in the simulation are mapped using (2.1) to obtain synthetic caustic patterns. A representative sequence of these caustic patterns for one particular time is shown in Figure 4.11a. These were obtained for the same instant of simulation and for the same set of z_0s as were used in the two-dimensional case. The role of three-dimensionality is thus clearly brought out. The graphic contrast that emerges between the caustic patterns obtained under two-dimensional assumptions and the actual three-dimensional conditions can be seen by comparing Figures 4.8a and 4.11a. In comparison to the corresponding two-dimensional results, it is noted that for small r_o/h, the shadow spots in Figure 4.11a are less epicycloidal in shape and much smaller in size. This is not surprising considering the angular variations of u_3 which deviated markedly from the asymptotic as $r \rightarrow 0$. Compare this with the results of the plane-stress analysis (see Figure 4.8a) where the qualitative agreement with the asymptotic field appears to be much better over a wider range of r/h. If, now, one were to relate the caustic diameters to the stress-intensity factor through (2.7), then the resulting value of K_{caus}/K_j (shown for two times) is seen to vary quite substantially with increasing initial-curve radius as shown in Figure 4.11b. From the figure, it is seen that as $r_0/h \rightarrow 0$ the measured stress-intensity factor value becomes substantially less than the value obtained from the domain integral. Further, for larger initial-curve radii, it is possible for caustics to provide an overestimate of K_j. More importantly, the almost monotonically increasing K_{caus}/K_j vs r_o/h curve for the three-dimensional transient simulation case qualitatively captures essentially all the features observed experimentally. Thus, the apparent dynamic stress-intensity fac-

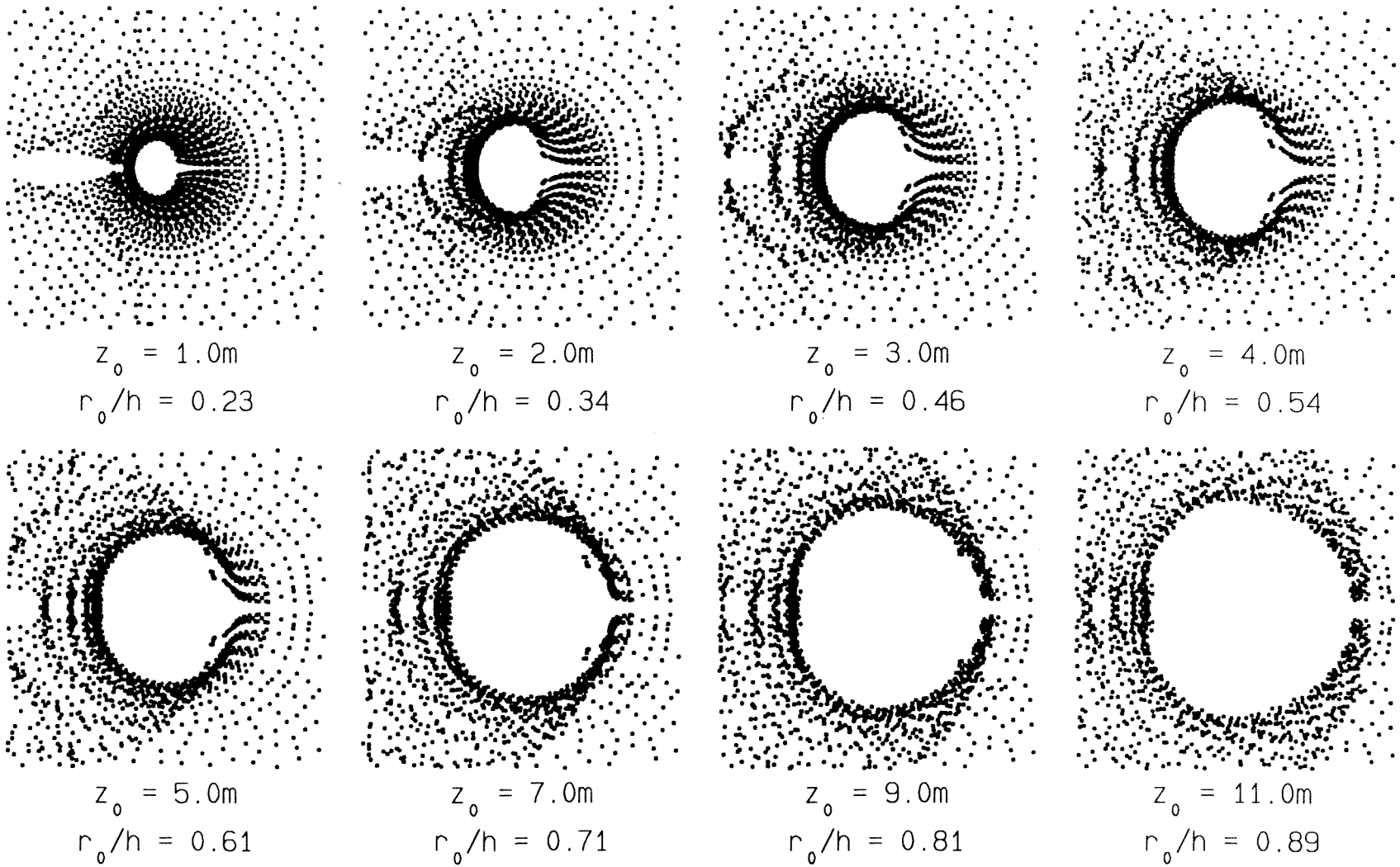

Figure 4.11a: Simulated caustics from the computed three dimensional free surface u_3-displacements.

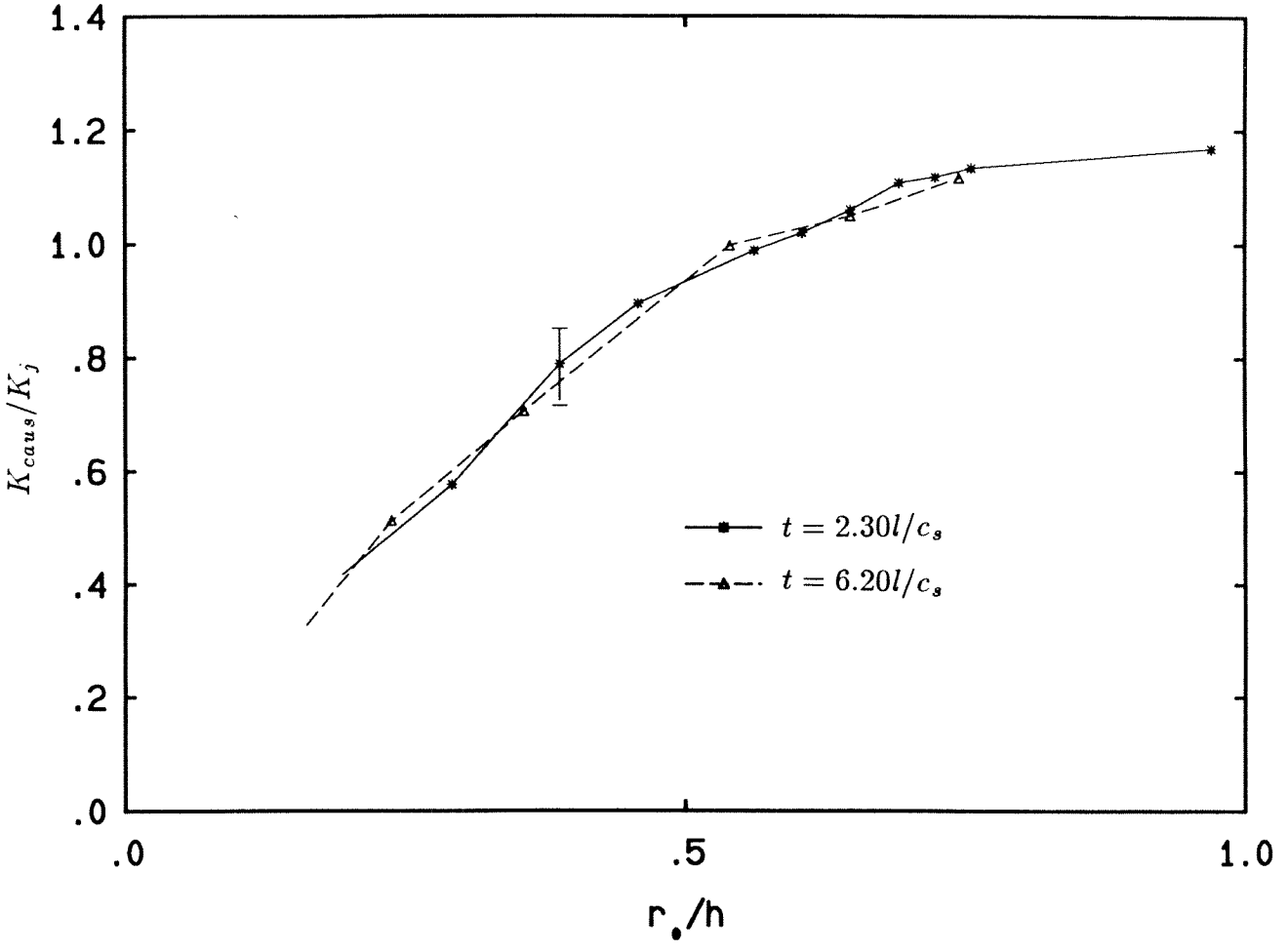

Figure 4.11b: Plot of K_{caus}/K_j versus r_0/h from the three-dimensional elastodynamic simulation.

tor as measured by caustics would seem to increase with increasing initial-curve radii. Also, in view of the lack of a sizeable domain of dominance of K_I^d, it would appear that the agreement between the measured dynamic stress-intensity factor history and that computed through the J-integral cannot be expected to be any better than obtained in Figures 4.4a,b.

As a parenthetical note, it is interesting that the variation in K_{I1}^d and K_{I2}^d – the two values for the dynamic stress-intensity factor as measured from pairs of bifocal caustics – turns out to be in quite good *quantitative* agreement with the results of Figure 4.11b. That is, the ratio of K_{I1}^d to K_{I2}^d as obtained from experiments seem to be in close agreement with that obtained from Figure 4.11b for the corresponding initial-curve radii. This can be seen in Figure 4.12 where the numerically generated results of Figure 4.11b are used to "scale" the results of one particular experiment. To do this, *assume* that the results of Figure 4.11b (K_{caus}/K_j vs r_0/h) hold for the whole duration of the loading. The experimental data (corresponding to the two z_0s) shown in Figure 4.12a can then be scaled, for each time, to the corresponding 'K_j' value by means of Figure 4.11b. The resulting "scaled" dynamic stress-intensity factor histories corresponding to the two z_0s are shown in Figure 4.12b. It is seen that by this procedure the deviation between the K_I^d values observed in the experiments from pairs of bifocal caustics essentially reduce to within expected experimental scatter for the whole duration of loading. Thus it would appear that the main reasons for the observed experimental variation are accounted for by the three-dimensional elastodynamic simulation. Note that it is purely to highlight this point that the above "scaling" procedure was adopted. It is not the intention here to offer Figure 4.11b as some kind of an empirical "correction curve" for experimental data.

Finally, it is instructive to look into some additional features of the near-tip field

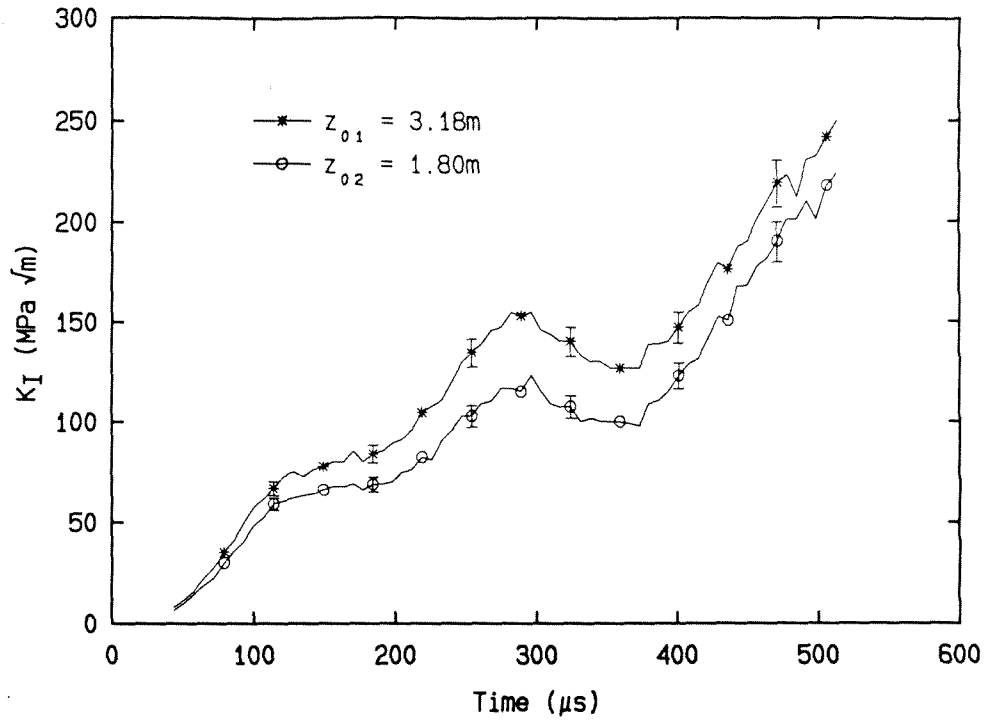

(a)

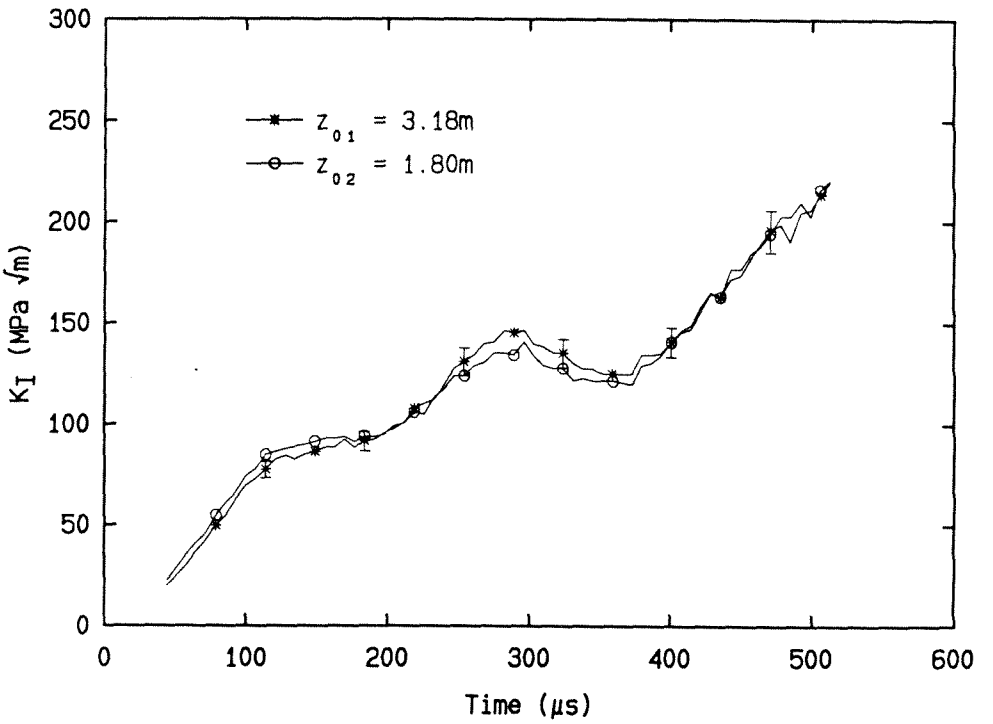

(b)

Figures 4.12a,b: Raw and "scaled" experimental data for specimen $(3q)$.

quantities. Figures 4.13-14 show the radial variation along the $\theta = 45^o$ line of the three-dimensional stresses and displacements for different planes along the thickness direction. This is done for one representative time. Note that in all these plots, the three-dimensional quantities are normalized by the corresponding quantities from the full-field dynamic plane-stress analysis. This is done in an attempt to highlight the effects of three-dimensionality. It also has the added virtue that it minimizes variations due to dynamic effects. One point to note is that the three-dimensional results seem to show maximum deviation from the two-dimensional results as the free-surface is approached. Further, the plane-stress solution seems to be recovered within about one-plate thickness from the crack-front. It is interesting that the deviation in the in-plane displacements u_1 are much less pronounced than in the other quantities. In Figure 4.15, the ratio of the three-dimensional free-surface u_2-displacement to its two-dimensional counterpart is shown as a contour plot. This again shows that three-dimensional effects seem to be confined to within a radial distance of at most one-plate thickness all around the crack-front. Note that symmetry requirement forces the two- and three-dimensional u_2-displacements to agree exactly along the crack-line. This manifests as a sharp turning in of the contour lines as the crack-line is approached. Figure 4.16 is a plot of the so-called plane-strain constraint which should be unity in regions where plane-strain conditions are obtained and zero where plane-stress conditions prevail. This is shown for one typical time in the simulation. It is seen that, by this measure, plane-stress conditions are obtained at radial distances greater than about one-half plate thickness.

The thickness variations of the plane-strain constraint and also representative stress components (σ_{11} and σ_{22}) are shown in Figures 4.17a,b,c for a range of radial distance from the crack-tip along the $\theta = 45^o$ line. Once again it can be seen that the deviation in stresses from the two-dimensional fields is largest toward the

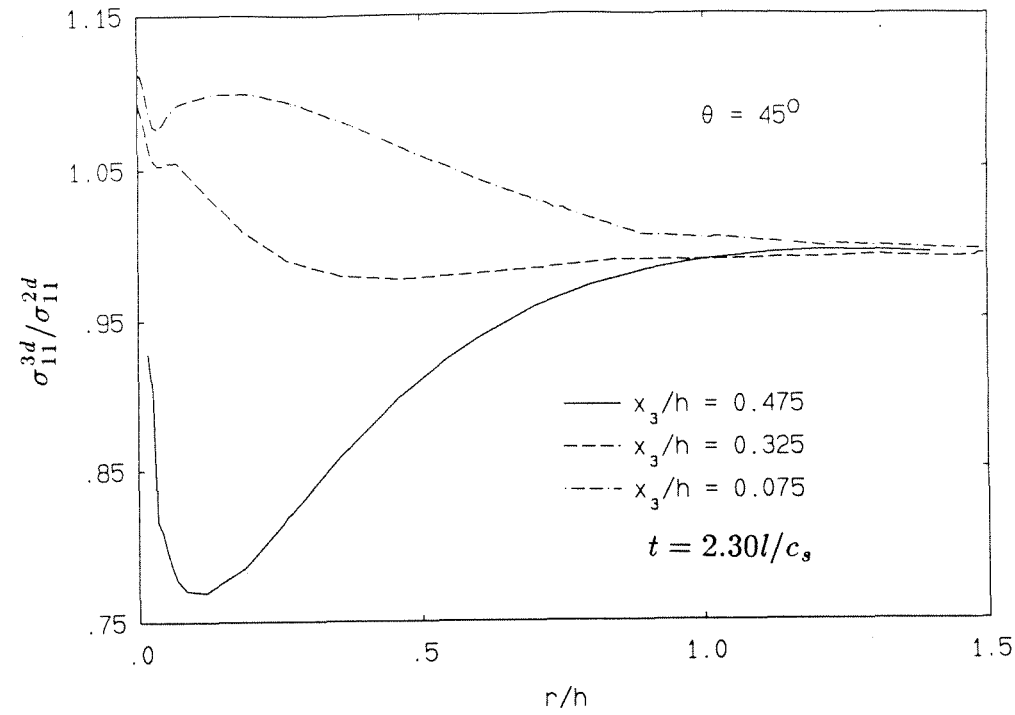

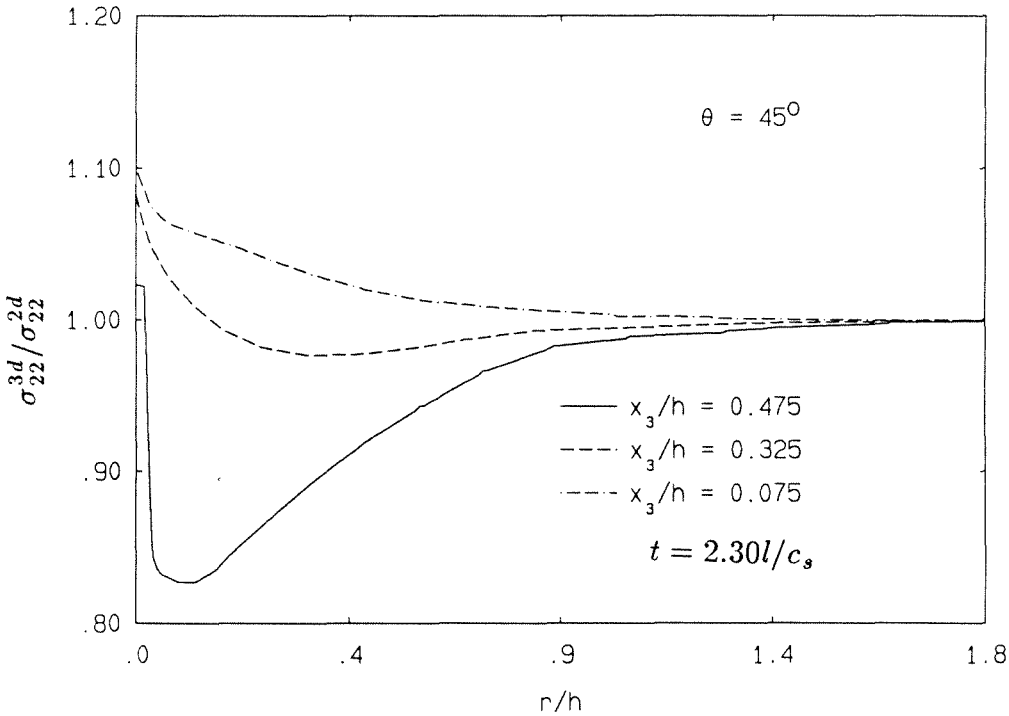

Figure 4.13: Radial variation of typical stress-components compared with the corresponding plane-stress values.

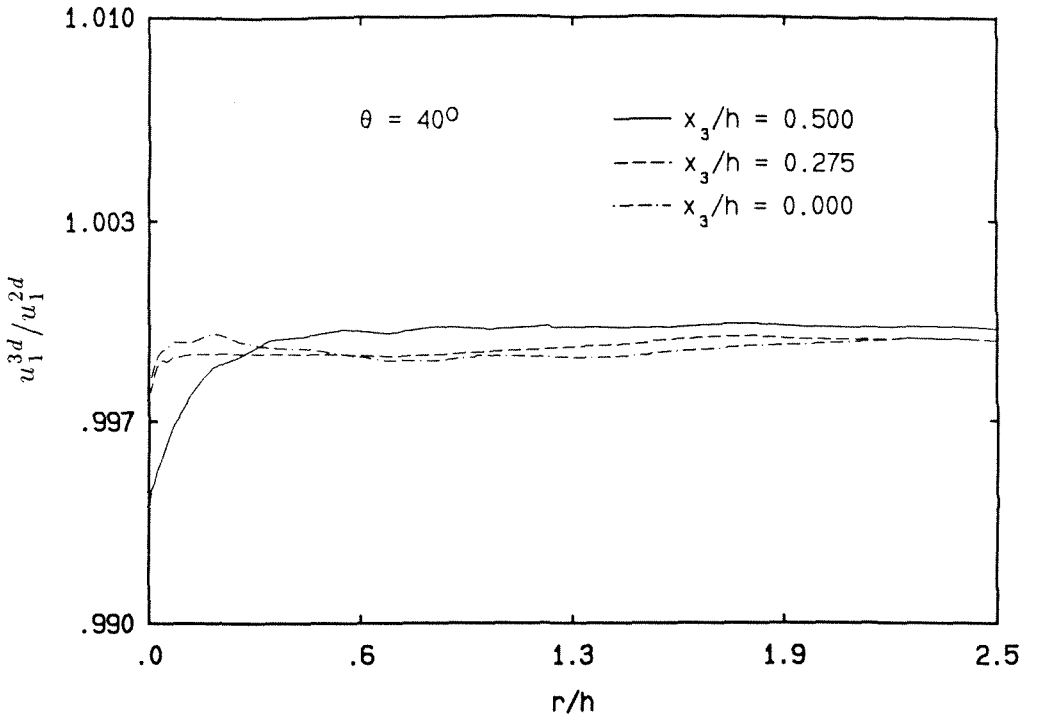

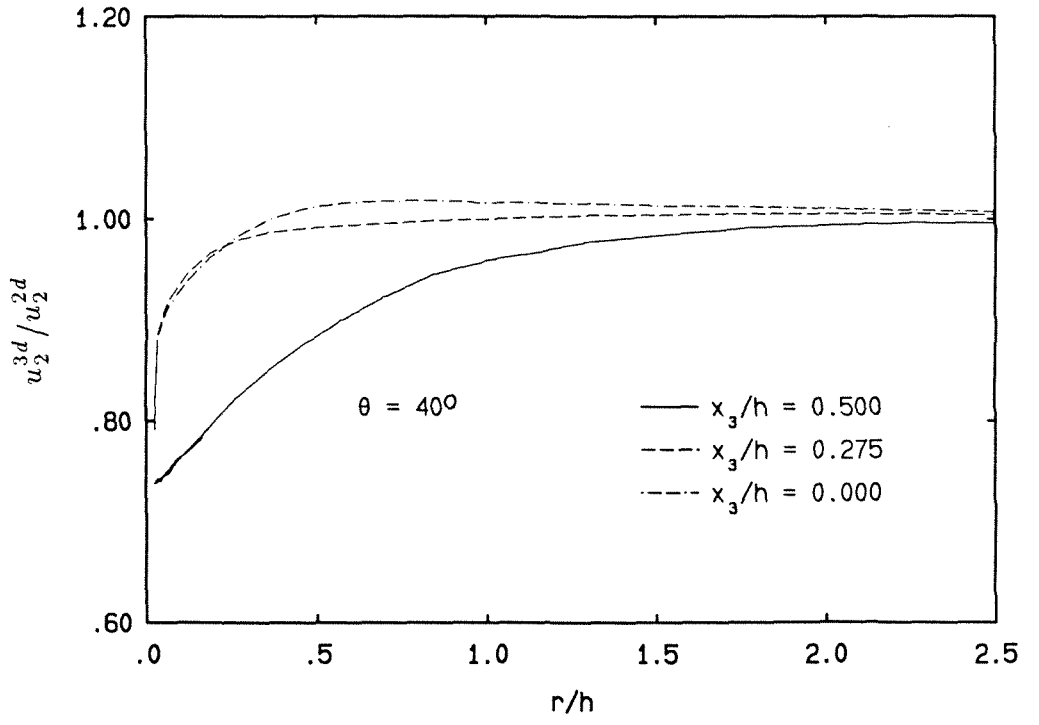

Figure 4.14: Radial variation of the displacements in comparison with the corresponding plane-stress values.

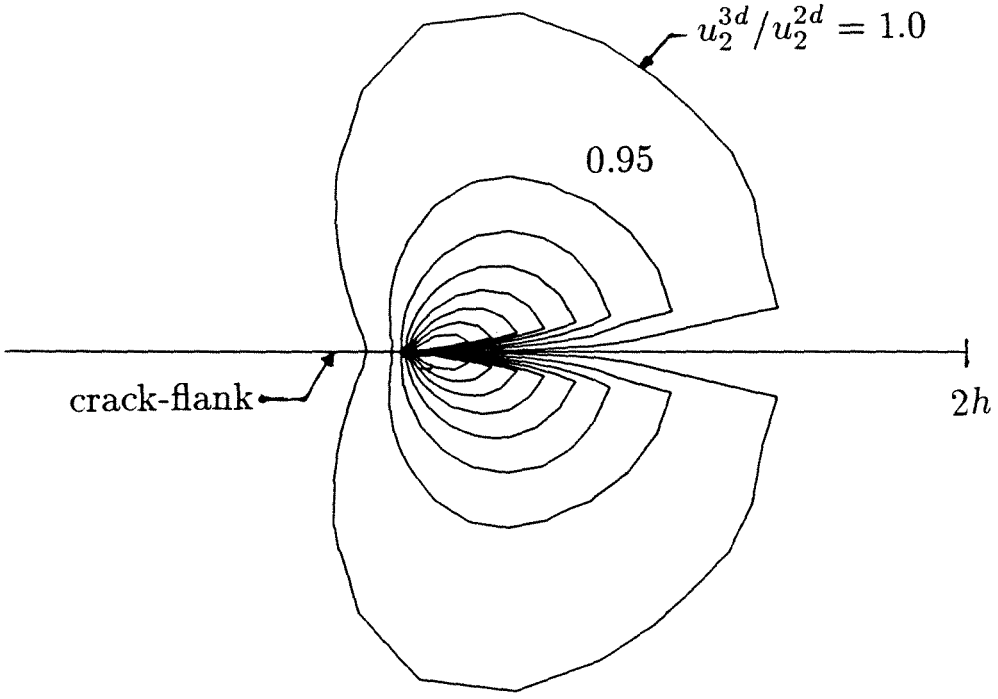

Figure 4.15: Contour plot of free-surface u_2-displacements normalized by the corresponding plane-stress values.

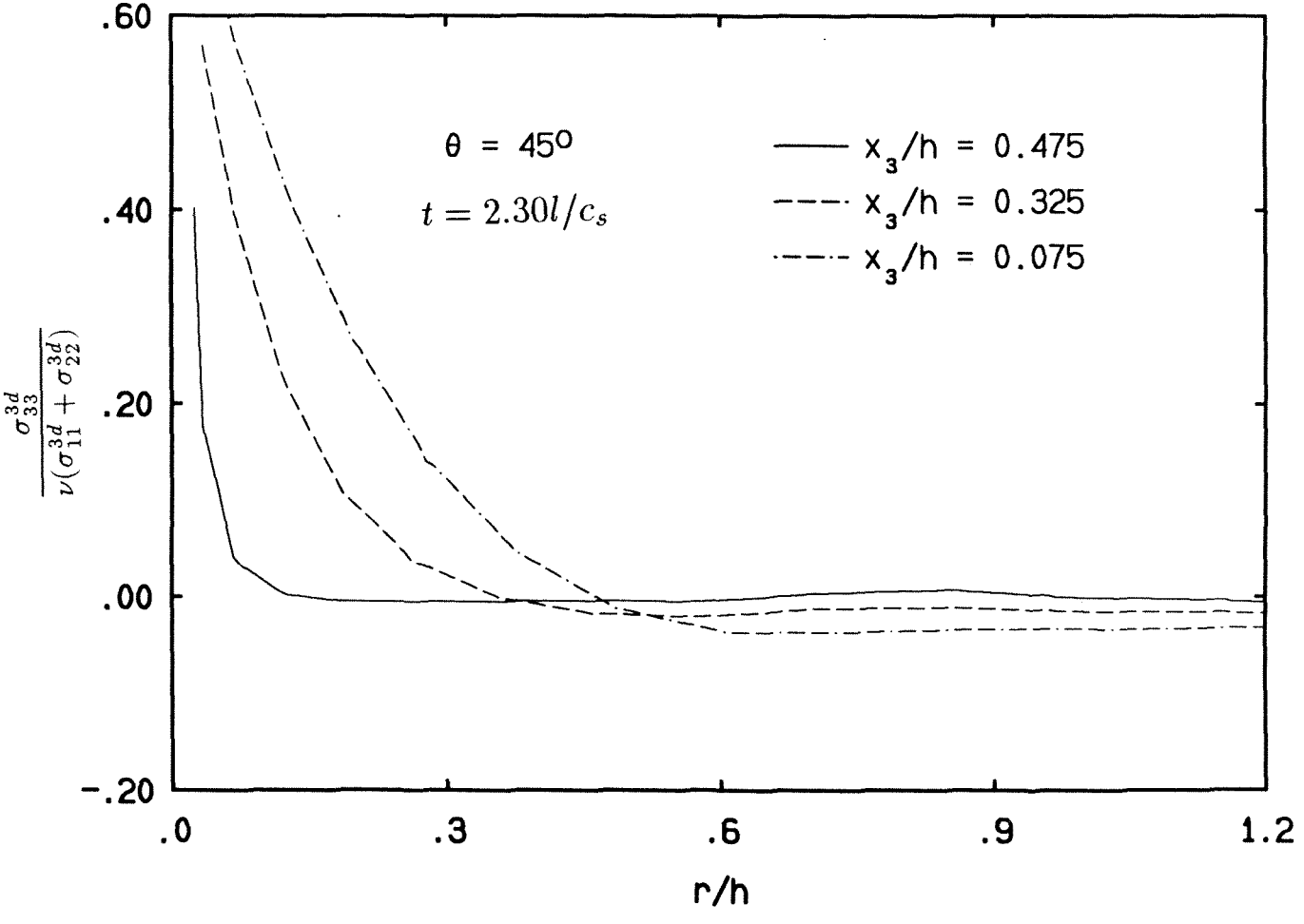

Figure 4.16: Radial variation of the plane-strain constraint for various planes through the specimen thickness.

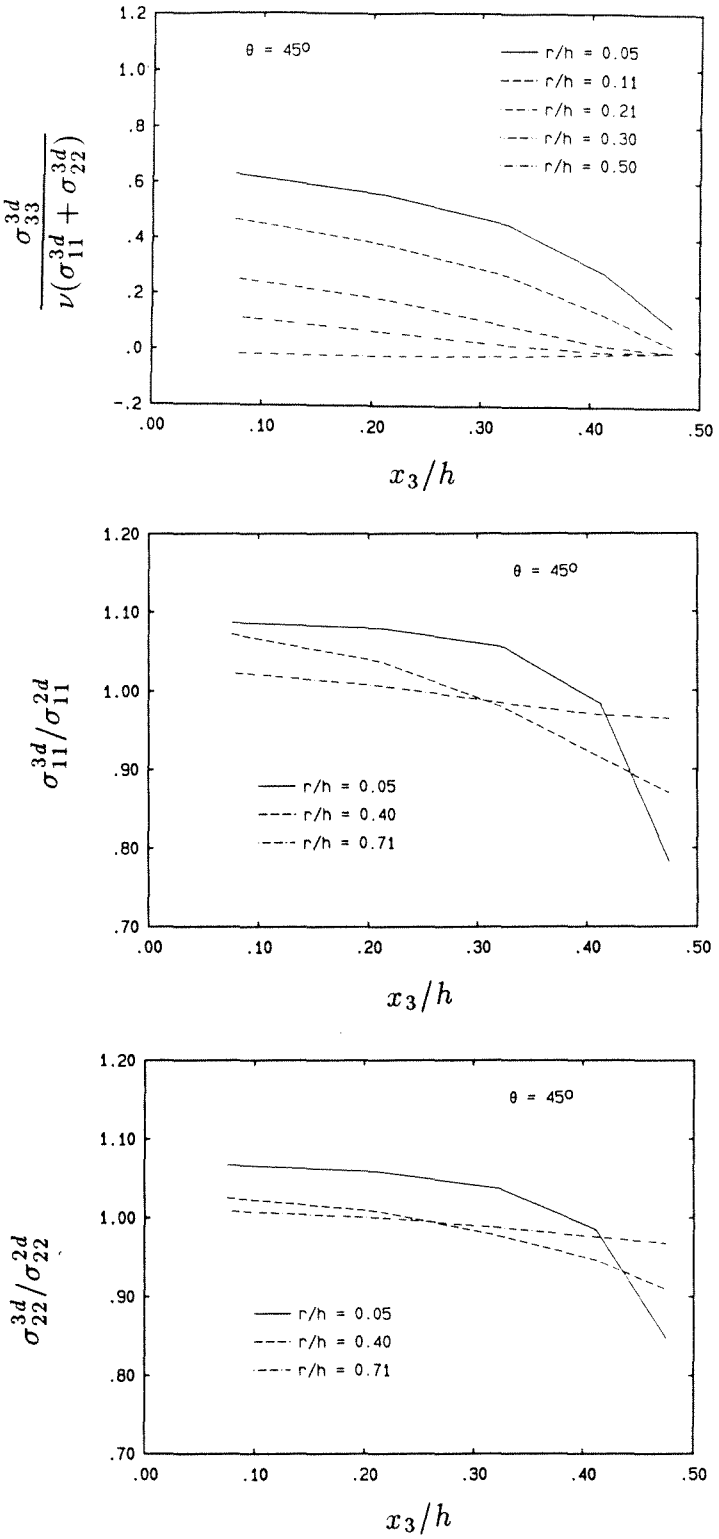

Figure 4.17: Through-thickness variation of a) the plane-strain constraint, b) σ_{11} and c) σ_{22}.

free-surface. Also, all these plots underscore the point that the assumption of plane-stress is indeed a good one for regions of radial extent greater than about one plate thickness away from the crack-front. This might conceivably be of use to the experimentalist.

4.3 Summary of Results

Based on two- and three-dimensional elastodynamic simulations of the drop-weight tests, the following conclusions can be drawn:

i. The dynamic asymptotic field, while sufficiently accurate for $r/h \rightarrow 0$, becomes increasingly inadequate for larger radial distances even in a purely two-dimensional setting.

ii. The three-dimensional nature of the dynamic crack-tip field, which is seen to be confined to within at most one-plate thickness radial extent around the crack-tip, exhibits largest deviation from the full-field plane-stress results for $r/h \rightarrow 0$.

iii. The above two results together imply that the three-dimensional structure of the near-tip surface, coupled with the transient nature of the local fields, appear to preclude any sizeable region of K_I^d-dominance around the crack-tip.

The experiments of the previous chapter had also indicated the lack of an underlying K_I^d-dominant field. This was observed experimentally for both the dynamically loaded stationary crack as well as for the rapidly propagating crack. As stated in the introductory chapter, this result is true for the configuration studied. Whether a similar result holds for other configurations is still an open question. It is felt that this point needs to be considered in evaluating the array of somewhat conflicting experimental results that have been used in support of one or the other of the mostly empirical theories of the mechanics of dynamic fracture. The main endeavor of the concluding chapter will be to investigate whether the assumed K_I^d-dominance could

have been violated in some of the experiments in the literature and, if so, whether those experimental results are amenable to an alternate interpretation.

CHAPTER V

CONCLUSION

The purpose of this investigation was to identify the domain of dominance of the asymptotic K_I^d-field for elastodynamic crack problems – both for dynamically loaded stationary cracks and for rapidly propagating cracks. The effort was undertaken in an attempt to verify the premise on which much of the experimental and analytical work in dynamic fracture mechanics rests. For example, a host of material properties to characterize various aspects of dynamic fracture have been postulated based on the dynamic stress-intensity factor field. Thus, there is the dynamic fracture toughness K_{ID} to characterize initiation and propagation; K_{Ia} is said to model crack arrest; cracks are supposed to branch when the dynamic stress-intensity factor reaches a critical material value K_{Ib}; and so on. With such importance attached to the stress-intensity factor as a parameter governing various aspects of dynamic fracture of nominally brittle materials, it is essential that the domain of dominance of the K_I^d-field be mapped out prior to experimentally extracting any stress-intensity factor-based material properties.

In this work, the issue of the domain of dominance of the K_I^d-field was studied for the case of the three-point bend specimen subjected to impact loading. This study was done in two phases. In the main phase, a series of experiments was performed using the bifocal caustics technique described in Chapter II. This allowed for the simultaneous experimental acquisition (during both the loading and the subsequent crack propagating regimes) of dynamic caustics from two different regions (initial-curves) around the crack-tip. As pointed out in Chapter II, if the two initial-curves of the caustics lie in a K_I^d-dominant region, the corresponding values for the dynamic stress-intensity factor must agree to within experimental error. The experimental results, however, showed differences of up to 60% in the

stress-intensity factor obtained from caustics whose initial-curve radii differed by less than 20% of the specimen thickness. No substantial range of r_0/h was found for which the bifocal caustics gave values for the dynamic stress-intensity factor within expected experimental scatter. Thus it was concluded that the K_I^d-field did not adequately characterize the out-of-plane displacement field over any sizeable region around the crack-tip.

In the second part of the study, numerical simulations of the experiments were performed in an attempt to throw more light on the experimental results. The simulations involved using the experimentally obtained boundary loads as inputs into two- and three-dimensional elastodynamic finite-element analyses of the three-point bend specimen. Only the dynamically loaded uninitiated crack was considered. The results of the simulations also showed that the interaction of the full-field transient and three-dimensional effects were such as to preclude the possibility of any sizeable K_I^d-dominant region around the crack-front.

The experimental results for both the stationary and propagating cracks, combined with the numerical results for the uninitiated crack, lead to the conclusion that the near-tip dynamic fields seem to differ substantially from the asymptotic K_I^d-field. Indeed, these differences are such as to lead to large scatter in the measured "stress-intensity factor" above and beyond that caused by measurement errors. Note that this scatter is of the same order as some of the observed variations cited in the literature as evidence of possible parametric dependence of the dynamic fracture toughness. In view of the results of the current experiments, one must wonder whether the observed variations in the literature might not also be due to violation of K_I^d-dominance presumed in the interpretation of the experimental data. While it is recognized that the results of this work are specific to the situation studied, it is not inconceivable, especially in view of lack of countervailing evidence, that similar

results could hold in other settings. It might thus be instructive to speculate on the validity of the presumed K_I^d-dominance in some of the experiments reported in the literature.

5.1 Some Implications of Lack of K_I^d-Dominance

As far as the dominance of a K_I-field is concerned, the ratio of the smallest pertinent in-plane length to the specimen thickness can be thought of as a relevant geometry parameter. As pointed out in chapter II, the possible extent of a K_I-dominant annulus around the crack-tip is bounded from within by the maximum extent of a) the process zone, b) the non-linear region and c) the three-dimensional region. For nominally brittle materials such as those considered in this work, it appears that three-dimensionality is the most critical of the three. Also, the outer bound for a K_I-dominant annulus around the crack-tip is expected to depend on a relevant in-plane length scale. Thus, under static conditions at least, it is expected that the ratio a/h (where 'a' is the smallest relevant in-plane length and 'h' is the specimen thickness) must be sufficiently large for a K_I-field to survive the three-dimensional region and establish its dominance over some finite domain. In dynamic problems, the issue is much more involved with additional requirements dictated by the nature of the loading and the time required for stress-wave information to reach regions outside the three-dimensional zone (see, for example, Ravi-Chandar and Knauss (1987)). These, however, would seem to only further restrict the possibility of obtaining a K_I^d-dominant region in a real experiment. Thus, if a/h fails to be sufficiently large, it is not expected that a K_I^d-dominant field would prevail over any finite domain around the crack-tip. In particular, note that in the experiments reported in this work, a/h is about 9 (based on the uncracked ligament as the relevant in-plane length) and, for this value, a K_I^d-dominant field was not observed. It might thus be expected that the existence of a K_I^d-dominant region is not assured

for specimens for which a/h is of the same order as in this work. It is not the author's intention here to make a detailed review of the experimental literature with a view to ascertaining whether K_I^d-dominance prevailed in these experiments or not. Rather, the parameter a/h is suggested here as one measure by which the interested reader might gauge the relevance of the results of this work to other experiments. In the following, some experiments to which the results of this work might have a bearing are briefly discussed.

On $K_{ID} - \dot{a}$ relations: The question of the precise functional dependence of the dynamic fracture toughness on the crack velocity has appropriated a substantial share of the resources devoted to the study of dynamic fracture. The argument, for the most part, has centered around the issue of uniqueness of relationship between K_I^d and $\dot{a}$. The results of Kobayashi and Mall (1978) and Ravi-Chandar and Knauss (1984) – using photo-elasticity and the method of caustics respectively – suggest that there is no such one-to-one correspondence (see Figures 5.1a,b). Kobayashi and Dally (1980), Rosakis, Duffy and Freund (1984), Zehnder and Rosakis (1988) among others, however, provide data sets that seem to indicate that the $K_{ID} - \dot{a}$ relation is indeed (to within experimental error) a unique material property (see Figures 5.2a-c). As can be seen from the figures, there is substantial scatter in many of these data sets. Is the scatter observed in some of the experiments due to a lack of a unique correspondence between K_{ID} and $\dot{a}$, or due to a more fundamental lack of a K_I^d-dominant field in the experiments? Also, in all these experiments, the question of whether it is indeed the dynamic stress-intensity factor that is being measured needs to be looked into.

On impact-response curves: The first attempts to obtain dynamic initiation fracture toughness values using impact loading of a three-point bend specimen were highly simplistic in that they used the dynamically obtained impact loads and in-

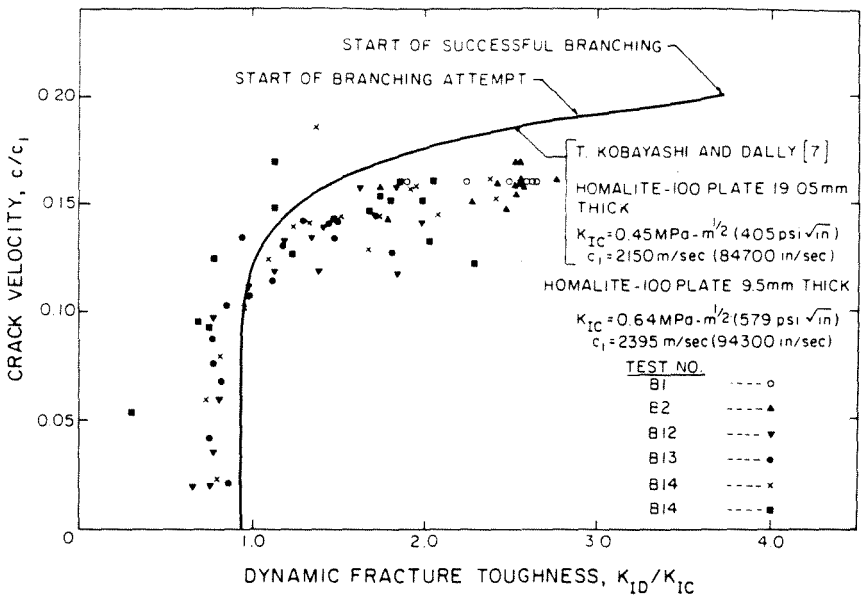

(a)

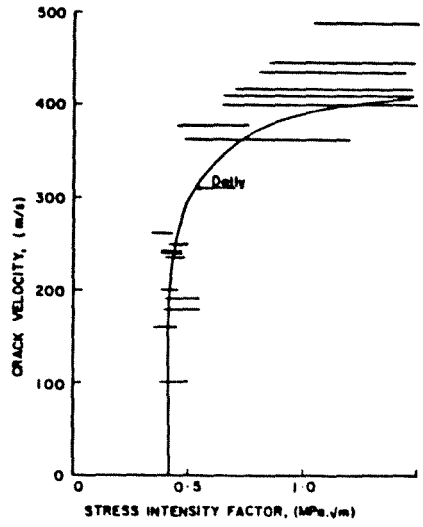

(b)

Figures 5.1a,b: Experiments indicating lack of a unique correspondence between K_I^d and $\dot{a}$: from a) Kobayashi and Mall (1978) and b) Ravi-Chandar and Knauss (1984).

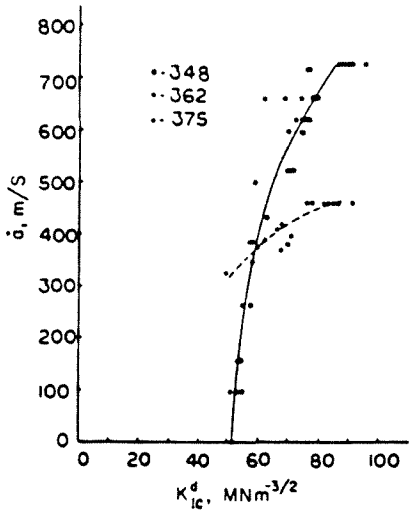

(a)

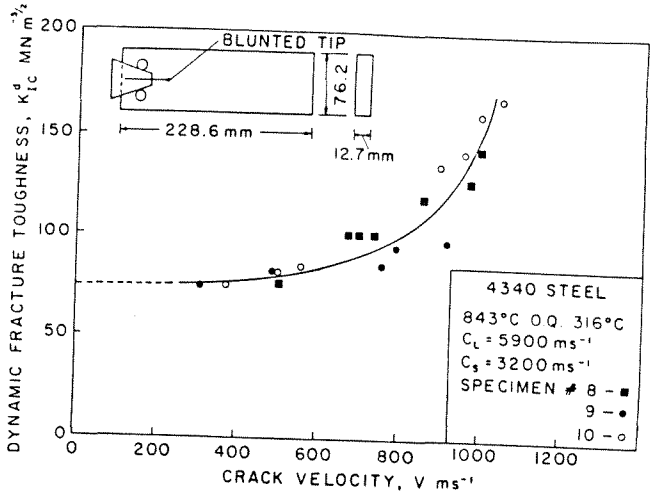

(b)

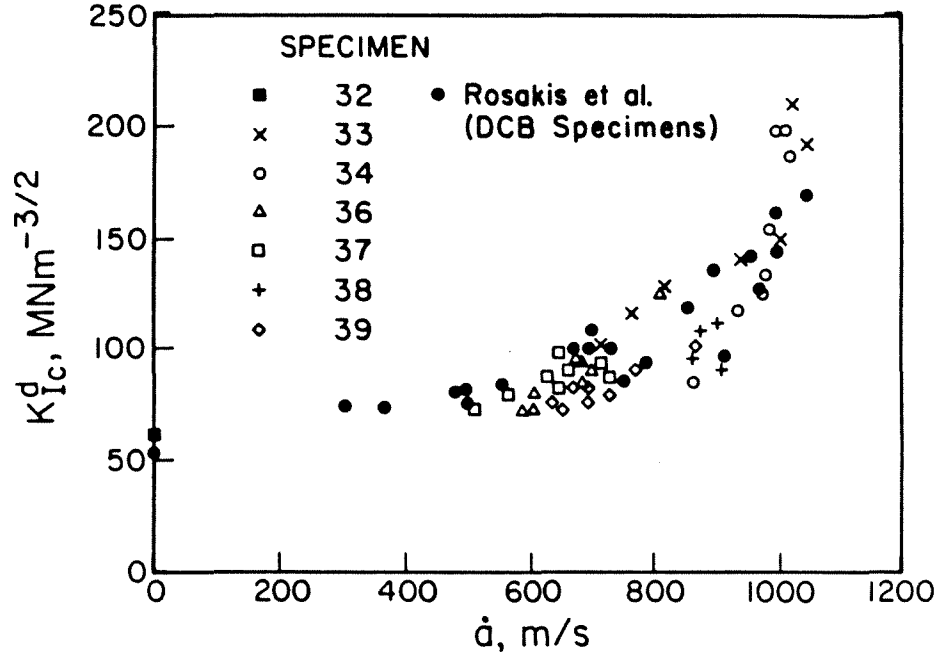

(c)

Figures 5.2a-c: Experiments showing unique correspondence between K_I^d and $\dot{a}$: from a) Kobayashi and Dally (1977) b) Rosakis, Duffy and Freund (1984) and c) Zehnder and Rosakis (1988).

terpreted them through *static* analyses. Recognizing that this was tantamount to neglecting inertial effects, the concept of impact-response curves was suggested by Kalthoff (1985). This is essentially a calibration curve (see Figure 5.3a) based on the assumption that the stress-intensity factor value obtained through the method of caustics gives the 'true' value. A preliminary experiment using the method of caustics is conducted to obtain the time history of stress-intensity factor which is then used as a master curve for all other tests involving similar geometry. That is, in subsequent tests, only the time to fracture (from the time of impact) is monitored and the dynamic initiation toughness is simply read off the master curve. The question that arises from this work is one of reliability of the master curve. In particular, by how much would the impact-response curve change if, in the caustics experiment used to obtain it, a different choice of z_o (leading to a different range of r_0/h) had been used?

On specimen dependence of K_{ID}: By far the most troubling of all the experimental results are those that indicate that the dynamic fracture toughness could be specimen dependent (Kalthoff (1983) and Dahlberg, Nilsson and Brickstad (1985)). These results (see Figure 5.3c), rather than merely contending about the parametric dependence of a material property – the fracture toughness – would, if true, seem to indicate that the stress-intensity factor-based fracture criterion is fundamentally flawed. However, it is possible to attribute the apparent observed specimen dependence of K_{ID} to specimen-dependent differences in the near-tip field (i.e., the near-tip fields, not being K_I^d-dominant, might have a different structure from specimen to specimen). Moreover, as has been shown in this work, much larger differences (than the 20% or so that is seen in Fig. 5.3c) could possibly have been obtained for the *same* type of specimen if, in the caustics experiments used to obtain the results of Figure 5.3c, a different range of initial-curves had been used by changing

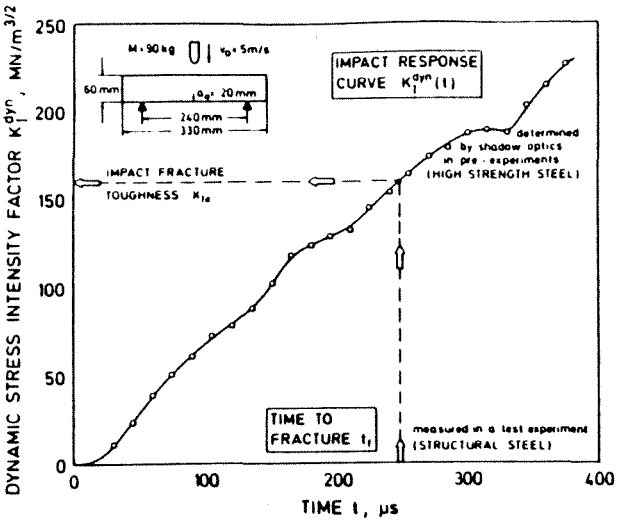

(a)

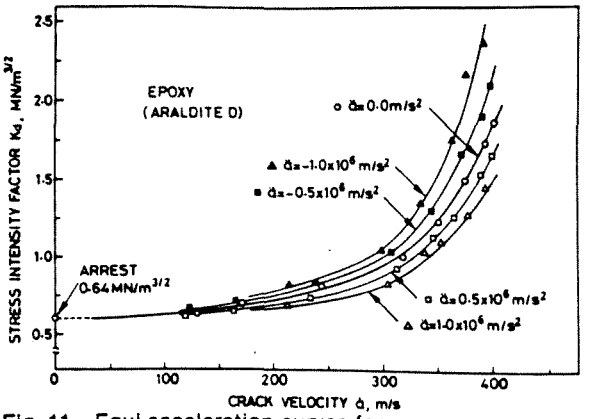

Fig. 11—Equi-acceleration curves for epoxy as a function of $\dot{a}$

(b)

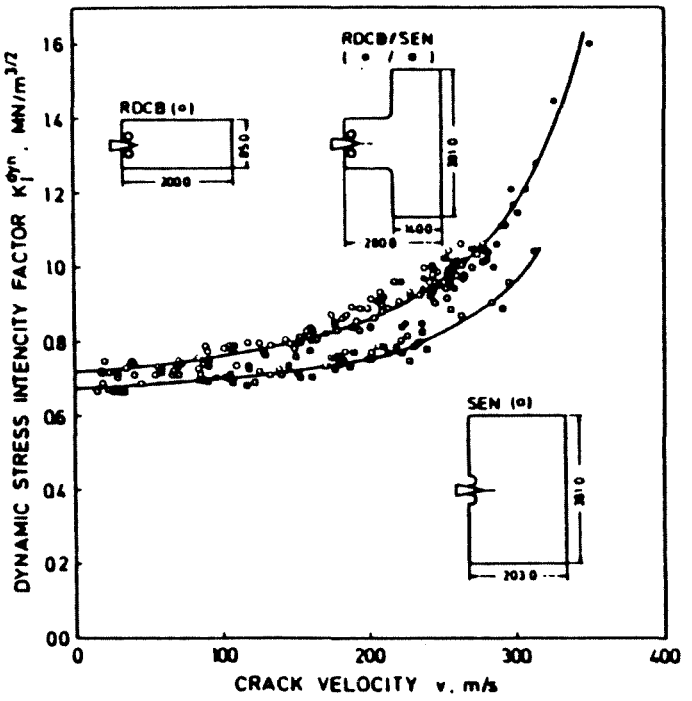

(c)

Figures 5.3a-c: a) Impact response curve suggested by Kalthoff (1985), b) acceleration dependence of K_{ID} noted by Takahashi and Kanazawa (1987) and c) specimen dependence of the dynamic fracture toughness observed by Kalthoff (1983).

the specimen to image plane distance z_0.

On $K_{ID} - \ddot{a}$ relations: Finally, attempts by Takahashi and Arakawa (1987) – using the method of caustics again – to show acceleration dependence of the dynamic fracture toughness (Figure 5.3b) can also be deemed inconclusive for precisely the same reasons as above.

It is thus possible that many of the apparent discrepancies in the experimental literature might arise from the lack of an underlying K_I^d-dominant region assumed in the interpretation of the experimental data.

5.2 Suggestions for Future Work

Two issues need to be addressed. First, if it is observed that in most practical situations a stress-intensity factor approach is acceptable for the characterization of dynamic fracture, then the question of scaling of specimens for laboratory study needs to be worked out in greater detail. In this case, the primary interest is in determining the parametric dependence of the dynamic fracture toughness on crack velocity, acceleration, temperature, et cetera. A stress-intensity factor-based fracture criterion such as (1.11) would then be appropriate. Since this approach inherently assumes the existence of a dominant K_I^d-field around the crack-tip region, it is imperative that such conditions also be obtained in the laboratory specimens used to obtain K_{ID} values. Preliminary experimental and numerical studies such as those undertaken in this work can possibly be used to tailor the geometric and loading conditions of the test configuration so that a region of K_I^d-dominance is attained.

More fundamentally, however, it must be recognized that fracture also occurs in structures (such as the specimens used in this work) where no K_I^d-dominance is observed. One must wonder what characterizes fracture in such cases. Thus, if the study of dynamic fracture is not to become the mere characterization of fracture

given a K_I^d-field, one needs to consider situations of a more general nature. A theoretical framework for fracture which possibly includes the failure criterion as part of the constitutive behavior of the material could be considered. This would then be an attempt to characterize the fracture process at a more fundamental level than possible with the stress-intensity factor. In the realm of experiments, techniques that are not based on any assumption about the structure of the near-tip continuum field need to be developed. A promising start is currently being made with the adaptation of interferometric techniques to dynamic fracture (Pfaff (1988)). Hybrid techniques combining experimental and numerical methods along the lines described in Chapter IV, can be refined and possibly adapted for the propagating regime as well. Analytical studies of three-dimensional and non-linear effects could be undertaken without resorting to a far-field stress-intensity factor field. The boundary layer approach of embedding linear, non-linear and non-continuum regions could probably be used without the restrictive requirement of a surrounding K_I-field; for example, one might seek the details of the three-dimensional crack-tip region under the requirement that it give way to a plane-stress region in the far-field rather than necessarily the plane-stress *asymptotic* field. Until such steps are taken, however, one must wonder whether the prevailing tendency to characterize most aspects of dynamic fracture by means of the stress-intensity factor merely for purposes of analytical tractability might not, in the end, prove to be as futile an endeavor as that of the proverbial Goha of Arabia, who, losing his wallet in the desert, nonetheless chooses to search for it in his house for the inarguably simple reason that 'it is dark outside, and here I have a light.'

REFERENCES

Achenbach J.D., (1973), "Wave Propagation in Elastic Solids," North Holland Publishing Company.

Bathe K., (1982), "Finite Element Procedures in Engineering Analysis," Prentice Hall.

Baker B.R., (1962), "Dynamic Stresses Created by a Moving Crack," *Journal of Applied Mechanics*, vol.29, pp 449-458.

Beinert J., and Kalthoff J.F.,(1981), "Experimental Determination of Dynamic Stress-Intensity Factors by Shadow Patterns," in 'Mechanics of Fracture,' vol VII, edited by G.Sih, Sijthoff and Noordhoff, pp 281-330.

Bilek Z., (1980), "Some Comments on Dynamic Crack Propagation in a High Strength Steel," in 'Crack Arrest Methodology and Applications', ASTM STP 711, American Society for Testing and Materials, pp 240-247.

Broberg K.B., (1960), "The Propagation of a Brittle Crack," *Arkiv für Fysik*, vol. 18, pp 159-192.

Craggs J.W., (1960), "On the Propagation of a Crack in an Elastic-Brittle Material," *Journal of Mechanics and Physics of Solids*, vol. 8, pp 66-75.

Dahlberg L., Nilsson F., and Brickstad B., (1980), "Influence of Specimen Geometry on Crack Propagation and Arrest Toughness," in 'Crack Arrest Methdology and Applications,' edited by Hahn G.T., et al, ASTM STP 711, pp 89-108.

Dally J.W., Fourney W.L., and Irwin G.R., (1985), "On the Uniqueness of $K_{ID} - \dot{a}$ Relation," *International Journal of Fracture*, vol. 27, pp 159-168.

de Hoop A.T., (1958), "Representation Theorems for the Displacement in an

Elastic Solid and Their Applications to Elastodynamic Diffraction Theory," Technishe Hogeschool, Delft.

Ellis T.A., (1954), doctoral dissertation, California Institute of Technology.

Eshelby J.D., (1969), "The Elastic Field of a Crack Extending Non-Uniformly under General Anti-Plane Loading," *Journal of Mechanics and Physics of Solids*, vol. 17.

Freund L.B., (1972), "Crack Propagation of a Crack in an Elastic Solid Sujected to General Loading-I. Constant Rate of Extension," *Journal of Mechanics and Physics of Solids*, vol. 20, pp 129-140.

Freund L.B., (1972), "Energy Flux into the Tip of an Extending Crack in an Elastic Solid," *Journal of Elasticity*, vol. 2, pp 341-349.

Freund L.B., (1973), "Crack Propagation of a Crack in an Elastic Solid Sujected to General Loading-III. Stress Wave Loading," *Journal of Mechanics and Physics of Solids*, vol. 21, pp 47-61.

Freund L.B., and Clifton R.J., (1974), "On the Uniqueness of Plane Elastodynamic Solutions for Running Cracks," *Journal of Elasticity*, vol. 4, No. 4, pp 293-299.

Freund L.B., and Douglas A., (1982), "The Influence of Inertia on Elastic Plastic Anti-Plane Shear Crack-Growth," *Journal of Mechanics and Physics of Solids*, vol. 30, pp 59-74.

Freund L.B., and Hutchinson J.W., (1985), "High Strain-Rate Crack Growth in Rate-Dependent Plastic Solids," *Journal of Mechanics and Physics of Solids*, vol. 33, pp 169-191.

Hinton E., and Campbell J.S., (1974), "Local and Global Smoothing of Discontinuous Finite Element Functions Using A Least Squares Method," *International Journal for Numerical Methods in Engineering*, vol. 8, pp 461-480.

Hughes T.J.R., and Belytschko T., (1983), "A Precis of Developments in Computational Methods for Transient Analysis," *Journal of Applied Mechanics*, vol. 50, pp 1033-1041.

Kalthoff J.F., (1983), "On Some Current Problems in Experimental Fracture Mechanics," in 'Workshop on Dynamic Fracture,' edited by Knauss W.G. et al., California Institute of Technology, pp 11-35.

Kalthoff J.F., (1985), "On the Measurement of Dynamic Fracture Toughness – A Review of Recent Work," *International Journal of Fracture*, vol. 27, pp 277-298.

Kalthoff J.F., (1985), "Concept of Impact Response Curves," in Metals Handbook, vol. 8, Mechanical Testing, American Society for Metals, Metals Park.

Kim K.S., (1985), "A Stress-Intensity Factor Tracer," *Journal of Applied Mechanics*, vol. 52, pp 291-297.

Knauss W.G., and Ravi-Chandar K., (1985), "Some Basic Problems in Stress Wave Dominated Fracture," *International Journal of Fracture*, vol. 27, pp 127-143.

Kobayashi A.S., and Mall S., (1978), "Dynamic Fracture Toughness of Homalite 100," *Experimental Mechanics*, vol. 18, pp 11-18.

Kobayashi T., and Dally J.W., (1977), "Relation Between Crack Velocity and the Stress Intensity Factor in Birefringent Polymers," in 'Fast Fracture and Crack Arrest,' ASTM STP 627, edited by Hahn G.T. et al., pp 257-273.

Kobayashi T., and Dally J.W. (1980), "Dynamic Photo-elastic Determination of the $\dot{a} - K$ Relation for the 4340 Steel," in 'Crack Arrest Methodology,' edited

by Hahn G.T., et al., ASTM STP 711, pp 89-108.

Krishnaswamy S., and Rosakis A.J. (1988), (under preparation), California Institute of Technology, Pasadena.

Lam P.S., and Freund L.B., (1985), "Analysis of Dynamic Crack Growth of a Tensile Crack in an Elastic-Plastic Material," *Journal of Mechanics and Physics of Solids*, vol.33, pp 153-167.

Manogg P., (1964), "Anwendungen der Schattenoptik zur Untersuchung des Zerreissvorgags von Platten," doctoral dissertation, Freiburg, West Germany.

Nakamura T., and Parks D.M., (1987), "Three-Dimensional Field Near the Crack Front of a Thin Elastic Plate," presented at the 24th Annual Meeting of the Society of Engineering Science, Sept. 21-23, 1987, Salt Lake City, Utah.

Parsons I.D., Hall J.F., and Rosakis A.J., (1986), "A Finite Element Investigation of the Elastostatic State Near a Three-Dimensional Edge Crack," GALCIT Report SM 86-29, California Institute of Technology.

Pfaff R., (1988), (private communication), California Institute of Technology, Pasadena, California.

Ravi-Chandar K., (1982), "An Experimental Investigation into the Mechanics of Dynamic Fracture," doctoral dissertation, California Institute of Technology, Pasadena, California.

Ravi-Chandar K., and Knauss W.G., (1984), *International Journal of Fracture*, vol. 25, pp 247-262.

Ravi-Chandar K., and Knauss W.G., (1987), "On the Characterization of the Transient Stress Field Near the Tip of a Crack," *Journal of Applied Mechanics*, vol. 54, pp 72-78.

Rice J.R., (1968), "Mathematical Analysis in the Mechanics of Fracture," in 'Fracture – An Advanced Treatise', vol. II, edited by Leibowitz H., Academic Press, New York, pp 191-308.

Rosakis A.J., (1980), "Analysis of the Optical Method of Caustics for Dynamic Crack Propagation," *Engineering Fracture Mechanics*, vol 13. pp 331-347.

Rosakis A.J., and Freund L.B., (1981), "The Effect of Crack-Tip Plasticity on the Determination of the Dynamic Stress-Intensity Factor by the Optical Method of Caustics," *Journal of Applied Mechanics*, vol. 48., pp 302-308.

Rosakis A.J., (1982), "Experimental Determination of the Fracture Initiation and Dynamic Crack Propagation Resistance of Structural Steels by the Optical Method of Caustics," doctoral dissertation, Brown University, Providence, Rhode Island.

Rosakis A.J., Duffy J., and Freund L.B., (1983), "Dynamic Crack Growth Criteria in Structural Metals," in 'Workshop on Dynamic Fracture,' edited by Knauss W.G. et al., California Institute of Technology, Pasadena.

Rosakis A.J., Duffy J., and Freund L.B., (1984), "The Determination of Dynamic Fracture Toughness of AISI 4340 Steel by the Shadow Spot Method," *Journal of the Mechanics of Physics of Solids*, vol. 32, pp 443-460.

Rosakis A.J., and Zehnder A.T., (1985), "On the Method of Caustics: An Exact Analysis Based on Geometrical Optics," *Journal of Elasticity*, vol. 15, No. 4, pp 347-368.

Rosakis A.J., and Ravi-Chandar K., (1986), "On Crack-Tip Stress State: An Experimental Evaluation of Three-Dimensional Effects," *International Journal of Solids and Structures*, vol. 22, No. 2, pp 121-134.

Shih C.F., Moran B., and Nakamura T., (1986), "Energy Release Rate Along A Three-dimensional Crack Front in a Thermally Stressed Body," *International Journal of Fracture*, vol. 30, pp 79-102.

Smith R.H., and Freund L.B., (1980), "Three-Dimensional Finite Element Analysis of Steady Elastodynamic Crack Growth in a Plate," presented at the joint ASME-SES Conference, June 1988, held at Berkeley, California.

Takahashi K., and Arakawa K., (1987), "Dependence of Crack Initiation on the Dynamic Stress-Intensity Factor in Polymers," *Experimental Mechanics*, vol. 27, No. 2, pp 195-199.

Taylor R.L., (1977), "Computer Procedures for Finite Element Analysis," in 'The Finite Element Method,' by Zienkiwiecz O.C., 3rd edition, McGraw-Hill.

Williams M.L., (1957), "On the Stress Distribution at the Base of Stationary Crack," *Journal of Applied Mechanics*, vol. 24, pp 109-114.

Yoffe E. H., (1951), "The Moving Griffith Crack," *Philosophical Magazine*, vol. 42, pp 739-750.

Yang W., and Freund L.B., (1985), "Transverse Shear Effects for Through Cracks in an Elastic Plate," *International Journal of Solids and Structures*, vol. 21, No. 9, pp 977-994.

Zehnder A.T., (1987), "Dynamic Fracture Initiation and Propagation in Metals: Experimental Results and Techniques," doctoral dissertation, California Institute of Technology, Pasadena, California.

Zehnder A.T., and Rosakis A.J., (1988), (private communication), California Institute of Technology, Pasadena.

APPENDIX A1

ENERGY-RELEASE RATE INTEGRALS

In this appendix, an average energy-release rate integral will be defined for a stationary crack in a three-dimensional body subject to dynamic loading. The equivalence of this (surface) integral to a numerically more desirable volume integral over a finite domain will be shown. The analysis given here is a specialization of a scheme given in Shih, Moran and Nakamura (1986) pertinent to the experiments reported in this work.

Consider a planar straight-fronted crack in an elastic plate of width h (Fig A1.1). Let x_1, x_2, x_3 be a Cartesian coordinate system such that crack flanks are given by $x_1 \leq 0 : x_2 = 0^{\pm} : x_3 \in [-h/2, h/2]$. The crack flanks and the lateral faces of the plate ($x_3 = \pm h/2$) are traction free. Consider a surface $\mathcal{S}$ enclosing the crack front consisting of a cylindrical region $\mathcal{S}_l$ and end-caps ${\mathcal{S}_h}^{\pm}$ at $x_3 = \pm h/2$. Let the intersection of $\mathcal{S}_l$ with any plane $x_3 = constant$ be the line Γ.

By an argument of virtual crack extension in the x_1-direction, an 'average' energy-release rate for this problem can be defined as

$$J = \frac{1}{h} \lim_{\Gamma \to 0} \int_{\mathcal{S}} \left((U + T) n_1 - \sigma_{ij} n_j \frac{\partial u_i}{\partial x_1} \right) dS$$

where U is the strain-energy density, T the kinetic energy density, σ_{ij} the stress tensor, u_i the displacement vector and $\underline{n}$ is the unit outward normal to $\mathcal{S}$. The limit $\Gamma \to 0$ symbolically indicates that the cylindrical surface $\mathcal{S}_l$ is to be shrunk onto the crack-front. It has been shown that this limit exists (under some weak restrictions) and is indeed independent of the actual shape of the surface (see Freund (1972)). Recognizing that the kinetic energy density is bounded for a stationary crack and that on the lateral surfaces ${\mathcal{S}_h}^{\pm}$ the traction as well as n_1 are zero, define $\overline{J} = hJ$.

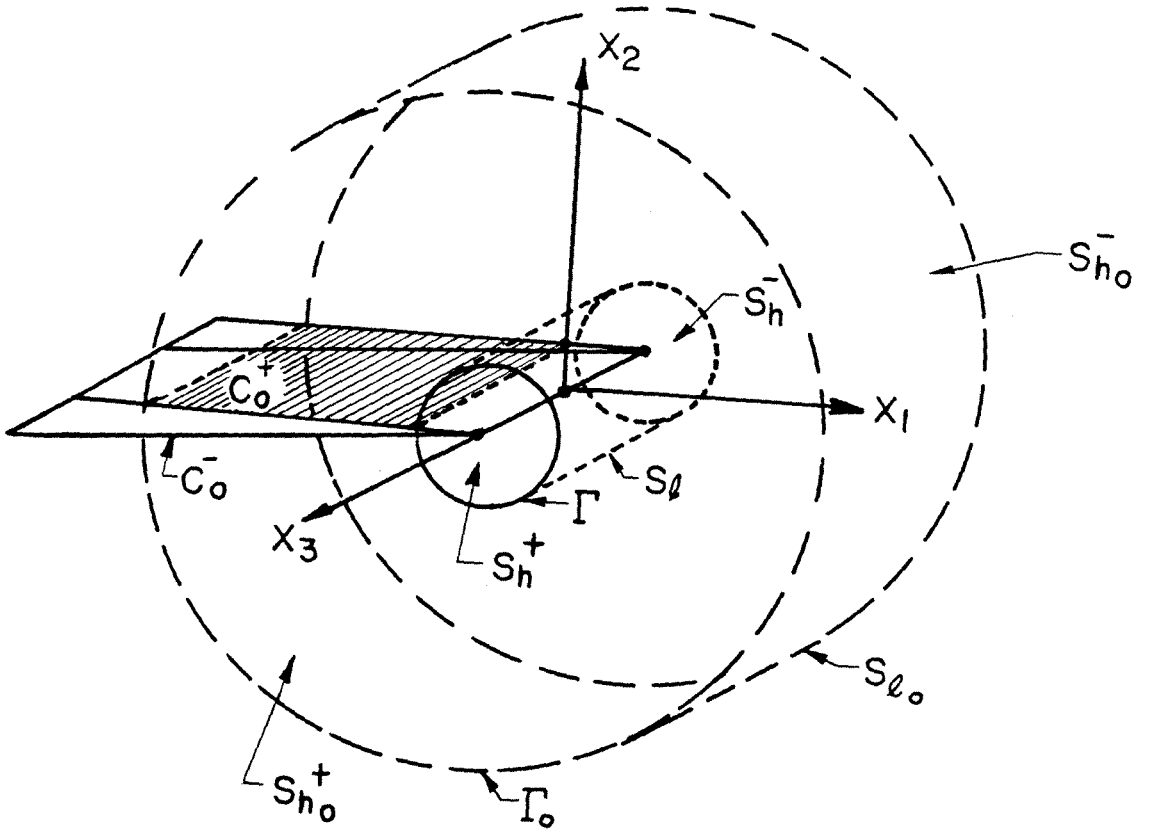

Figure A1.1: Domain of integration for the J-integral.

Thus

$$\overline{J} = \lim_{\Gamma \to 0} \int_{\mathcal{S}_l} \left(U n_1 - \sigma_{ij} n_j \frac{\partial u_i}{\partial x_1} \right) dS. \qquad (*)$$

Since it is numerically impossible to evaluate the above expression to any reasonable degree of accuracy, an alternate form of the above integral will now be developed. Consider another surface $\mathcal{S}_o$ enclosing the surface $\mathcal{S}_l$. This consists of a tubular surface $\mathcal{S}_{lo}$ (whose generator is Γ_o), the end-caps $\mathcal{S}_{ho}{}^{\pm}$ on $x_3 = \pm h/2$ which contain the region between Γ and Γ_o and that part of the crack-flanks $\mathcal{C}_o^+$ and $\mathcal{C}_o^-$ which lie between $\mathcal{S}_{lo}$ and $\mathcal{S}_o$. Let $\mathcal{V}_o$ be the volume enclosed by $\mathcal{S}_o$ and $\mathcal{S}_l$. Let ϕ be a scalar-valued function defined in $\mathcal{V}_o$ such that a) ϕ is once continuously differentiable in $\mathcal{V}_o$ (b) $\phi = 1$ on $\mathcal{S}_l$ and (c) $\phi = 0$ on $\mathcal{S}_{lo}$. Equation (*) can be cast into the form

$$\overline{J} = \lim_{\Gamma \to 0} \int_{\mathcal{S}_o + \mathcal{S}_l} \left(U n_1 - \sigma_{ij} n_j \frac{\partial u_i}{\partial x_1} \right) \phi \; dS \qquad (**)$$

since the contribution from the crack-flanks and the end-caps is zero and ϕ is zero on $\mathcal{S}_{lo}$ and one on $\mathcal{S}_l$. Applying the divergence theorem to the closed surface integral in (**) and making use of the balance of linear momentum, it can be shown that

$$\overline{J} = \lim_{\Gamma \to 0} \int_{\mathcal{V}_o} \left(\sigma_{ij} \frac{\partial u_i}{\partial x_1} \frac{\partial \phi}{\partial x_j} - U \frac{\partial \phi}{\partial x_1} + \rho \frac{\partial^2 u_i}{\partial t^2} \frac{\partial u_i}{\partial x_1} \phi \right) dV$$

where ρ is the material density. Defining $\mathcal{V}$ to be the volume enclosed by $\mathcal{S}_o$ and $\mathcal{S}_l$ in the limit $\Gamma \to 0$, one obtains

$$J = \frac{1}{h} \int_{\mathcal{V}} \left(\sigma_{ij} \frac{\partial u_i}{\partial x_1} \frac{\partial \phi}{\partial x_j} - U \frac{\partial \phi}{\partial x_1} + \rho \frac{\partial^2 u_i}{\partial t^2} \frac{\partial u_i}{\partial x_1} \phi \right) dV. \qquad (\ddagger)$$

This is the so-called domain integral form for the average energy-release rate. Its advantage lies chiefly in the fact that the surface $\mathcal{S}_{lo}$ can be so chosen as to minimize the percent error caused by the numerical uncertainties in the field quantitities near the crack-front.

Remarks:

(i) Specialization to elastostatics is immediate. Note that in this case there is path independence of the J-integral and so one need not take the limit $\Gamma \rightarrow 0$. The equivalent domain integral would now be over the volume $\mathcal{V}_o$ without the necessity of shrinking the inner tube onto the crack-front.

(ii) For two-dimensional problems, the above arguments go through exactly with a line integral now being converted to a surface integral. The domain integral form thus becomes

$$J = \lim_{\Gamma \rightarrow 0} \int_{\mathcal{S}} \left(\sigma_{ij} \frac{\partial u_i}{\partial x_1} \frac{\partial \phi}{\partial x_j} - U \frac{\partial \phi}{\partial x_1} + \rho \frac{\partial^2 u_i}{\partial t^2} \frac{\partial u_i}{\partial x_1} \phi \right) dS$$

where $\mathcal{S}$ is the area between the outer contour Γ_o and the inner contour Γ which, of course, is shrunk onto the crack-tip.

The accuracy of the domain integral scheme as well as the effect of the particular choice of the weighting function ϕ were studied by Shih, Moran and Nakamura (1986) who, using an explicit time integration scheme, found the method to be highly satisfactory. Since the simulations reported in this work were all done using an implicit time integration scheme (with relatively coarser time steps), a calibration problem will now be studied in order to determine the time steps that would be appropriate for these problems. The test problem is a two-dimensional, plane-strain problem of a semi-infinite crack in an infinite medium under mode-I conditions. The crack is loaded by a step pulse parallel to the crack line. The asymptotic solution to this problem can be obtained from Freund (1973). The numerical simulation of this problem of course requires a finite geometry but the analytical solution is still applicable till such time as the effects of the boundary are felt by the crack-tip. A rather coarse finite-element mesh was chosen (Figure A1.2a) as being adequate for the purpose at hand. An unconditionally stable, implicit Newmark predictor-corrector time integration scheme was used. Figure A1.2b shows the results of

the analysis for different time steps. Also shown is the exact analytical value. It is seen that for the finer time steps chosen, results for J are within 5 percent of the analytical values. It should be noted that even finer time steps and finer mesh discretization were used in the simulations of the experiments, and so, it is expected that the numerically induced errors in the computation of the energy-release rates would be even smaller.

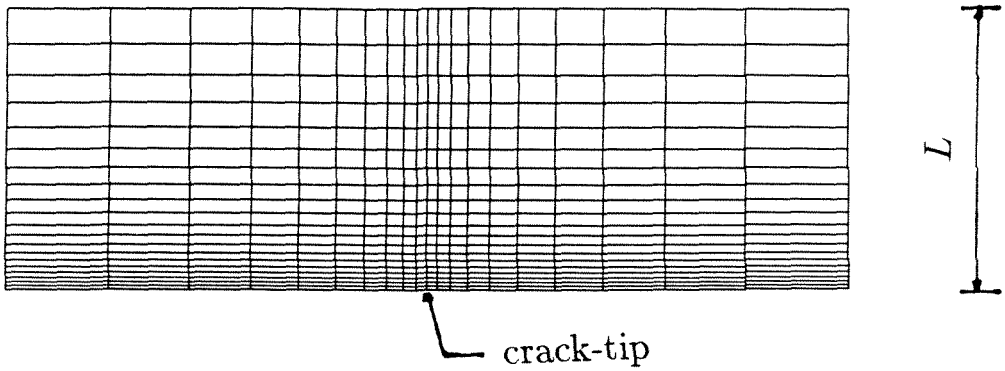

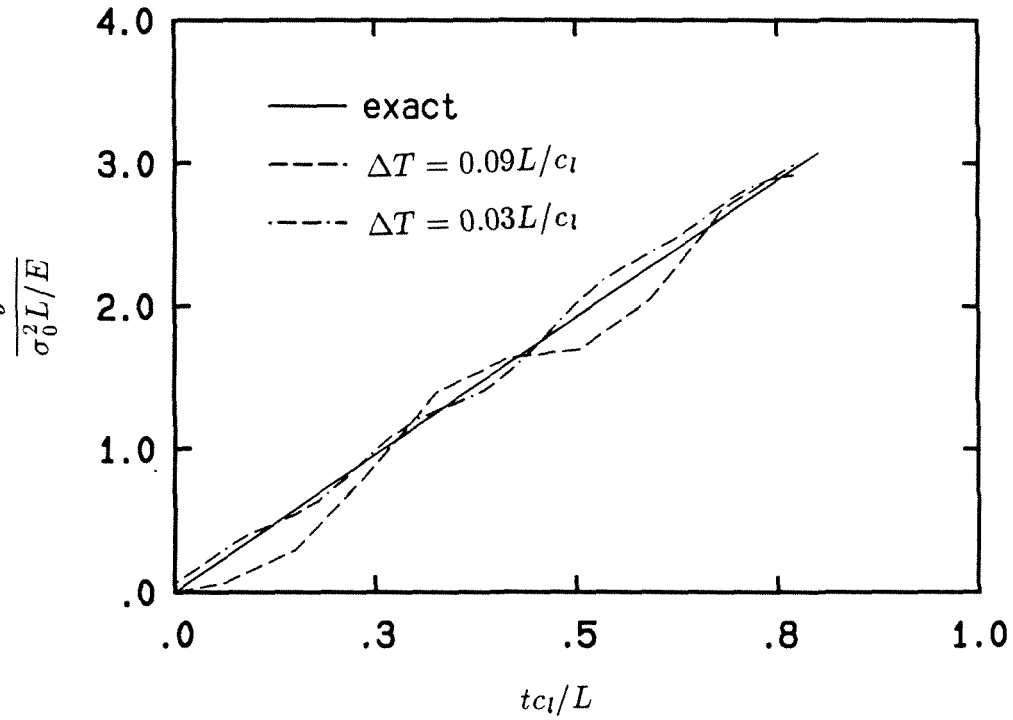

Figures A1.2: a) Mesh geometry and b) comparison of the analytical (exact) stress-intensity factor history with the numerically obtained values.

APPENDIX A2

THE NEWMARK PREDICTOR-CORRECTOR ALGORITHM

The finite-element spatial discretization of the elastodynamic problem and the subsequent time integration of the discretized equations are described here. These follow fairly standard practice and are given here essentially for the sake of completeness.

A displacement based finite-element scheme is used for the spatial discretization (see Bathe (1982)). Using the principle of virtual work, one obtains the semi-discrete equation of motion for $t \in [0, T]$

$$\mathbf{M}\ddot{\underline{x}}(t) + \mathbf{K}\underline{x}(t) = \underline{f}(t)$$

$$\underline{x}(0) = \underline{x}_o \qquad (\dagger)$$

$$\dot{\underline{x}}(0) = \dot{\underline{x}}_o$$

where $\mathbf{M} = \int_{\mathcal{R}} \rho \mathbf{H}^T \mathbf{H} dV$ is the mass matrix, $\mathbf{K} = \int_{\mathcal{R}} \mathbf{B}^T \mathbf{D} \mathbf{B} dV$ is the stiffness matrix, $\underline{f}(t) = \int_{\partial R} \mathbf{H}^T \underline{\tau} dS$ is the applied load vector and $\underline{x}(t)$ is the vector of nodal displacements at time t, $\mathbf{H}$ is the interpolation function matrix, $\mathbf{B}$ is the strain-displacement matrix, $\mathbf{D}$ is the elasticity matrix and $\underline{\tau}$ is the applied boundary traction.

Once the spatial discretization is done, the mass and stiffness matrices, as well as the load vector, are known and it remains only to integrate (†) in time to obtain the nodal displacements, velocities and accelerations. To do this, the Newmark predictor-corrector algorithm is used. The time interval $[0, T]$ is discretized and suppose that the solution at time t_n is known; i.e., $\underline{x}_n \approx \underline{x}(t_n)$, $\underline{v}_n \approx \dot{\underline{x}}(t_n)$ and $\underline{a}_n \approx \ddot{\underline{x}}(t_n)$ have been computed. The solution at time t_{n+1} is required. Let $h = t_{n+1} - t_n$.

The Newmark algorithm for (†) is:

$$\mathbf{M}\underline{a}_{n+1} + \mathbf{K}\underline{x}_{n+1} = \underline{f}_{n+1}$$

$$\underline{x}_{n+1} = \underline{x}_n + h\underline{v}_n + h^2\big((1/2-\beta)\underline{a}_n + \beta\underline{a}_{n+1}\big) \qquad (\ddagger)$$

$$\underline{v}_{n+1} = \underline{v}_n + h\big((1-\gamma)\underline{a}_n + \gamma\underline{a}_{n+1}\big)$$

where $\beta \in [0, 1/2]$ and $\gamma \in [0, 1]$ are Newmark parameters chosen to meet desired stability and convergence properties. The solution to (‡) is obtained by an iterative Newton-Raphson procedure as follows:

(i) *Newmark Predictor:*

$$k = 0$$

$$\underline{x}_{n+1}^{(0)} = \underline{x}_n + h\underline{v}_n + h^2(1/2-\beta)\underline{a}_n$$

$$\underline{v}_{n+1}^{(0)} = \underline{v}_n + h(1-\gamma)\underline{a}_n$$

$$\underline{a}_{n+1}^{(0)} = 0$$

(ii) *Solve:*

$$\widehat{\mathbf{K}}\Delta\underline{x} = \hat{r}_{n+1}^{(k)}$$

where

$$\widehat{\mathbf{K}} = \mathbf{K} + \frac{1}{\beta h^2}\mathbf{M}$$

$$\hat{\underline{r}}_{n+1}^{(k)} = \underline{f}_{n+1} - \mathbf{K}\underline{x}_{n+1}^{(k)} - \mathbf{M}\underline{a}_{n+1}^{(k)}$$

(iii) *Newmark Corrector:*

$$\underline{x}_{n+1}^{(k+1)} = \underline{x}_{n+1}^{(k)} + \Delta\underline{x}$$

$$\underline{v}_{n+1}^{(k+1)} = \underline{v}_{n+1}^{(k)} + \frac{\gamma}{\beta h}\Delta\underline{x}$$

$$\underline{a}_{n+1}^{(k+1)} = \underline{a}_{n+1}^{(k)} + \frac{1}{\beta h^2}\Delta\underline{x}$$

(iv) *Convergence check:*

$$||\underline{r}_{n+1}^{(k)}|| \leq ||\underline{r}_{n+1}^{(0)}|| * TOLERANCE$$

Check for convergence of solution to desired tolerance. If convergence is achieved, the solution $\underline{x}_{n+1}$, $\underline{v}_{n+1}$ and $\underline{a}_{n+1}$ is deemed known and the procedure is repeated for the next time step. If convergence is *not* achieved, set $k \leftarrow (k+1)$ and go to step (ii).

Remark:

It is easy to show (see Hughes and Belytshcko (1983)) that the choice $\beta = 0.25$ and $\gamma = 0.5$ for the Newmark parameters leads to an unconditionally stable, implicit algorithm. This is the algorithm used in the analyses reported in this thesis.

	4340	4340var
C %	0.42	0.42
Mn %	0.71	0.46
P %	0.007	0.009
S %	0.013	0.001
Si %	0.23	0.28
Ni %	1.78	1.74
Cr %	0.83	0.89
Mo %	0.25	0.21
Cu %	0.12	0.19
Sn %	0.005	-
Al %	0.033	0.031
N %	-	0.005
O %	-	0.001
H(ppm)	-	1.0

Table T1: Material composition.

Specimen	2l (in)	b (in)	a (in)	h (in)	Notch	Temper	Material
60	12.00	5.00	1.5	0.38	edm	315°C	4340
61	12.00	5.00	1.5	0.38	edm	315°C	4340
62	12.00	5.00	1.5	0.38	edm	315°C	4340
$\alpha - 3$	12.06	5.00	1.5	0.45	edm	200°C	4340var
$\alpha - 4$	12.00	5.00	1.5	0.46	edm	200°C	4340var
$\alpha - 5$	12.06	5.00	1.3	0.45	edm	200°C	4340var
$v3s$	12.06	4.94	1.5	0.46	edm	200°C	4340var
$v36f$	12.03	4.97	1.5	0.41	fatigue	200°C	4340var
31	12.06	4.94	1.5	0.47	edm	200°C	4340
$3q$	12.06	4.97	1.5	0.48	edm	200°C	4340
$v63$	12.06	4.94	1.5	0.46	edm	350°C	4340var
$65f$	12.06	4.97	1.5	0.48	fatigue	350°C	4340

Table T2: Specimen dimensions.